

**Preparation and Application of Fluoroalkyl End-Capped
Vinyltrimethoxysilane Oligomeric Silica/Butadiene
Copolymers Nanocomposites**

Doctoral Course
Graduate School of Science and Technology
Hirosaki University

Doctoral Thesis

March 2018

Arissara Ratcha

Contents

General Introduction	1
Chapter 1. Preparation and Thermal Stability of Fluoroalkyl End-Capped Vinyltrimethoxysilane Oligomeric Silica/ Poly(acrylonitrile-<i>co</i>-butadiene) Nanocomposites - Application to the Separation of Oil and Water	24
1.1. Introduction	25
1.2. Experimental	27
1.2.1. Measurements	27
1.2.2. Materials	28
1.2.3. Preparation of fluoroalkyl end-capped vinyltrimethoxysilane oligomeric silica nanocomposites - encapsulated poly(acrylonitrile- <i>co</i> -butadiene) [R _F -(VM-SiO ₂) _n -R _F /NBR]	29
1.2.4. Preparation of modified glass treated with the R _F -(VM-SiO ₂) _n -R _F /NBR nanocomposites by casting method	30
1.3. Results and discussion	31
1.3.1. Preparation of the fluoroalkyl end-capped vinyltrimethoxysilane oligomeric silica nanocomposites - encapsulated NBR	31
1.3.2. Thermal stability of the fluoroalkyl end-capped vinyltrimethoxysilane oligomeric silica nanocomposites - encapsulated NBR	36

1.3.3.	Surface modification of glass by the use of fluoroalkyl end-capped vinyltrimethoxysilane oligomeric silica nanocomposites - encapsulated NBR	39
1.4.	Conclusions	50
Chapter 2.	Preparation and Thermal Stability of Initiator Fragments	56
	End-Capped Oligomers/Silica Nanocomposites	
2.1.	Introduction	57
2.2.	Experimental	60
2.2.1.	Measurements	60
2.2.2.	Materials	61
2.2.3.	Synthesis of initiator fragments end-capped oligomers by using APS as a radical initiator	62
2.2.3.1.	Initiator fragments end-capped <i>N,N</i> -dimethylacrylamide oligomer	62
2.2.3.2.	Initiator fragments end-capped acrylic acid oligomer	63
2.2.4.	Synthesis of initiator fragments end-capped oligomers by using VA-086 as a radical initiator	64
2.2.4.1.	Initiator fragments [2-methyl- <i>N</i> -(2-hydroxyethyl)propionamide] end-capped <i>N,N</i> -dimethylacrylamide oligomer	64
2.2.5.	Synthesis of initiator fragments end-capped <i>N,N</i> -dimethylacrylamide oligomers by using AIBN as a radical initiator	66

2.2.6.	Preparation of initiator fragments end-capped <i>N,N</i> -dimethylacrylamide oligomers/silica nanocomposites	66
2.3.	Results and discussion	68
2.3.1.	Synthesis and solubility of initiator fragments end-capped oligomers	68
2.3.2.	Preparation and thermal stability of the sulfate ester fragments end-capped oligomers/silica nanocomposites	73
2.3.3.	Preparation and thermal stability of the 2-methyl- <i>N</i> -(2-hydroxyethyl)propionamide fragments end-capped oligomers/silica nanocomposites	81
2.3.4.	Preparation and thermal stability of nitrile fragments end-capped <i>N,N</i> -dimethylacrylamide oligomers/silica nanocomposites	90
2.3.5.	Discussion on the thermal stability of the initiator fragments end-capped oligomers/silica nanocomposites	94
2.4.	Conclusions	102
Chapter 3.	Wettability Control Between Superoleophobic and Superoleophilic Characteristics on the Modified Superhydrophobic Surfaces Treated with Fluoroalkyl End-Capped Vinyltrimethoxysilane Oligomeric Silica/ Poly(styrene-<i>co</i>-butadiene) Nanocomposites : Application to the Separation of Oil and Water	107
3.1.	Introduction	108
3.2.	Experimental	110

3.2.1.	Measurements	110
3.2.2.	Materials	111
3.2.3.	Preparation of the $R_F-(VM-SiO_2)_n-R_F/SBR$ nanocomposites	111
3.2.4.	Preparation of modified glass treated with the $R_F-(VM-SiO_2)_n-R_F/SBR$ nanocomposites by casting method	112
3.3.	Results and discussion	114
3.3.1.	Preparation of the $R_F-(VM-SiO_2)_n-R_F/SBR$ nanocomposites	114
3.3.2.	Surface modification of glass by using the $R_F-(VM-SiO_2)_n-R_F/SBR$ nanocomposites	117
3.3.3.	Separation of the mixture of oil and water and W/O emulsion by using the $R_F-(VM-SiO_2)_n-R_F/SBR$ nanocomposites as a packing material	129
3.4.	Conclusions	134
	Conclusions	139
	Publications	142
	Acknowledgements	144

General Introduction

1. Fluoropolymer

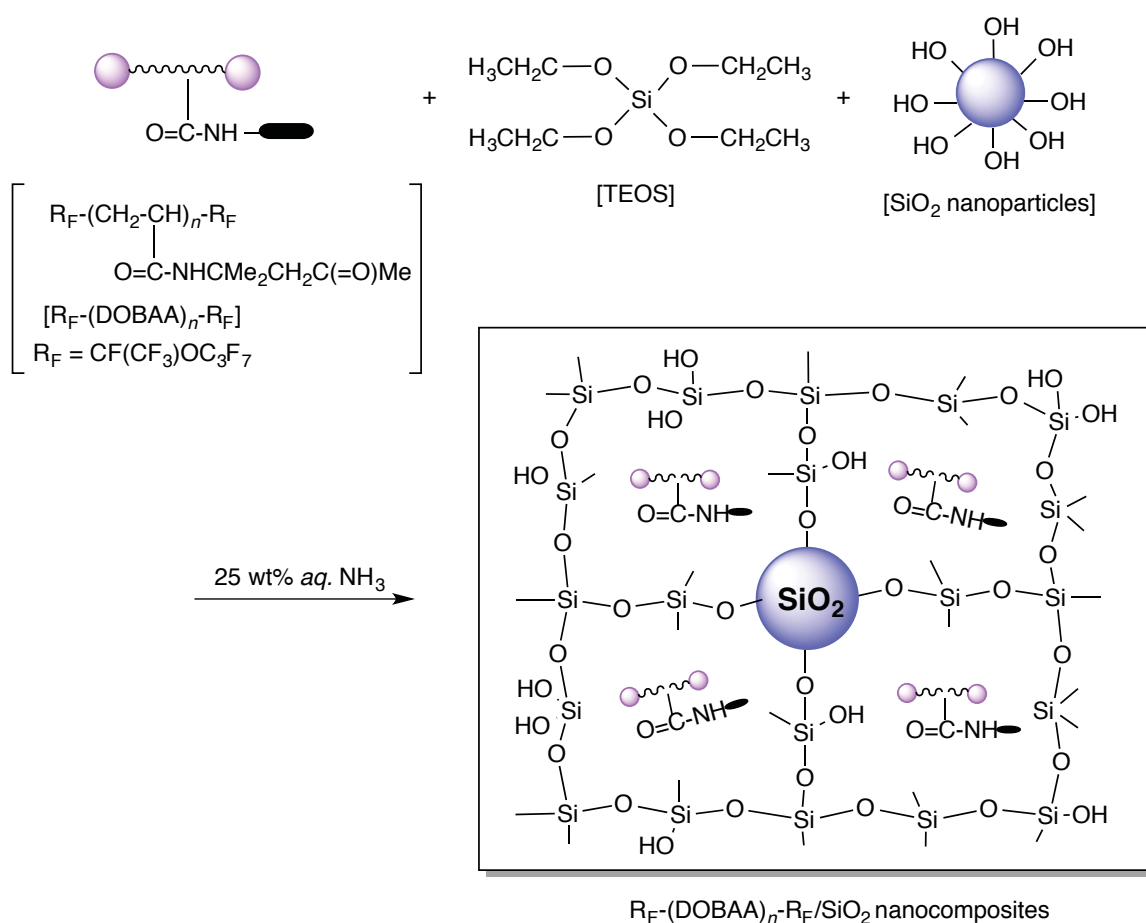
Much attention has been hitherto focused on fluoropolymers, due to exhibiting their excellent properties such as high thermal and oxidative stability, low moisture absorption, weather stability, low flammability, chemical resistance and low surface energies, which cannot be achieved by the corresponding non-fluorinated polymers.^{1~6)} Some of typical fluoropolymers are listed in Table 1.^{7, 8)}

Table 1 Some of typical fluoropolymers

Structure	Name
$\left[\begin{array}{c} \text{F} \quad \text{F} \\ \quad \\ \text{---C---C---} \\ \quad \\ \text{F} \quad \text{F} \end{array} \right]_n$	Poly(tetrafluoroethylene) (PTFE)
$\left[\begin{array}{c} \text{F} \quad \text{H} \\ \quad \\ \text{---C---C---} \\ \quad \\ \text{F} \quad \text{H} \end{array} \right]_n$	Poly(vinylidene fluoride) (PVDF)
$\left[\begin{array}{c} \text{F} \quad \text{F} \quad \text{F} \quad \text{F} \\ \quad \quad \quad \\ \text{---}(\text{C} \text{---} \text{C})\text{---} \text{C} \text{---} \text{C} \text{---} \\ \quad \quad \quad \\ \text{F} \quad \text{F} \quad \text{F} \quad \text{CF}_3 \end{array} \right]_n$	Perfluoroethylene-propylene copolymer (PFEP)
$\left(\begin{array}{c} \text{F} \quad \text{F} \\ \quad \\ \text{---C---C---} \\ \quad \\ \text{O} \quad \text{O} \\ \diagdown \quad / \\ \text{F}_3\text{C} \quad \text{CF}_3 \end{array} \right)_x \text{---} (\text{CF}_2\text{---CF}_2)_y$	Teflon AF [®]
$\left(\begin{array}{c} \text{F}_2\text{C---F}_2\text{C} \quad \text{CF}_2\text{---CF}_2 \\ \diagdown \quad / \\ \text{CF---FC} \\ \quad \\ \text{O} \quad \text{CF}_2 \\ \\ \text{F}_2 \end{array} \right)_n$	Cytop [®]

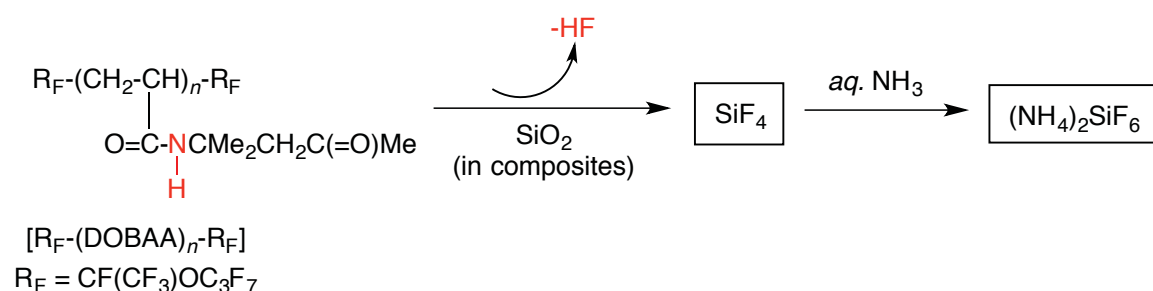
In these fluoropolymers, poly(tetrafluoroethylene) (PTFE or Teflon[®]) is one of the most important polymeric materials in the fluorochemical industry, owing to its chemically outstanding resistance and high thermal stability.^{6, 9)} Up to now, there are a wide variety of commercially available products related to the fluoropolymers such as perfluoroethylene-propylene copolymer (PFEP) and poly(vinylidene fluoride) (PVDF). However, these fluoropolymers are poor solubility in organic solvents, limiting their applications into numerous fields.^{10 ~ 12)} The novel amorphous perfluoropolymers such as Teflon AF[®] and cytop[®] have been already developed to improve the solubility of fluoropolymers toward the selected organic solvents.¹¹⁾ From this point of view, it is of much interest to develop fluorinated polymers possessing an excellent solubility toward the traditional organic solvents including water. In fact, two fluoroalkyl end-capped oligomers [$R_F-(M)_n-R_F$; R_F = fluoroalkyl groups; M = radical polymerizable monomers] are attractive functional materials, because these oligomers can exhibit a variety of unique properties such as high solubility toward not only water but also traditional organic solvents, surface-active properties and nanometer size-controlled self-assembled aggregates through the aggregation of terminal fluoroalkyl segments, which cannot be achieved by the corresponding non-fluorinated one.^{13 ~ 16)} Therefore, the developmental viewpoint of new fluorinated functional materials, it is of particular interest to explore the fluoroalkyl end-capped oligomeric nanoparticles possessing a variety of unique characteristics imparted by fluorine.

For example, the fluoroalkyl end-capped *N*-(1,1-dimethyl-3-oxobutyl)acrylamide oligomer/silica nanocomposites $[R_F-(\text{DOBAA})_n-R_F/\text{SiO}_2]$ were prepared by the sol-gel reactions of the corresponding oligomers with tetraethoxysilane under alkaline conditions as shown in Scheme 1.^{17, 18)} Interestingly, the $R_F-(\text{DOBAA})_n-R_F/\text{SiO}_2$ nanocomposites can exhibit no weight loss behavior even after calcination at 800 °C, although the polytetrafluoroethylene (PTFE)/ SiO_2 composites can exhibit a clear weight loss corresponding to the content of PTFE in the composites at around 600 °C.¹⁹⁾



Scheme 1 Preparation of the $R_F-(\text{DOBAA})_n-R_F/\text{SiO}_2$ nanocomposites

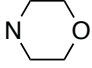
Such no weight loss behavior is due to the formation of ammonium hexafluorosilicate, which would be derived through the dehydrofluorination between the amide protons and fluorines in the oligomer catalyzed by ammonia in the presence of silica nanoparticles as the co-catalyst, and then reacting with silica nanoparticles as shown in Scheme 2.¹⁷⁾



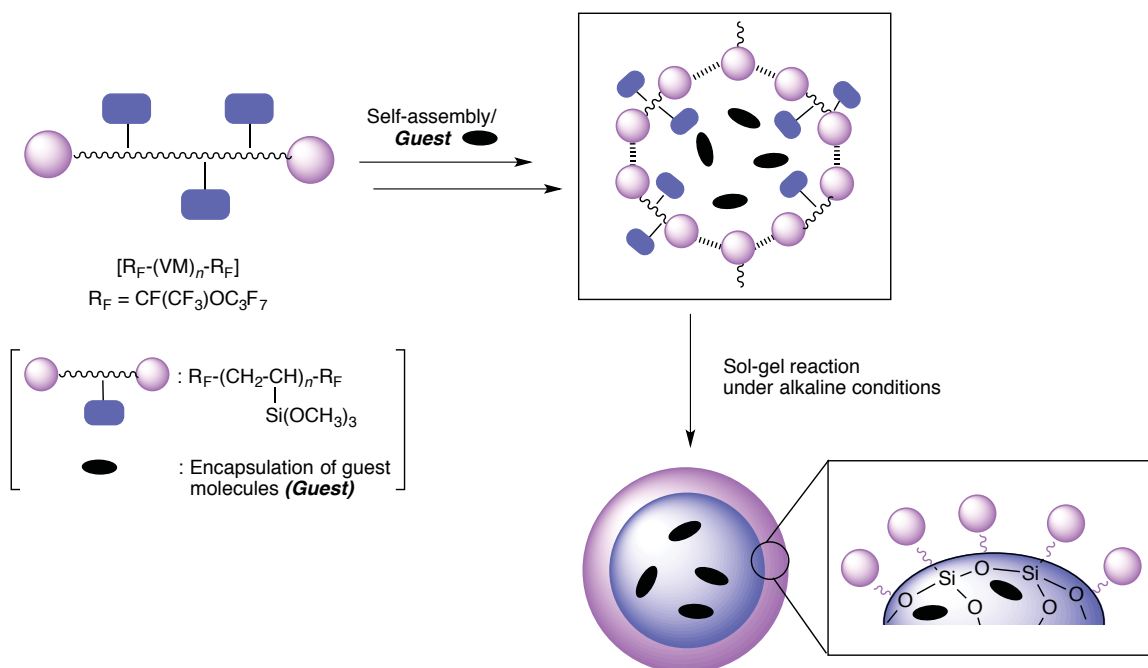
Scheme 2 The formation of ammonium hexafluorosilicate

In this way, fluoroalkyl end-capped oligomers/silica composites can be classified according to their structures into the fluorinated oligomers/silica composites possessing non-flammable and flammable characteristics after calcination at 800 °C, respectively, as shown in Table 2. The fluoroalkyl end-capped oligomers/silica composites containing amido protons and more acidic protons such as sulfo groups can exhibit a non-flammable characteristic even after calcination at 800 °C through the formation of ammonium hexafluorosilicate during nanocomposite reactions.¹⁷⁾

Table 2 A variety of fluoroalkyl end-capped oligomers/SiO₂ nanocomposites possessing flammable and non-flammable characteristics after calcination at 800 °C [R_F = CF(CF₃)OC₃F₇]

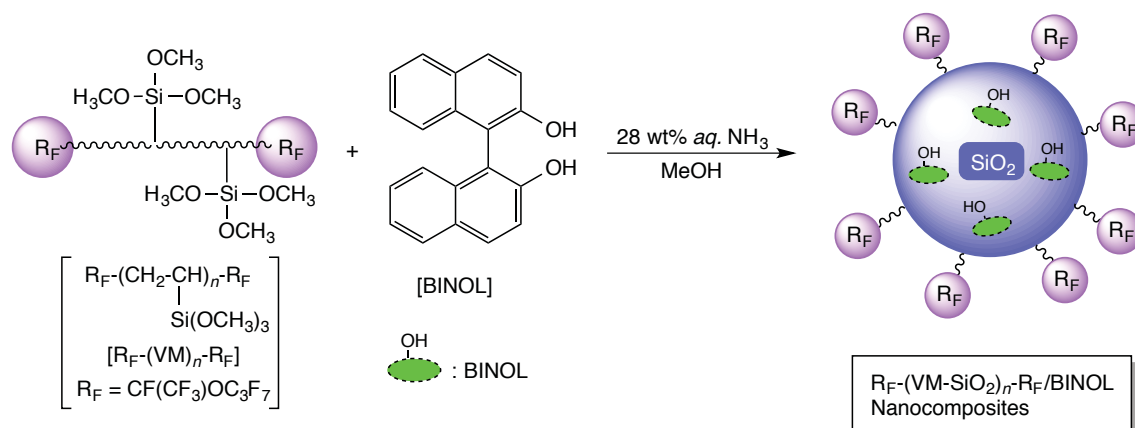
Property	Structure		Name
Flammable	$\begin{array}{c} \text{R}_F\text{-(CH}_2\text{-CH)}_n\text{-R}_F \\ \\ \text{O=C-R} \end{array}$	R = NMe ₂	[R _F -(DMAA) _n -R _F]
		OH	[R _F -(ACA) _n -R _F]
			[R _F -(ACMO) _n -R _F]
		N ⁺ H ₂ CMe ₂ CHSO ₄ ⁻	[R _F -(AMPS) _n -R _F]
		R' = OH	[R _F -(MACA) _n -R _F]
Non-flammable	$\begin{array}{c} \text{R}_F\text{-(CH}_2\text{-CH)}_n\text{-R}_F \\ \\ \text{O=C-R} \end{array}$	R = NHMe ₂ CHC(=O)Me	[R _F -(DOBAA) _n -R _F]
		NHCHMe ₂	[R _F -(NIPAM) _n -R _F]
		R = OCH ₂ CHSO ₃ H	[R _F -(MES) _n -R _F]
		$\begin{array}{c} \text{R}_F\text{-(CH}_2\text{-CMe)}_x\text{-(CH}_2\text{C)}_y\text{-R}_F \\ \qquad \qquad \\ \text{O=C-OH} \quad \text{O=C-OH} \\ \text{CF}_3 \\ x : y = 51 : 49 \end{array}$	[R _F -(MACA) _x -(TFMA) _y -R _F]

On the other hand, two fluoroalkyl end-capped vinyltrimethoxysilane oligomers [R_F-(VM)_n-R_F: R_F-(CH₂CHSi(OMe)₃)_n-R_F; n = 2, 3; R_F = fluoroalkyl groups] are of particular interest due to exhibiting the higher surface active characteristic, compared with that of the traditional monomeric fluoroalkyl end-capped silane coupling agents [R_F-CH₂CH₂Si(OMe)₃; R_F = fluoroalkyl group].²⁰⁾ These fluoroalkyl end-capped oligomers can undergo the sol-gel reactions under alkaline conditions to produce the fluoroalkyl end-capped oligomeric silica nanoparticles [R_F-(VM-SiO₂)_n-R_F] as shown in Scheme 3.²¹⁾ Especially, these R_F-(VM-SiO₂)_n-R_F oligomeric nanoparticles exhibit a good dispersibility and stability in organic media.²¹⁾ The modified glass surface treated with the



Scheme 4 The formation of self-assembled molecular aggregates of the $R_F-(VM)_n-R_F$ oligomers and the formation of the $R_F-(VM-SiO_2)_n-R_F$ oligomeric nanocomposites - encapsulated guest molecules through the sol-gel reactions under alkaline conditions

For example, novel cross-linked fluoroalkyl end-capped vinyltrimethoxysilane oligomeric nanoparticles $[R_F-(VM-SiO_2)_n-R_F]$ - encapsulated 1,1'-bi(2-naphthol) (BINOL) were prepared by the sol-gel reaction of fluoroalkyl end-capped vinyltrimethoxysilane oligomer in the presence of BINOL under alkaline conditions as shown in Scheme 5.²²⁾



Scheme 5 Preparation of fluoroalkyl end-capped vinyltrimethoxysilane oligomeric nanoparticles $[\text{R}_F-(\text{VM-SiO}_2)_n-\text{R}_F]$ - encapsulated 1,1'-bi(2-naphthol) (BINOL)

Unexpectedly, the $\text{R}_F-(\text{VM-SiO}_2)_n-\text{R}_F/\text{BINOL}$ nanocomposites were found to exhibit no weight loss even after calcination at 800°C corresponding to the content of BINOL in the nanocomposites. Therefore, from the developmental viewpoint of new fluorinated functional materials, it will become of particular interest to study on the encapsulation of not only low molecular weight aromatic compound such as BINOL but also others organic compounds into the fluoroalkyl end-capped oligomeric composite cores.

2. Rubbers

Rubbers or elastomers are a special class of polymeric materials such as natural rubber (NR), butadiene rubber (BR), (acrylo)nitrile-butadiene rubber (NBR), styrene-butadiene rubber (SBR), ethylene-propylene-diene monomer (EPDM) and silicone rubber.^{23 ~ 26)}

These rubbers are the most commonly used in industrial fields such as automotives,

packaging, aircraft, electrical and coating industry. Among the numerous rubbers, butadienes as raw material such as NBR and SBR have been widely used in automotive, civil construction, plastic and footwear products due to the unique properties.^{27, 28)}

NBR or poly(acrylonitrile-*co*-butadiene) is the copolymer which consists of butadiene and acrylonitrile, while SBR or poly(styrene-*co*-butadiene) is copolymer which consists of butadiene and styrene. The chemical structures of both copolymers are illustrated in Figure 1.^{29 ~ 31)}

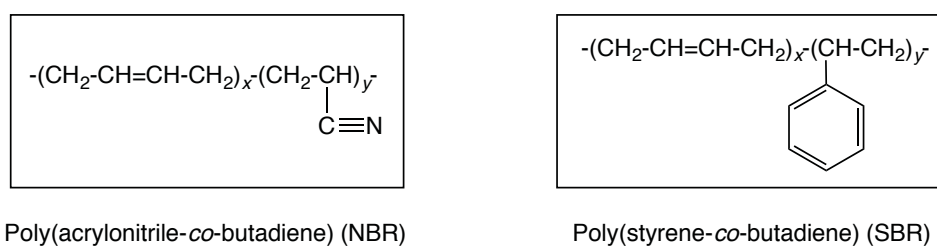


Figure 1 Chemical structures of poly(acrylonitrile-*co*-butadiene) (NBR) and poly(styrene-*co*-butadiene) (SBR)

The significantly different structures between NBR and SBR, NBR possesses the aliphatic electron withdrawing acrylonitrile ($-\text{CN}$) groups and SBR contains the phenyl groups on the polymer main chain, respectively.³²⁾ Especially, NBR bearing the acrylonitrile units can provide good oil-resistance ability toward a variety of solvents, while SBR has poor oil-resistance ability due to the presence of benzene ring on the polymer main chain. In addition, both of NBR and SBR have poor ozone- and weather-resistance due to the presence of the highly unsaturated units on the polymer

main chain.^{23, 30, 32)} Therefore, it is deeply desirable to explore novel rubber derivatives possessing an excellent oil-resistance ability. From this point of view, the nanocomposite reaction of such traditional rubbers with the fluoroalkyl end-capped oligomers are of particular interest, in order to improve the oil-resistance ability of the parent rubbers, because the fluorinated polymers have in general good oil repellent characteristic.

3. Development of rubbers/inorganic composites

“Composites” or “organic/inorganic hybrid materials” have been widely used in a variety of applicable fields such as cosmetics, agriculture, food packaging, textiles, medicine, semiconductor devices, catalysis and fire-resistant hybrid membranes.^{33 ~ 36)} Polymeric composites which consist of inorganic nanoparticles and organic polymers can exhibit the improved performance such as mechanical, stiffness, strength, and flame retardancy, compared to the original polymers.^{37 ~ 39)} Among the traditional organic polymers, rubbers are of the great interest owing to good heat resistance, ease of deformation at ambient temperatures and high flexibility.^{40, 41)} There have been hitherto numerous studies on the fabrication of rubber/inorganic composites by the incorporation of fillers such as layered silicate clays, carbon nanotube (CNT), carbon black (CB), graphene oxide, silica, and titanium dioxide (TiO₂) into rubbers. In fact, several rubber/inorganic composites have been already reported as shown in Table 3.^{42 ~ 50)}

Table 3 Some properties of rubber/inorganic composite materials

Rubber compounds	Inorganic materials	Properties	Ref.
BR ^{a)}	SiO ₂	Enhancement of mechanical properties	44
NR/CR ^{b)} blends	SiO ₂	Enhancement of thermal stability, modulus and tensile strength	45
SBR	SiO ₂	High wet skid resistance and low rolling resistance	46
NR ^{c)}	TiO ₂	Strong antibacterial and good resistance of UV radiation	47
SBR	HNT ^{d)}	Enhancement of mechanical properties and solvent resistance	48
NBR, SBR	CB ^{e)}	Low swelling oil values and increasing compression set	49
NR, NBR, SBR	Clay	Good flame retardance	50

a) BR: Butadiene rubber

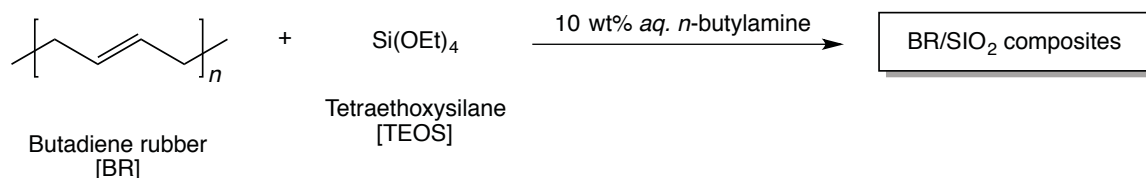
b) CR: Chloroprene rubber

c) NR: Natural rubber

d) HNT: Halloysite nanotube

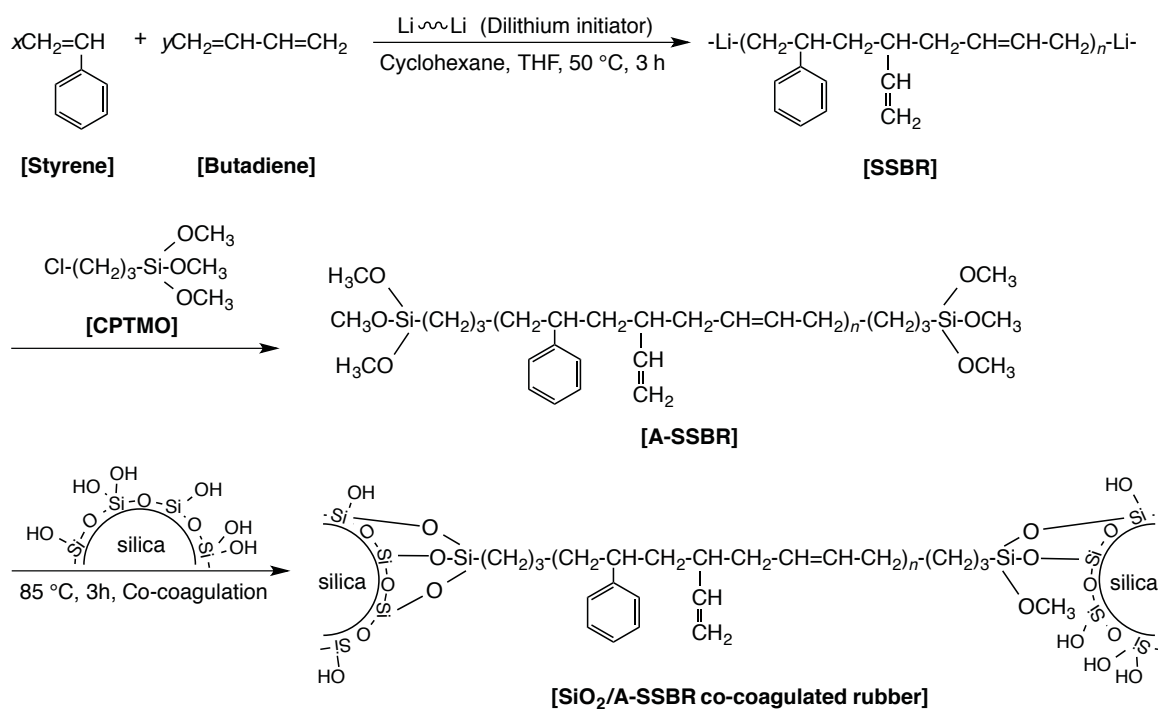
e) CB: Carbon black

Especially, there have been of particular interest in rubber composites materials containing silica particles from the applicable point of view in the industrial areas, because of their improved thermal stability, mechanical properties, gas barrier properties, oil-resistance and the low rolling resistance.^{51 ~ 53)} For example, Ikeda et al. reported on the fabrication of cross-linked butadiene rubber (BR)/SiO₂ composites by the sol-gel reaction of tetraethoxysilane (TEOS) in the presence of cross-linked BR under alkaline conditions as shown in Scheme 6.⁴⁴⁾



Scheme 6 Preparation of cross-linked butadiene rubber/silica (BR/SiO₂) composites

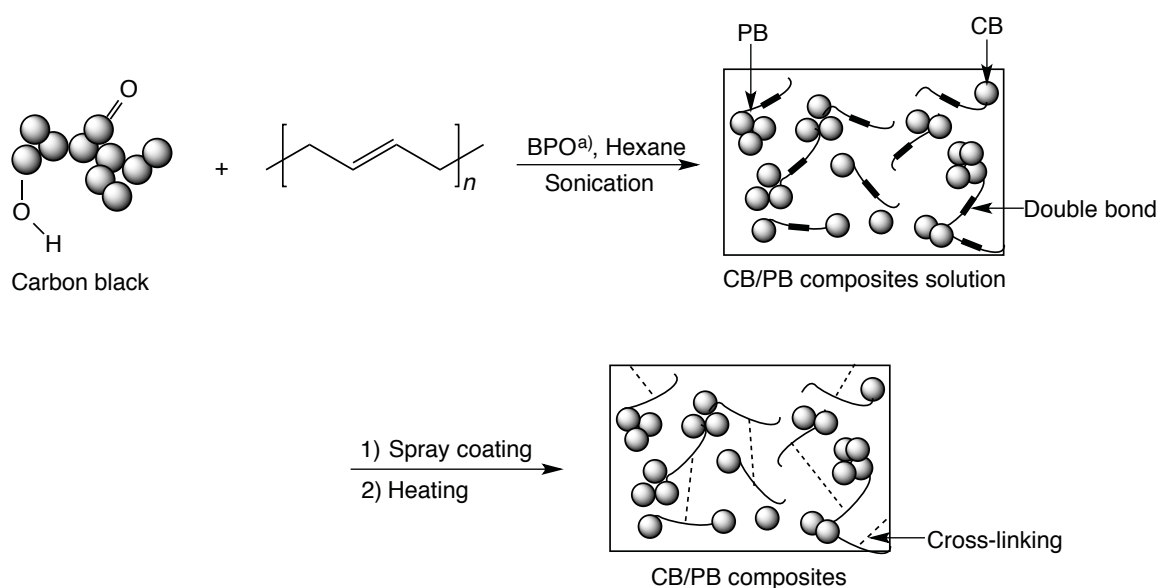
Liu et al. reported on the synthesis of styrene-butadiene rubber with alkoxy-silane-functionalization at two ends of macromolecular chains (A-SSBR) by anionic polymerization with dilithium derivative as an initiator under the solution-polymerization technique as shown in Scheme 7.⁴⁶⁾



Scheme 7 The synthesis process for A-SSBR and condensation reaction between A-SSBR and silica

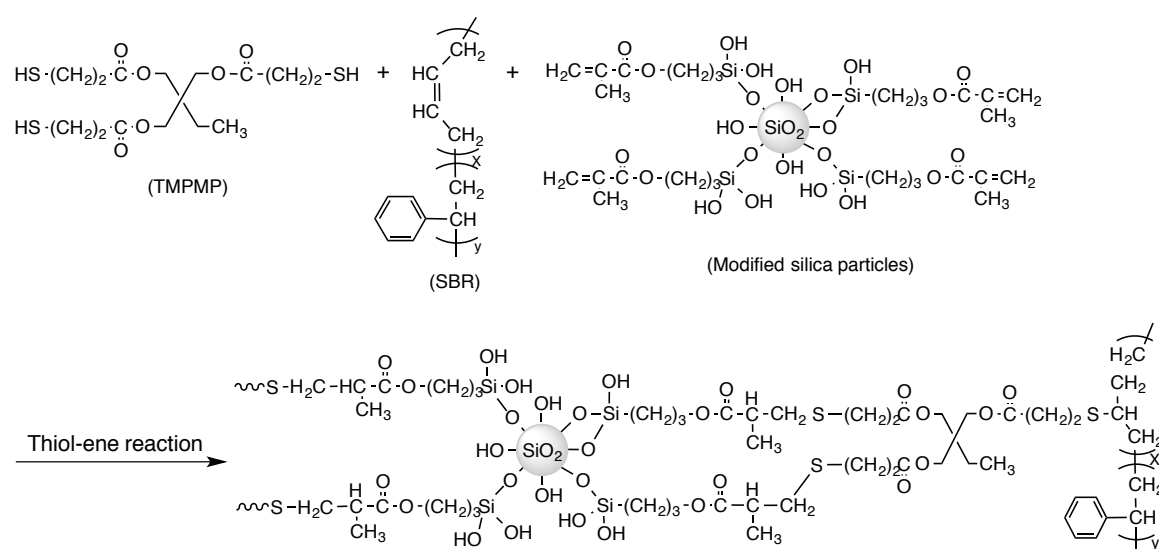
The presence of modified silica into BR and SBR composites can improve the mechanical properties and low rolling resistance due to the good dispersibility of silica in the rubber matrix.^{44, 46)}

Hitherto, rubber/inorganic composite materials have been considerably studied and have been successfully applied to automotive industry.^{54, 55)} With the development of the application of rubber composites, some special properties such as superhydrophobicity are required for fabrication of new composite materials. For example, Hu et al. reported that the fabrication of carbon black (CB)/polybutadiene (PB) elastomeric composites can be prepared by suspension polymerization as shown in Scheme 8. The surface modification of CB/PB composites on a rubber substrate by spray coating technique can exhibit the superhydrophobic property on the surface, because the water contact angle is 171 degree.⁵⁶⁾



Scheme 8 The fabrication of CB/PB composite coating by spraying followed by thermal curing
a) BPO: benzoyl peroxide

Moreover, as shown in Scheme 9, Ye et al. reported that the modified SBR surfaces with silica/ γ -methacryloxypropyltrimethoxysilane (γ -MPTMS) particles in the presence of trimethylolpropane tris(3-mercaptopropionate) (TMPMP) can be prepared by thiol-ene click reaction. The obtained modified SBR films with SiO_2/γ -MPTMS particles can exhibit the superhydrophobic characteristic (water contact angle value: 152°).⁵⁷⁾



Scheme 9 Preparation of hydrophobic modification of styrene-butadiene rubber (SBR) with silica nanoparticles

In this way, rubber/silica composites possessing not only the improved mechanical properties but also the special requirements properties such as the superhydrophobicity will become mostly applicable into the tire industry. However, studies on the rubber/silica composites possessing fluorines or fluoroalkyl groups have been hitherto very limited. Therefore, from the developmental viewpoints of novel fluorinated functional polymeric materials, it is of particular interest to explore the novel fluorinated polymers/rubber

compounds such as NBR and SBR composites possessing not only a surface-active characteristic imparted by fluorine but also unique property related to rubber compounds containing nitrile and styrene moieties.

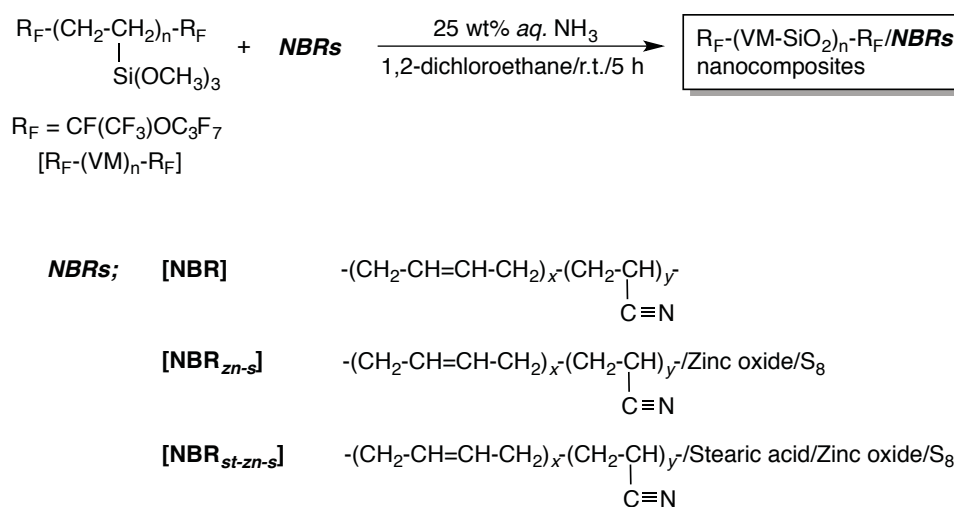
4. Thesis outline

As indicated above, fluoroalkyl end-capped vinyltrimethoxysilane oligomeric silica $[R_F-(VM-SiO_2)_n-R_F]/BINOL$ nanocomposites have been already prepared by the sol-gel reactions of the corresponding fluoroalkyl end-capped vinyltrimethoxysilane oligomer in the presence of BINOL as a low molecular weight compound under alkaline conditions. The $R_F-(VM-SiO_2)_n-R_F/BINOL$ nanocomposites can also exhibit nonflammable characteristic even after calcination at 800 °C through the architecture of rigid BINOL-containing silica gel matrices and the formation of ammonium hexafluorosilicate during the sol-gel process.²²⁾ Therefore, from the developmental viewpoints of new fluorinated functional materials, it is of particular interest to explore the novel fluorinated oligomeric silica nanocomposites impart by the macromolecular compounds such as poly(acrylonitrile-*co*-butadiene) (NBR) and poly(styrene-*co*-butadiene) (SBR).

In this study, preparation and applications of fluoroalkyl end-capped vinyltrimethoxysilane oligomeric silica nanocomposites - encapsulated macromolecular compounds such as poly(acrylonitrile-*co*-butadiene) and poly(styrene-*co*-butadiene) will

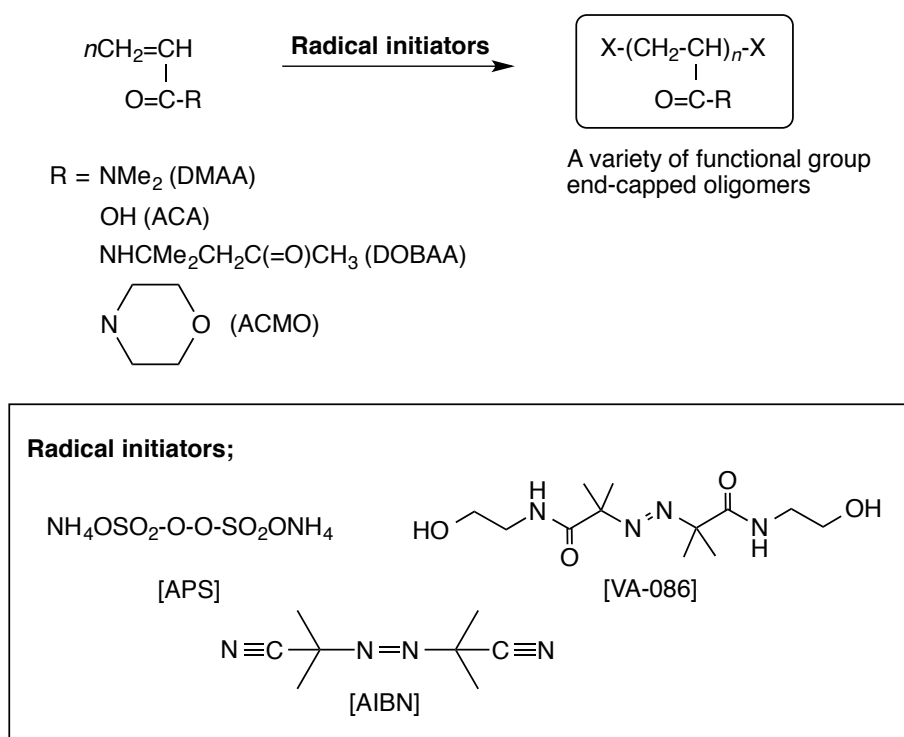
be described. In addition, preparation and properties of the initiator fragments end-capped oligomers by using a variety of radical initiators are also discussed, compared with those of the corresponding oligomers/silica nanocomposites in order to clarify the thermal stability of the nitrile units-containing oligomers in the composite cores.

In chapter 1, preparation and thermal stability of fluoroalkyl end-capped vinyltrimethoxysilane oligomeric silica/poly(acrylonitrile-*co*-butadiene) (NBR) nanocomposites containing nitrile segments are described (see Scheme 10). Not only the NBR but also the NBR containing stearic acid, zinc oxide and sulfur (NBR_{st-zn-s}), and the NBR containing zinc oxide and sulfur (NBR_{zn-s}) are also encapsulated into the fluoroalkyl end-capped vinyltrimethoxysilane oligomeric silica nanocomposite cores. Thermal stability and surface modification of these nanocomposites are also described including their application to the separation of oil/water.



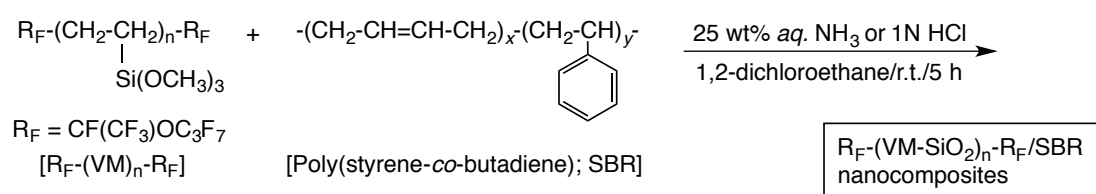
Scheme 10 Preparation of fluoroalkyl end-capped vinyltrimethoxysilane oligomeric silica/NBRs nanocomposites

In chapter 2, synthesis of a variety of initiator fragments end-capped oligomers by the oligomerizations of the corresponding monomer initiated by a variety of radical initiator containing not only nitrile groups but also 2-methyl-*N*-(2-hydroxyethyl)propionamide and sulfate ester units is described (see Scheme 11). In addition, thermal stability of the obtained initiator fragments end-capped oligomeric nanocomposites is also discussed, compared with those of the corresponding oligomers/silica nanocomposites, in order to clarify the thermal stability of the nitrile units-containing oligomer in the fluorinated oligomeric silica nanocomposites cores.



Scheme 11 Synthesis of initiator fragments end-capped oligomers

In chapter 3, preparation and surface modification of glass by using fluoroalkyl end-capped vinyltrimethoxysilane oligomeric silica/poly(styrene-*co*-butadiene) (SBR) nanocomposites are described (see Scheme 12). In this chapter, wettability control between the superoleophobic and superoleophilic characteristics on the modified surface is also described including the application to the separation of oil/water.



Scheme 12 Preparation of fluoroalkyl end-capped vinyltrimethoxysilane oligomeric silica/SBR nanocomposites

References

- 1) K. Johns and G. Stead, *J. Fluorine Chem.*, **104**, 5 (2000).
- 2) B. Ameduri and B. Boutevin (Eds.), *Well-Architected Fluoropolymers: Synthesis, Properties and Applications*, Plenum Press, New York (1999).
- 3) B. Ameduri and H. Sawada (Eds.), *Fluorinated polymers: Volume 1, "Synthesis, Properties, Processing and Simulation"*. Cambridge, RSC, UK (2016).
- 4) B. Ameduri and H. Sawada (Eds.), *Fluorinated polymers: Volume 2, "Application"*. Cambridge, RSC, UK (2016)
- 5) P. Graham, M. Stone, A. Thorpe, T. G. Nevell, and J. Tsibouklis, *J. Fluorine Chem.*, **104**, 529 (2000).
- 6) S. Lee, J.-S. Park, and T. R. Lee, *Langmuir*, **24**, 48117 (2008).
- 7) M. Kutz (Ed), *Introduction of Fluoropolymers*, Elsevier (2011).
- 8) H. Teng, *Appl. Sci.*, **2**, 496 (2012).
- 9) J. P. Badey, E. Espuche, Y. Jugnet, B. Chabert, and T. M. Duc, *Int. J. Adhesion and Adhesives*, **16**, 173 (1996).
- 10) J. Scheirs (Ed). *Modern Fluoropolymer*, John Wiley & Sons, New York (1997).
- 11) B. Ameduri, *Fluorinated (co)polymers: Synthesis, Properties, and Applications*, Encyclopedia of Polymer Science and Technology, John Wiley & Sons, New York (2012).

- 12) Y. Wang, M. Wang, and X. Ge, *Langmuir*, **30**, 10840 (2014).
- 13) H. Sawada, *J. Fluorine Chem.*, **101**, 315 (2000).
- 14) H. Sawada, *Chem. Rev.*, **96**, 1779 (1996).
- 15) H. Sawada, *Polym. J.*, **39**, 637 (2007).
- 16) H. Sawada, *Polym. Chem.*, **3**, 46 (2012).
- 17) H. Sawada, T. Tashima, H. Kakehi, Y. Nishiyama, M. Kikuchi, M. Miura, Y. Sato, and N. Isu, *Polym. J.*, **42**, 167 (2010).
- 18) H. Sawada, T. Tashima, Y. Nishiyama, M. Kikuchi, G. Kostov, Y. Goto, and B. Ameduri, *Macromolecules*, **44**, 1114 (2011).
- 19) T. S. Light, L. F. Fitzpatrick, and J. P. Phaneuf, *Anal. Chem.*, **37**, 79 (1965).
- 20) T. Kawase, T. Fuj, M. Minagawa, H. Sawada, T. Matumoto, and M. Nakayama, *J. Adhes. Sci. Technol.*, **10**, 1031 (1996).
- 21) H. Sawada, T. Suzuki, H. Takashima, and K. Takishita, *Colloid Polym. Sci.*, **286**, 1569 (2008).
- 22) H. Sawada, Y. Matsuki, Y. Goto, S. Kodama, M. Sugiya, and Y. Nishiyama, *Bull. Chem. Soc. Jpn.*, **83**, 75 (2010).
- 23) “*Rubber Chemistry*” Matador rubber (2007).
- 24) Richard B. Simpson, “*Rubber Basics*” Rapra Technology Limited, United Kingdom (2002).
- 25) L. T. Vo, S. H. Anastasiadis, and E. P. Giannelis, *Macromolecules*, **44**, 6162 (2011).

- 26) D. Lopes, M. J. Ferreira, R. Russo, and J. M. Dias, *J. Clean. Prod.*, **92**, 230 (2015).
- 27) K. G. Gatos and J. Karger-Kocsis, “*Rubber-Clay Nanocomposites Based On Nitrile Rubber*” Science, Technology, and Applications, 1st Ed. (2011).
- 28) M. Frounchi, M. Mehrabzadeh, and M. Parvary, *Polym. Int.* **49**, 163 (2000).
- 29) R. Sreeja, S. Najidha, S. J. Remya, P. Predeep, M. Mazur, and P. D. Sharna, *Polymer*, **47(2)**, 617 (2006).
- 30) S.-S. Choi and S.-H. Ha, *J. Ind. Eng. Chem.* **16**, 238 (2010).
- 31) W. Du, H. Zou, M. Tian, L. Zhang, and W. Wang, *Polym. Adv. Technol.* **23**, 1029 (2012).
- 32) Y. Changjie, Q. Zhang, G. Junwei, Z. Junping, S. Youqiang, and W. Yuhang, *J. Polym. Res.* **18**, 2487 (2011).
- 33) S. Thomas and R. Stephen (Eds), *Rubber Nanocomposites: Preparation, Properties, and Applications*, Wiley, Singapore (2010).
- 34) S. Kango, S. Kalia, A. Celli, J. Njuguna, Y. Habibi, and R. Kumar, *Prog. Polym. Sci.*, **38**, 1232 (2013).
- 35) H. Zou, S. Wu, and J. Shen, *Chem. Rev.*, **108**, 3893 (2008).
- 36) J. Hu, M. Chen, and L. Wu, *Polym. Chem.*, **2**, 760 (2011).
- 37) J. Wen and G. L. Wilkes, *Chem. Mater.*, **8**, 1667 (1996).
- 38) D. R. Paul and L. M. Robeson, *Polymer*, **49**, 3187 (2008).

- 39) X. Zhao, L. Lv, B. Pan, W. Zhang, S. Zhang, and Q. Zhang, *Chem. Eng. J.*, **170**, 381 (2011).
- 40) L. R. G. Treloar (Ed), *The Physics of Rubber Elasticity*, Oxford University Press Inc., New York (2005).
- 41) D. G. Pagageorgiou, I. A. Kinloch, and R. J. Young, *Carbon*, **95**, 460 (2015).
- 42) S. Varghese and J. Karger-Kocsis, *Polymer*, **44**, 4921 (2003).
- 43) X. Liu, W. Kuang, and B. Guo, *Polymer*, **56**, 553 (2015).
- 44) Y. Ikeda and S. Kohjiya, *Polymer*, **38**, 4417 (1997).
- 45) B. P. Kapgate and C. Das, *RSC Adv.*, **4**, 58816 (2014).
- 46) X. Liu, S. Zhao, Z. Zhang, X. Li, and Y. Bai, *Polymer*, **55**, 1964 (2014).
- 47) B. Seentrakoon, B. Junhasavasdikul, and W. Chavasiri, *Polym. Degrad. Stab.*, **98**, 566 (2013).
- 48) Z. Jia, T. Xu, S. Yang, Y. Luo, and D. Jia, *Polym. Test.*, **54**, 29 (2016).
- 49) A. Mostafa, A. Abouel-Kasem, M. R. Bayoumi, and M. G. El-Sebaie, *Mater. Design*, **30**, 1561 (2009).
- 50) Y. Wu, H. Huang, W. Zhao, H. Zhang, Y. Wang, and L. Zhang, *J. Appl. Polym. Sci.*, **107**, 3318 (2008).
- 51) T. Tancharernrat, G. L. Rempel, and P. Prasassarakich, *Chem. Eng. J.*, **258**, 290 (2014).

- 52) R. Scotti, L. Wahba, M. Crippa, M. D'Arienzo, R. Donetti, N. Santo, and F. Morazzoni, *Soft Matter*, **8**, 2131 (2012).
- 53) Z. Peng, L. X. Kong, S.-D. Li, Y. Chen, and M. F. Huang, *Compos. Sci. Technol.*, **67**, 3130 (2007).
- 54) M. Galimberti (Ed.), *Advanced Elastomers - Technology, Properties and Application "Rubber Clay Nanocomposites"*, John Wiley & Sons, New York (2011).
- 55) A. Zanchel, N. Carli, M. Giovanela, R. N. Brandalise, and J. S. Crespo, *Mater. Design*, **39**, 437 (2012).
- 56) X. Hu, C. Tang, Z. He, H. Shao, K. Xu, J. Mei, and W.-M. Lau, *Small*, **13**, 1602353 (2017).
- 57) Y. Ye, C. Zhang, M. Tian, Z. Du, and J. Mi, *J. Phys. Chem. C*, **119** (36), 20957 (2015).

CHAPTER 1

**Preparation and Thermal Stability of Fluoroalkyl
End-Capped Vinyltrimethoxysilane Oligomeric Silica/
Poly(acrylonitrile-*co*-butadiene) Nanocomposites -
Application to the Separation of Oil and Water**

1.1. Introduction

Poly(acrylonitrile-*co*-butadiene) [NBR or nitrile rubber (cross-linked NBR)] has been hitherto applied to the gaskets and O-rings in fuel systems, due to exhibiting the unique properties such as oil resistance, tensile strength, abrasion resistance, and low-temperature resistance.^{1 ~ 9)} Original nitrile rubber has in general a poor release characteristic toward the numerous substrates.^{10 ~ 16)} Therefore, it is deeply desirable to develop the surface modification of the nitrile rubber derivatives possessing the good release characteristic on the modified surfaces.^{17 ~ 19)} Fluoroalkyl end-capped vinyltrimethoxysilane oligomer [$R_F-(CH_2CHSi(OMe)_3)_n-R_F$; R_F = fluoroalkyl groups; $n = 2, 3$; $R_F-(VM)_n-R_F$] is effective for the surface modification of nitrile rubber to exhibit a good release characteristic on the modified surface.²⁰⁾ $R_F-(VM)_n-R_F$ oligomer is also effective for the encapsulation of low-molecular weight aromatic compounds such as 1,1'-bi(2-naphthol) (BINOL) under alkaline conditions to afford the corresponding fluorinated oligomeric silica nanocomposites-encapsulated BINOL in good isolated yields. Interestingly, the encapsulated BINOL can afford no weight loss behavior in the fluorinated silica gel matrices even after calcination at 800 °C.^{21, 22)} In view of the

development of new NBR derivatives imparted by fluorine, it is of particular interest to prepare novel $R_F-(VM)_n-R_F$ oligomeric nanocomposites-encapsulated NBR through the sol-gel reactions in the presence of NBR under alkaline conditions to provide the corresponding oligomer. This chapter shows that the $R_F-(VM)_n-R_F$ oligomer undergoes the sol-gel reactions in the presence of NBR under alkaline conditions to provide the corresponding fluorinated oligomeric silica nanocomposites-encapsulated NBR. Interestingly, the encapsulated NBR in the fluorinated silica nanocomposite cores thus obtained was found to afford no weight loss behavior even after calcination at 800 °C. More interestingly, these fluorinated silica nanocomposites, which were prepared under cross-linking reaction at 150 °C for 30 min by using NBR containing zinc oxide and S_8 , were applied to the surface modification of glass to provide the superoleophilic/superhydrophobic characteristic on the surfaces. In addition, the fluorinated nanocomposites possessing such surface-active characteristic can be used for the packing material for the column chromatography to separate the mixture of oil and water. These results will be described in this chapter.

1.2. Experimental

1.2.1. Measurements

^1H NMR spectra were recorded using a JEOL JNM-ECA500 (500 MHz) FT NMR SYSTEM (Tokyo, Japan). Molecular weight and copolymer composition of NBR $[-(\text{CH}_2\text{-CH}=\text{CH-CH}_2)_x\text{-(CH}_2\text{-CHCN)}_y\text{-}$; $x : y = 66 : 34$; $M_n = 10780$, $M_w/M_n = 1.12$] were measured using a Shodex DS-4 (pump) and Shodex RI-71 (detector) gel permeation chromatography (Tokyo, Japan) calibrated with polystyrene standard using tetrahydrofuran (THF) as the eluent and ^1H NMR spectra, respectively. Thermal analyses were recorded by raising the temperature around 800 °C (the heating rate: 10 °C/min) under atmospheric conditions by the use of Bruker axis TG-DTA2000SA differential thermobalance (Kanagawa, Japan). Size [number - average diameter (average hydrodynamic diameter)] of nanocomposites was measured by using Otsuka Electronics DLS-7000HL (Tokyo, Japan). Field emission scanning electron micrographs (FE-SEM) were obtained using JEOL JSM-7000F (Tokyo, Japan). Contact angles were measured using a Kyowa Interface Science Drop Master 300 (Saitama, Japan).

Dynamic force microscope (DFM) was recorded by using SII Nano Technology Inc. E-sweep (Chiba, Japan). Optical and fluorescence microscopies were measured by using OLYMPUS Corporation BX51 (Tokyo, Japan).

1.2.2. Materials

Stearic acid and zinc oxide were used as received from New Japan Chemical Co., Ltd. (Osaka, Japan) and Mitsui Mining & Smelting Co., Ltd. (Tokyo, Japan), respectively. Sulfur (S₈) was purchased from Hosoi Chemical Industry Co., Ltd. (Tokyo, Japan). Vinyltrimethoxysilane was used as received from Dow Corning Toray Co., Ltd. (Tokyo, Japan). NBR (Nipol DN3380^{TR}) was used as received from Zeon Corporation (Tokyo, Japan). Fluoroalkyl end-capped vinyltrimethoxysilane oligomer [R_F-(CH₂-CHSi(OMe)₃)_n-R_F: the mixture of dimer and trimer; R_F = CF(CF₃)OC₃F₇] was synthesized by reaction of fluoroalkanoyl peroxide with the corresponding monomer according to the previously reported methods.²³⁾

1.2.3. Preparation of fluoroalkyl end-capped vinyltrimethoxysilane oligomeric silica nanocomposites – encapsulated poly(acrylonitrile-*co*-butadiene) [R_F -(VM-SiO₂)_n- R_F /NBR nanocomposites]

To an 1,2-dichloroethane solution (5.0 ml) containing the fluoroalkyl end-capped vinyltrimethoxysilane oligomer [100 mg; R_F -[CH₂CHSi(OMe)₃]_n- R_F ; R_F -(VM)_n- R_F ; R_F = CF(CF₃)OC₃F₇; n = 2, 3] were added NBR (10 mg) in toluene (35 mg) and 25 % aqueous ammonia solution (1.0 ml). The mixture was stirred with a magnetic stirring bar at room temperature for 5 h. After the solvent was evaporated off, 1,2-dichloroethane was added to the obtained crude products and stirred with magnetic stirring bar at room temperature for 1 day. After centrifugal separation of this solution, the obtained products were washed well with 1,2-dichloroethane several times, and dried in vacuo to afford the expected white powdery product (57 mg). Not only the NBR but also the NBR containing stearic acid (1 wt%), zinc oxide (5 wt%) and S₈ (1 wt%) [NBR_{st-zn-s}] and the NBR containing zinc oxide (5 wt%) and S₈ (1 wt%) [NBR_{zn-s}] were used for preparation of the R_F -(VM-SiO₂)_n- R_F /NBR_{st-zn-s} and R_F -(VM-SiO₂)_n- R_F /NBR_{zn-s} nanocomposites under similar conditions, respectively (see Scheme 1-1).

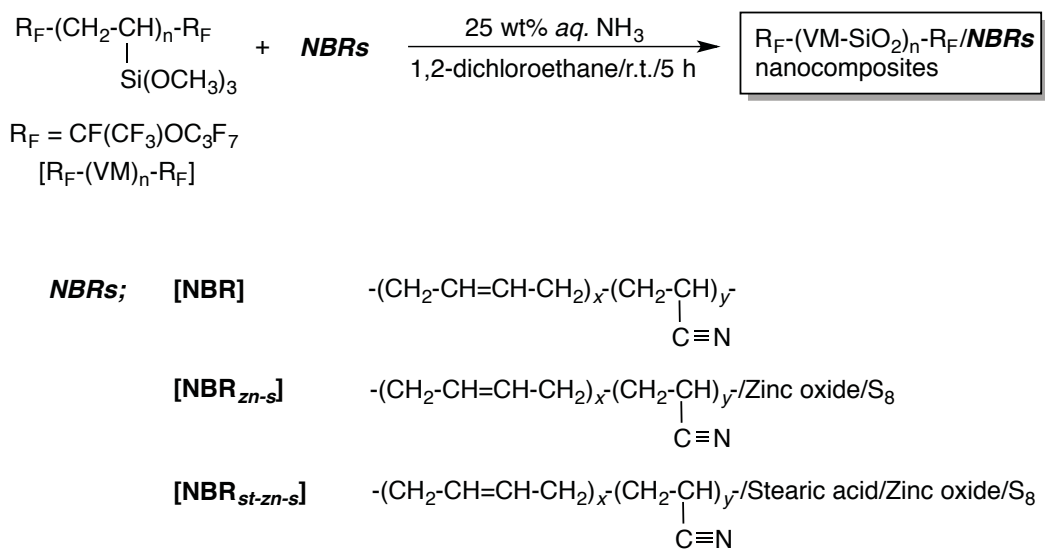
1.2.4. Preparation of modified glass treated with the $R_F-(VM-SiO_2)_n-R_F/NBR$ nanocomposites by casting method

To an 1,2-dichloroethane solution (5.0 ml) containing $R_F-(VM)_n-R_F$ oligomer (100 mg) were added NBR (20 mg) and 25 wt% aqueous ammonia solution (1.0 ml). The mixture was stirred with a magnetic stirring bar at 25 °C for 5 h. The modified glass was prepared by casting the 1,2-dichloroethane solution of the $R_F-(VM-SiO_2)_n-R_F/NBR$ nanocomposites thus obtained on glass plate ($18 \times 18 \text{ mm}^2$ pieces). The solvent was evaporated at room temperature, and dried at room temperature for 1 day under vacuum to afford the modified glass. Not only NBR but also $NBR_{st-zn-s}$ and NBR_{zn-s} were used for the surface modification of glass under similar conditions.

1.3. Results and discussion

1.3.1. Preparation of the fluoroalkyl end-capped vinyltrimethoxysilane oligomeric silica nanocomposites – encapsulated NBR

Fluoroalkyl end-capped vinyltrimethoxysilane oligomer [R_F-(CH₂CHSi(OMe)₃)_n-R_F; R_F = CF(CF₃)OC₃F₇; R_F-(VM)_n-R_F] underwent the sol-gel reaction under alkaline conditions in the presence of NBR to afford the corresponding oligomeric silica nanocomposites – encapsulated NBR [R_F-(VM-SiO₂)_n-R_F/NBR] in 43 ~ 54 % isolated yields as shown in Scheme 1-1 and Table 1-1



Scheme 1-1 Preparation of fluoroalkyl end-capped vinyltrimethoxysilane oligomeric silica/NBRs nanocomposites

Table 1-1 Preparation of the $R_F-(VM-SiO_2)_n-R_F/NBRs$ nanocomposites

Run	$R_F-(VM)_n-R_F$ (mg)	NBRs (mg)	Yield ^{a)} (%)	Size of composites ^{b)} (nm) \pm STD
NBR				
1	100	5	44	67.3 ± 4.3
2	100	10	52	13.8 ± 2.3
3	100	20	50	36.4 ± 3.5
4	100	50	54	41.7 ± 3.9

NBR _{st-zn-s}				
5	100	5	54	89.6 ± 12.6
6	100	10	71	66.5 ± 8.0
7	100	20	63	51.4 ± 11.2

NBR _{zn-s}				
8	100	5	22	80.8 ± 24.2
9	100	10	36	28.7 ± 3.5
10	100	20	24	66.5 ± 8.0

a) Yield was based on $R_F-(VM)_n-R_F$ and NBRs

b) Determined by dynamic light scattering (DLS) measurement in 1,2-dichloroethane

Similarly, NBR containing S_8 , stearic acid and zinc oxide as vulcanizing agent and cure activators, respectively, $[NBR_{st-zn-s}]$ and NBR containing S_8 and zinc oxide $[NBR_{zn-s}]$ were used for the composite reactions to afford the expected $R_F-(VM-SiO_2)_n-R_F/NBR_{st-zn-s}$ and $R_F-(VM-SiO_2)_n-R_F/NBR_{zn-s}$ nanocomposites in 54 ~ 71 % and 22 ~ 36 % isolated yields, respectively. The results are also shown in Scheme 1-1 and Table 1-1. It is well known that stearic acid (RCOOH) interacts with zinc oxide to provide zinc stearate $[(RCOO)_2Zn]$, and the obtained zinc stearate is useful for the preparation of the cross-linked NBR by the use of S_8 as a vulcanization agent.²⁴⁾ Thus, the

$R_F-(VM-SiO_2)_n-R_F/NBR_{st-zn-s}$ nanocomposites would be obtained in higher isolated yields than those of other nanocomposites under such conditions.

The obtained $R_F-(VM-SiO_2)_n-R_F/NBR$ nanocomposites were found to exhibit a good dispersibility and stability toward the traditional organic solvents such as methanol, ethanol, 2-propanol, tetrahydrofuran and 1,2-dichloroethane except for water. Thus, the size of these composites in 1,2-dichloroethane was studied by the use of dynamic light-scattering (DLS) measurements at 20 °C, and the results are also illustrated in Table 1-1. Table 1-1 shows that these fluorinated composites are nanometer size-controlled very fine particles from 14 to 90 nm.

In order to clarify the formation of fluorinated nanocomposite particles, the field emission scanning electron micrograph (FE-SEM) of well-dispersed methanol solutions (or mixed solutions of 2-propanol/methanol (50/50: vol/vol)) of the $R_F-(VM-SiO_2)_n-R_F/NBR$, the $R_F-(VM-SiO_2)_n-R_F/NBR_{zn-s}$, and the $R_F-(VM-SiO_2)_n-R_F/NBR_{st-zn-s}$ nanocomposites before and after heating at 150 °C for 30 min were measured, and the results were shown in Figs. 1-1 ~ 1-3.

Electron micrographs also show that these fluorinated composites are very fine nanoparticles with a mean diameter of 53 nm [Fig. 1-1-(A)], 54 nm [Fig. 1-2-(A)] and

71 nm [Fig. 1-3-(A)], respectively. The similar size values as those (14, 67 and 29 nm) of DLS were obtained in FE-SEM measurements. The slight increase of the sizes of the $R_F-(VM-SiO_2)_n-R_F/NBR$ nanocomposites and the $R_F-(VM-SiO_2)_n-R_F/NBR_{st-zn-s}$ nanocomposites from 53 ~ 54 to 66 ~ 77 nm was observed after the thermal treatment of these composites at 150 °C for 30 min (see Figs. 1-1 and 1-2). On the other hand, the effective increase of the size of the $R_F-(VM-SiO_2)_n-R_F/NBR_{zn-s}$ nanocomposites from 71 to 463 nm was observed under similar conditions, indicating that the cross-linking reaction should proceed rapidly to afford the corresponding fluorinated nanocomposites with increasing their particle size.

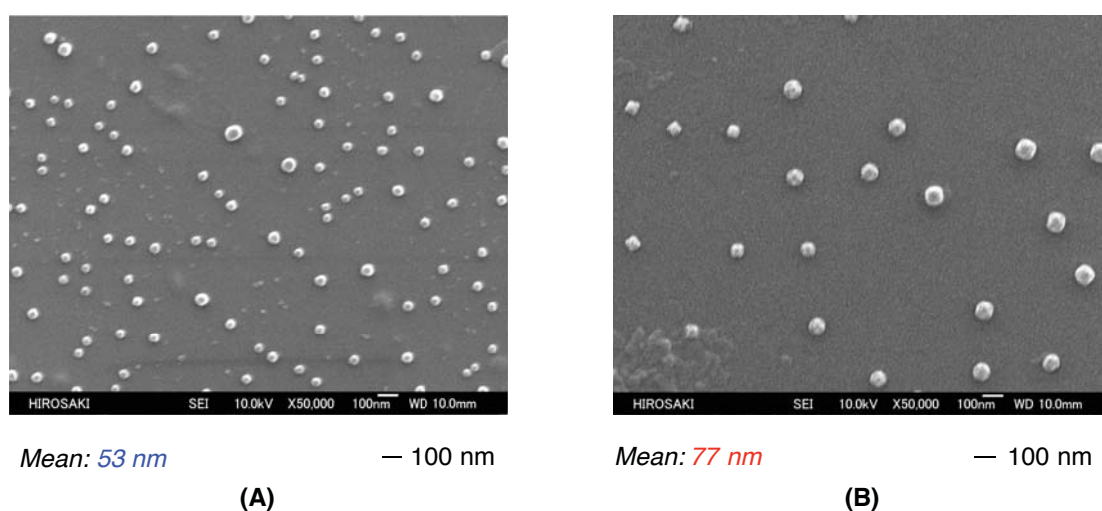


Fig. 1-1 FE-SEM (Field Emission Scanning Electron Microscopy) images of the $R_F-(VM-SiO_2)_n-R_F/NBR$ nanocomposites (Run 2 in Table 1-1) before (A) and after (B) heating at 150 °C for 30 min in methanol solutions

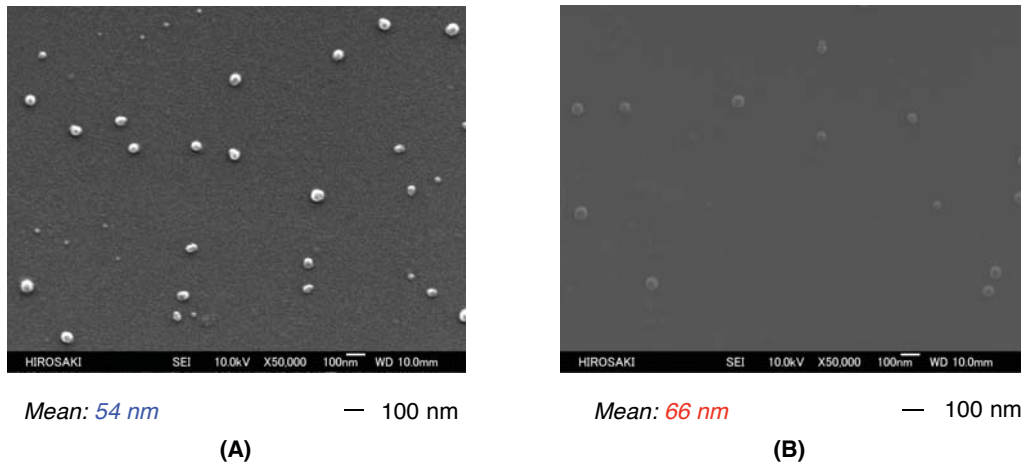


Fig. 1-2 FE-SEM (Field Emission Scanning Electron Microscopy) images of the $R_F-(VM-SiO_2)_n-R_F/NBR_{st-zn-s}$ nanocomposites (Run 6 in Table 1-1) before (A) and after (B) cross-linking reaction at 150 °C for 30 min in the mixture of methanol and 2-propanol solutions (50/50 vol/vol)

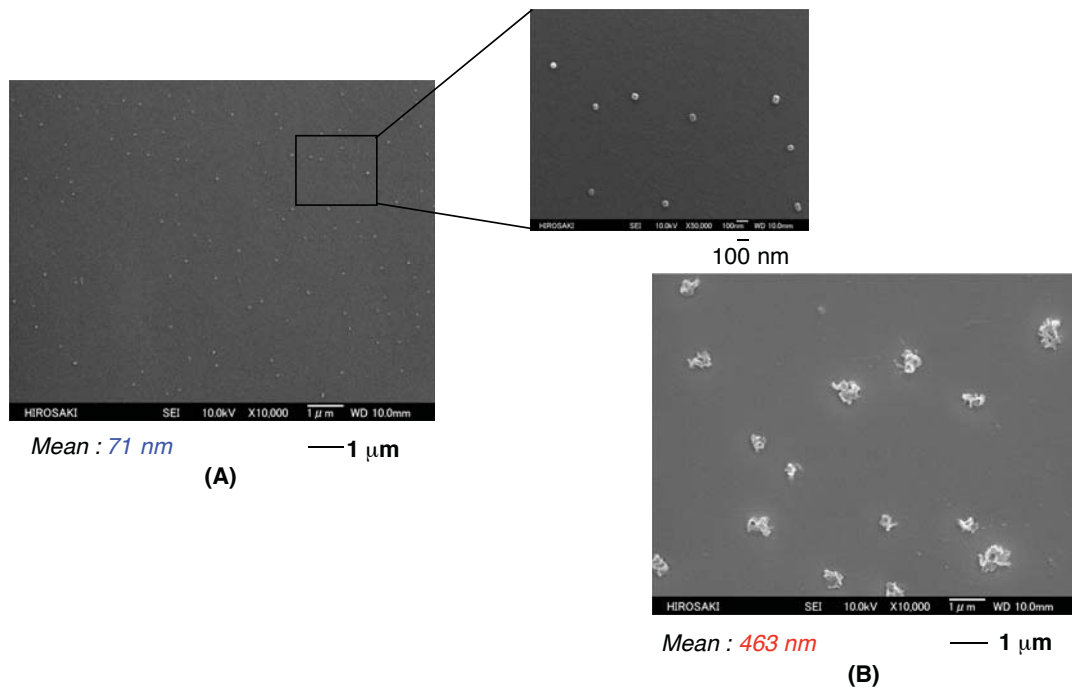


Fig. 1-3 FE-SEM (Field Emission Scanning Electron Microscopy) images of the $R_F-(VM-SiO_2)_n-R_F/NBR_{zn-s}$ nanocomposites (Run 9 in Table 1-1) before (A) and after (B) cross-linking reaction at 150 °C for 30 min in methanol solutions

1.3.2. Thermal stability of the fluoroalkyl end-capped vinyltrimethoxysilane oligomeric silica nanocomposites - encapsulated NBR

Thermal stability of the $R_F-(VM-SiO_2)_n-R_F/NBR$, the $R_F-(VM-SiO_2)_n-R_F/NBR_{zn-s}$ and the $R_F-(VM-SiO_2)_n-R_F/NBR_{st-zn-s}$ nanocomposites illustrated in Table 1-1 was studied by the use of thermogravimetric analyses (TGA), in which the weight loss of these nanocomposites was measured by raising the temperature around 800 °C at a 10 °C/min heating rate under air atmospheric conditions, and the results were shown in Figs. 1-4 ~ 1-6.

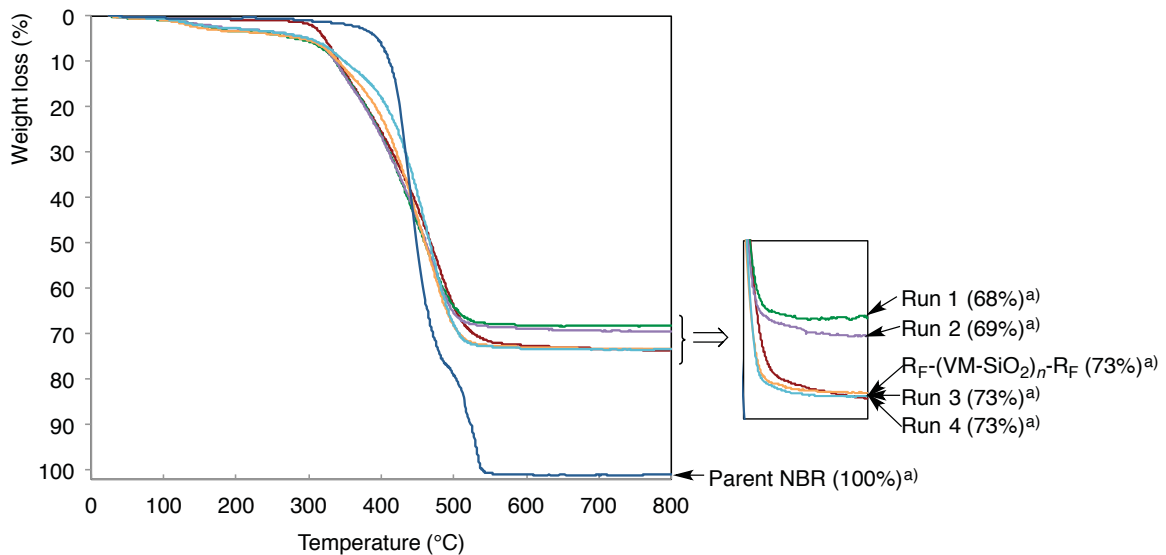


Fig. 1-4 Thermogravimetric analyses (TGA) of parent NBR, the $R_F-(VM-SiO_2)_n-R_F/NBR$ nanocomposites (Runs 1 ~ 4 in Table 1-1) and the $R_F-(VM-SiO_2)_n-R_F$ nanoparticles
a) Weight loss (%) at 800 °C

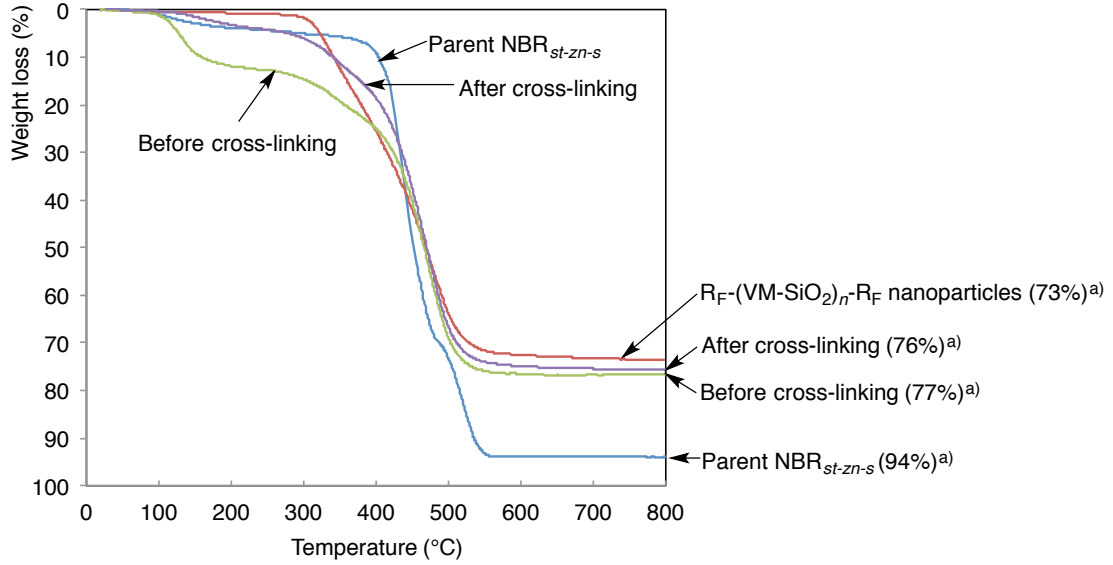


Fig. 1-5 Thermogravimetric analyses (TGA) of parent NBR_{st-zn-s}, the R_F-(VM-SiO₂)_n-R_F/NBR_{st-zn-s} nanocomposites (Run 6 in Table 1-1) before and after cross-linking reaction at 150 °C for 30 min, and the R_F-(VM-SiO₂)_n-R_F nanoparticles
 a) Weight loss (%) at 800 °C

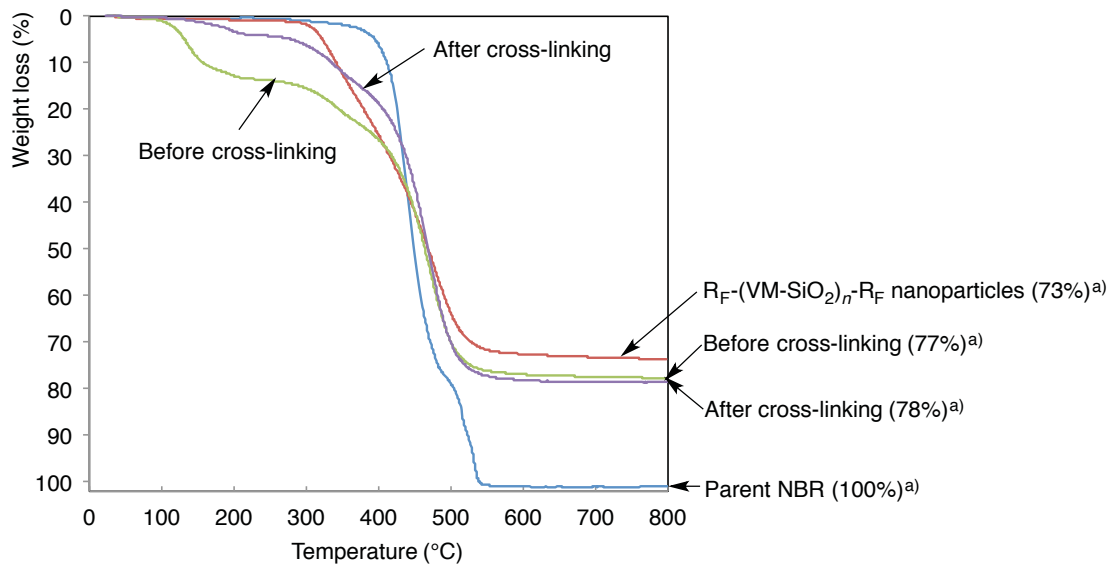


Fig. 1-6 Thermogravimetric analyses (TGA) of parent NBR, the R_F-(VM-SiO₂)_n-R_F/NBR_{zn-s} nanocomposites (Run 9 in Table 1-1) before and after cross-linking reaction at 150 °C for 30 min, and the R_F-(VM-SiO₂)_n-R_F nanoparticles
 a) Weight loss (%) at 800 °C

As shown in Figs. 1-5 and 1-6, the $R_F-(VM-SiO_2)_n-R_F/NBR_{st-zn-s}$ and $R_F-(VM-SiO_2)_n-R_F/NBR_{zn-s}$ nanocomposites before cross-linking reaction at 150 °C for 30 min can afford a clear weight loss around 150 ~ 300 °C, indicating that the cross-linking reaction of NBR by using zinc oxide, S₈ and stearic acid can proceed under such conditions to afford the corresponding cross-linked NBR in the composites. On the other hand, interestingly, the $R_F-(VM-SiO_2)_n-R_F/NBR$ nanocomposites illustrated in Fig. 1-4 were found to exhibit no weight loss behavior corresponding to the contents of the NBR in the composites even after calcination at 800 °C. It has been already reported that polyacrylonitrile (PAN) can enhance its thermal stability due to the cyclization of nitrile groups in PAN leading to the unsaturated >C=N- species.^{25 ~ 28)} Similarly, it has been already reported that the nitrile fragments end-capped *N,N*-dimethylacrylamide (DMAA) oligomers/silica nanocomposites [NC-CMe₂-(CN₂CH(C=O)NMe₂)_n-CMe₂-CN/SiO₂] can provide no weight loss behavior corresponding to the contents of the oligomer in the nanocomposites even after calcination at 800 °C.²⁹⁾ This no weight loss behavior would be due to the formation of the imine unit (>C=N-) during the calcination process.²⁹⁾ Therefore, since the $R_F-(VM-SiO_2)_n-R_F/NBR$ nanocomposites possess the nitrile units in the composites, such units would enable the encapsulated NBR in the composites to

afford no weight loss behavior even after calcination at 800 °C. The $R_F-(VM-SiO_2)_n-R_F/NBR$ nanocomposites would also give the slight weight loss at around 150 ~ 300 °C illustrated in Fig. 1-4 due to the formation of the imine units.

1.3.3. Surface modification of glass by the use of fluoroalkyl end-capped vinyltrimethoxysilane oligomeric silica nanocomposites - encapsulated NBR

The modified glasses treated with the fluorinated oligomeric silica nanocomposites - encapsulated NBR illustrated in Table 1-1 were prepared, and the contact angles of dodecane and water for these modified glasses were measured by depositing a droplet of dodecane or water (2 μ l) on these modified glass surfaces. These results are shown in Table 1-2.

As shown in Table 1-2, the modified glass surfaces treated with the $R_F-(VM-SiO_2)_n-R_F/NBR$ nanocomposites were found to exhibit the highly oleophobic and superhydrophobic characteristics on the surface, because dodecane and water contact angle values are 78 ~ 98 and 180 degrees, respectively. Especially, the $R_F-(VM-SiO_2)_n-R_F/NBR$ nanocomposites, which were prepared under the feed ratio:

oligomer/NBR = 100/10 (mg/mg) (see Run 2 in Table 1-1), afforded the highly oleophobic and superhydrophobic characteristics (dodecane and water contact angle values: 98 and 180 degrees) on the modified surface (see Run 2 in Table 1-2). A similar highly oleophobic (dodecane contact angle values: 78 ~ 92 degrees) and superhydrophobic (water contact angle value: 180 degree) characteristics were observed in the $R_F-(VM-SiO_2)_n-R_F/NBR_{st-zn-s}$ nanocomposites (see Runs 5 ~ 7 in Table 1-2). In the $R_F-(VM-SiO_2)_n-R_F/NBR$ nanocomposites, dodecane contact angle values were decreased from 95 (or 98) to 74 degrees with increasing the feed amounts of NBR from 5 (or 10) to 50 mg in the NBR and the $R_F-(VM)_n-R_F$ oligomer (see Runs 1 ~ 4 in Tables 1-1 and 1-2). A similar tendency was observed in the $R_F-(VM-SiO_2)_n-R_F/NBR_{st-zn-s}$ nanocomposites (see Runs 5 ~ 7 in Table 1-2). These findings are due to the presence of the oleophilic NBRs moieties in the composites, and highly amounts of NBRs in the composites are likely to afford the oleophilic characteristic on the modified surface. In addition, the cross-linking reaction at 150 °C for 30 min of the modified glass surface treated with the $R_F-(VM-SiO_2)_n-R_F/NBR_{st-zn-s}$ nanocomposites (Run 6 in Tables 1-1 and 1-2) was found to supply the similar highly oleophobic/superhydrophobic characteristic (dodecane and water contact angle values: 70 and 180 degrees) on the modified surface to

those (dodecane and water contact angle values: 80 and 180 degrees: Run 6 in Table 1-2) before cross-linking reaction. Such highly oleophobic characteristic has been already observed in the fluoroalkyl end-capped vinyltrimethoxysilane oligomeric silica/talc nanocomposites - encapsulated perfluoroalkanoic acid.³⁰⁾

Table 1-2 Contact angles of dodecane and water on the modified glass surface treated with the $R_F-(VM-SiO_2)_n-R_F/NBRs$ nanocomposites

Run ^{a)}	NBRs in the composites	Contact angle (Degree)							
		Dodecane ^{b)}	Water						
			Time (min)						
			0	5	10	15	20	25	30
1	NBR	95	180	-c)	-c)	-c)	-c)	-c)	-c)
2		98	180	-c)	-c)	-c)	-c)	-c)	-c)
3		86	180	-c)	-c)	-c)	-c)	-c)	-c)
4		74	180	-c)	-c)	-c)	-c)	-c)	-c)
5	$NBR_{st-zn-s}$	92	180	-c)	-c)	-c)	-c)	-c)	-c)
6		80	180	-c)	-c)	-c)	-c)	-c)	-c)
7		78	180	-c)	-c)	-c)	-c)	-c)	-c)
8	NBR_{zn-s}	0	180	-c)	-c)	-c)	-c)	-c)	-c)
9		0	180	-c)	-c)	-c)	-c)	-c)	-c)
10		0	180	-c)	-c)	-c)	-c)	-c)	-c)

a) Each Run No. corresponds to that of Table 1-1

b) After 5 min

c) No change

On the other hand, the $R_F-(VM-SiO_2)_n-R_F/NBR_{zn-s}$ nanocomposites were unable to provide the oleophobic/superhydrophobic characteristic on the modified surface (Runs 8 ~ 10 in Table 1-2). The same dodecane and water contact angle values (0 and 180 degrees) were observed on the modified glass surface treated with the $R_F-(VM-SiO_2)_n-R_F/NBR_{zn-s}$ nanocomposites (Run 9 in Table 1-1), of whose modified

glass was treated through cross-linking reaction at 150 °C for 30 min, as those (see Run 9 in Table 1-2) before the cross-linking reaction. In fact, Fig. 1-7-[I]-(B) shows the shape of water droplet on the modified glass surface treated with the $R_F-(VM-SiO_2)_n-R_F/NBR_{zn-s}$ nanocomposites (Run 9 in Table 1-1), and the water droplet cannot deposit on the modified surface due to the superhydrophobic coating surface (water contact angle value: 180 degree) even after pull-up process of the needle from the modified surface [see Fig. 1-7-[I]-(C)]. On the other hand, dodecane contact angle value on the modified surface can decrease smoothly from 25 to 0 degrees over 30 sec to afford the superoleophilic surface as shown in Fig. 1-7-[II]-(C).

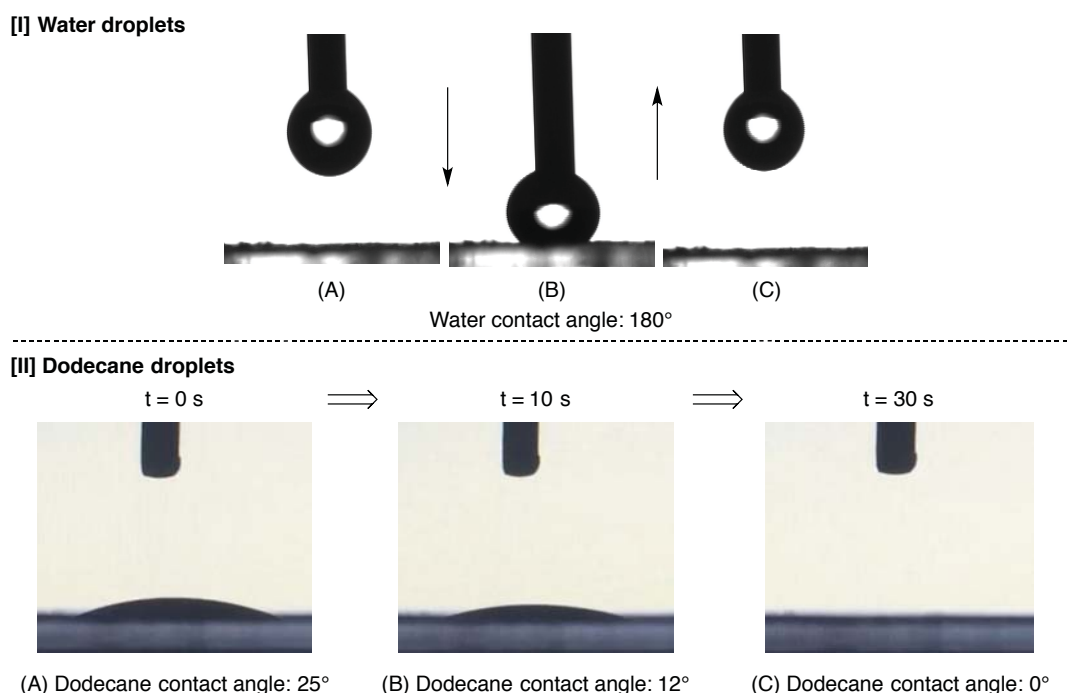


Fig. 1-7 Charge coupled device camera images of the water droplets [I] that adhered to the needle tip: (A) (process before adhesion of the water droplet on the modified glass surface), water droplet on the modified surface: (B), pull-up process of the needle from the modified surface: (C), and the dodecane droplets [II] on the modified surface

In order to clarify the creation of such superoleophilic/superhydrophobic surface, the surface roughness of the modified glass surface treated with the $R_F-(VM-SiO_2)_n-R_F/NBR_{st-zn-s}$ nanocomposites (Run 9 in Table 1-1) was studied by dynamic force microscopy (DFM) measurements. The $R_F-(VM-SiO_2)_n-R_F/NBR_{st-zn-s}$ nanocomposites (Run 6 in Table 1-1) and the $R_F-(VM-SiO_2)_n-R_F/NBR$ nanocomposites (Run 2 in Table 1-1) possessing highly oleophobic/superhydrophobic characteristic were also studied under similar conditions, for comparison. These results are shown in Figs. 1-8 and 1-9.

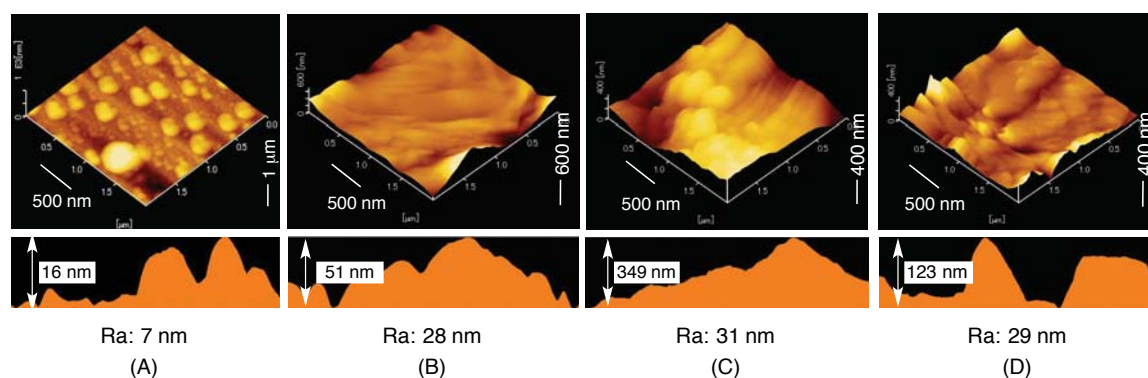


Fig. 1-8 DFM (Dynamic Force Microscopy) topographic images of the modified glass surface treated with the parent $R_F-(VM-SiO_2)_n-R_F$ oligomeric nanoparticles (A), the $R_F-(VM-SiO_2)_n-R_F/NBR_{st-zn-s}$ nanocomposites (Run 6 in Table 1-1) before (B) and after (C) cross-linking reaction at 150 °C for 30 min, and the $R_F-(VM-SiO_2)_n-R_F/NBR$ nanocomposites (Run 2 in Table 1-1) (D)

As shown in Fig. 1-8-(A), the topographical image of the original fluoroalkyl end-capped vinyltrimethoxysilane oligomeric silica nanoparticles [$R_F-(VM-SiO_2)_n-R_F$], which were prepared by the sol-gel reaction of the corresponding oligomer under alkaline

conditions, can provide a roughness property (the roughness average: $R_a = 7$ nm) to give the usual oleophobic/superhydrophobic surface (dodecane and water contact angle values: 48 and 180 degrees).³¹⁾ Higher R_a values (28 and 31 nm) were obtained in the $R_F-(VM-SiO_2)_n-R_F/NBR_{st-zn-s}$ nanocomposites before and after cross-linking reaction [see Figs. 1-8-(B) and 1-8-(C)], respectively. The $R_F-(VM-SiO_2)_n-R_F/NBR$ nanocomposites were also afforded the higher R_a value (29 nm) on the modified surface [Fig. 1-8-(D)]. However, the extremely higher R_a values (95 and 83 nm) on the modified surface treated with the $R_F-(VM-SiO_2)_n-R_F/NBR_{zn-s}$ nanocomposites before and after cross-linking reaction [see Figs. 1-9-(A) and 1-9-(B)]. This finding suggests that such higher R_a values would be derived into the superoleophilic/superhydrophobic surface.

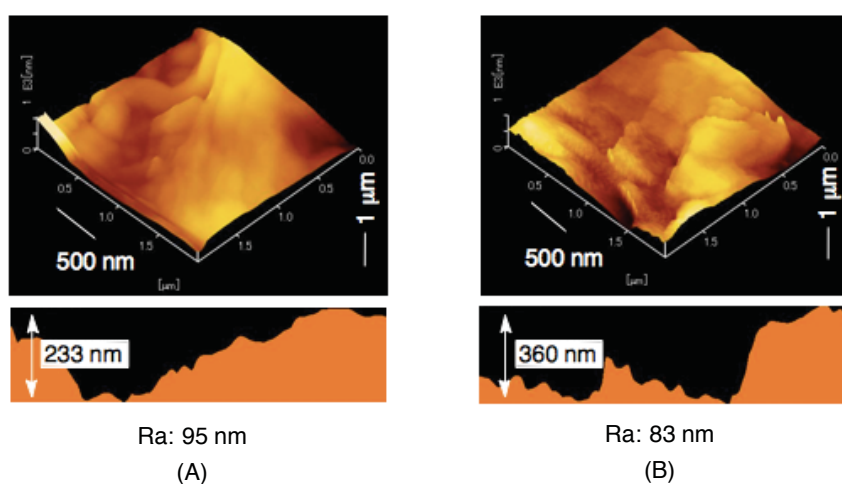


Fig. 1-9 DFM (Dynamic Force Microscopy) topographic images of the modified glass surface treated with the $R_F-(VM-SiO_2)_n-R_F/NBR_{zn-s}$ nanocomposites (Run 9 in Table 1-1) before (A) and after (B) cross-linking reaction at 150 °C for 30 min

In this way, it was verified that the $R_F-(VM-SiO_2)_n-R_F/NBR_{zn-s}$ nanocomposites before and after cross-linking reaction at 150 °C for 30 min can supply a superoleophilic/superhydrophobic characteristic. It is well known that superoleophilic/superhydrophobic materials are facile way to realize the oil/water separation.^{32 ~ 35)} In fact, a superhydrophobic surface can be realized by a water contact angle greater than 150°, and such surface creation has been comprehensively studied due to their possessing superior water repellency and self-cleaning property.^{32 ~ 38)} In general, superoleophilic surfaces have a strong affinity of organic oils. Thus, the surfaces possessing the superhydrophobic and superoleophilic characteristics can simultaneously repel water and strongly absorb oils. Such interesting behavior has been applied to the oil-water separating membranes and self-cleaning surface.^{30 ~ 33)} The $R_F-(VM-SiO_2)_n-R_F/NBR_{zn-s}$ nanocomposites were applied to the packing materials for column chromatography to separate the mixture of oil (1,2-dichloroethane)/water (blue-colored water treated with copper sulfate pentahydrate), and the results are illustrated in Fig. 1-10.

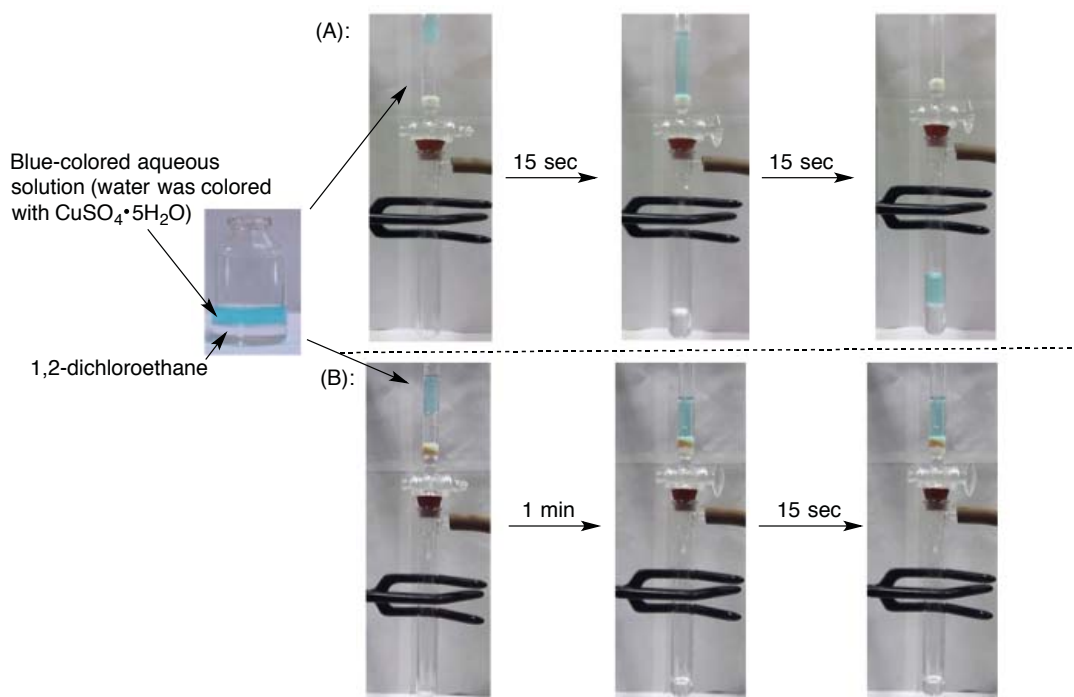


Fig. 1-10 Separation of the mixture of blue-colored water and 1,2-dichloroethane by using the $R_F-(VM-SiO_2)_n-R_F/NBR_{zn-s}$ nanocomposites (Run 9 in Table 1): (A) before and (B) after cross-linking reaction at 150 °C for 30 min under reduced pressure conditions

Furthermore, not only the mixture of oil and water but also the surfactant (span 80: 20 mg)-stabilized water (0.05 ml)-in-oil (1,2-dichloroethane: 5.0 ml) emulsion, which was prepared under ultrasonic conditions for 5 min at room temperature, by the use of the $R_F-(VM-SiO_2)_n-R_F/NBR_{zn-s}$ nanocomposite powders (Run 9 in Table 1-1) as the packing material for the column chromatography. The results are shown in Fig. 1-11.

As shown in Fig. 1-10-(A), the $R_F-(VM-SiO_2)_n-R_F/NBR_{zn-s}$ nanocomposites before cross-linking reaction were unable to separate the mixture of blue-colored water and oil, due to the good solubility of NBR in the composites toward the oil.

However, interestingly, it was demonstrated that the $R_F-(VM-SiO_2)_n-R_F/NBR_{zn-s}$ nanocomposites after cross-linking reaction are effective for the separation of blue-colored water and oil under reduced pressure conditions, and the colorless oil was easily detected [see Fig. 1-10-(B)].

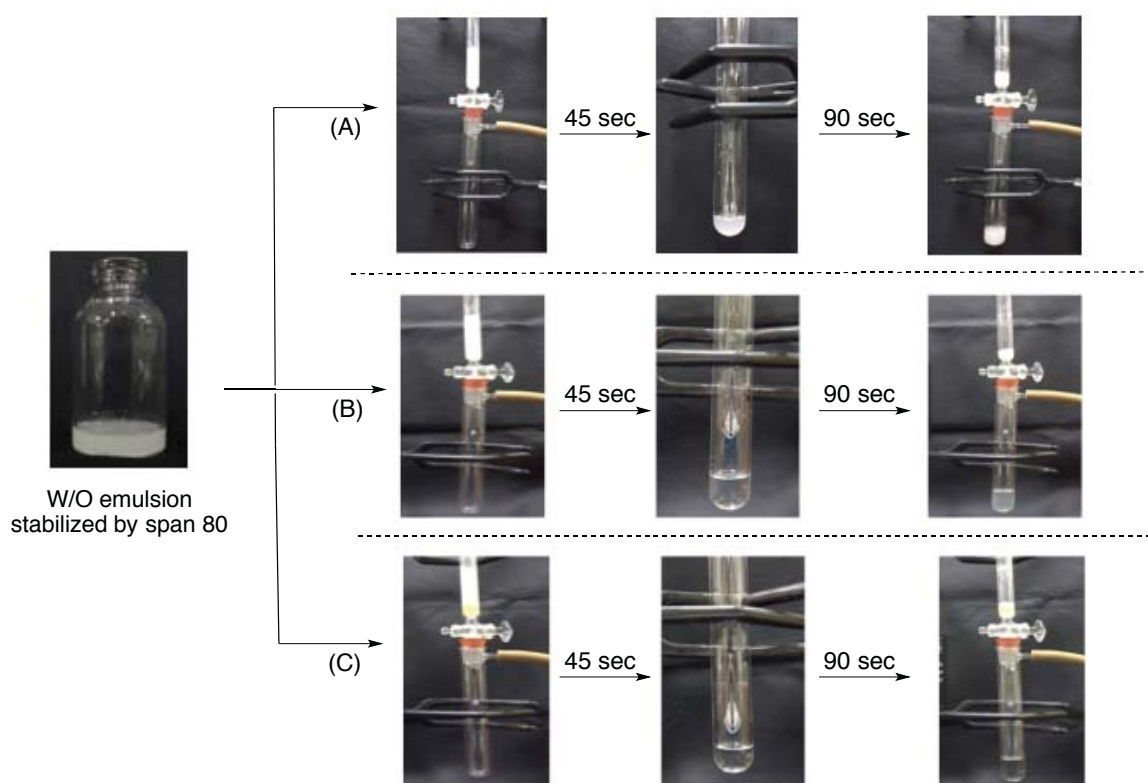


Fig. 1-11 Separation of the W/O (1,2-dichloroethane) emulsion by using the Wakogel^{TR} C500-HG (A), the $R_F-(VM-SiO_2)_n-R_F/NBR_{zn-s}$ nanocomposites (Run 9 in Table 1-1) before (B) and after (C) cross-linking reaction at 150 °C for 30 min under reduced pressure conditions

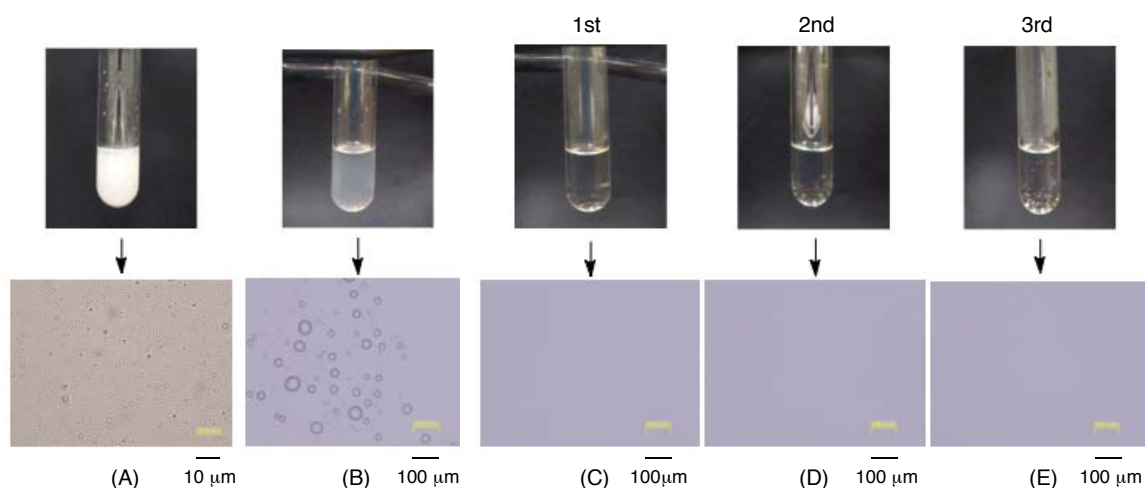


Fig. 1-12 Optical microscopy images of the eluent after the separation of the W/O (oil: 1,2-dichloroethane) emulsion stabilized by span 80 by using the column chromatography with Wakogel^{TR} C500-HG (A) and the $R_F-(VM-SiO_2)_n-R_F/NBR_{zn-s}$ nanocomposites (Run 9 in Table 1-1) before (B) and after [(C): 1st time; (D): 2nd time; (E): 3rd time] cross-linking reaction at 150 °C for 30 min as the packing materials, respectively, under reduced pressure conditions

As shown in Figs. 1-11-(A) and 1-11-(B), the silica gel (Wakogel[®] C-500 HG), which is well known as the packing material, and the $R_F-(VM-SiO_2)_n-R_F/NBR_{zn-s}$ nanocomposites before cross-linking reaction were unable to separate the W/O emulsion under reduced pressure conditions. However, the $R_F-(VM-SiO_2)_n-R_F/NBR_{zn-s}$ nanocomposites after cross-linking reaction were effective to separate the W/O emulsion under reduced pressure conditions to isolate the colorless oil (1,2-dichloroethane) [see Fig. 1-11-(C)], indicating that such cross-linking reaction enables the NBR in the composites to afford the good solvent resistance. In addition, the reusability of these nanocomposites as the packing material was also studied. The results show that the colorless oil was quantitatively isolated under similar conditions even after the use of

the W/O emulsion three times as the following recovered ratios: 1st time: 88 %; 2nd time: 86 %; 3rd time: 90 %. Moreover, optical micrograph images also showed that the water droplet cannot be detected at all in the isolated colorless oils [Figs. 1-12-(C), (D), and (E)] even after the reuse (2nd time and 3rd time) as the packing material; although the water droplet can easily detect in the isolated eluent by using the Wakogel [Fig. 1-12-(A)] and the $R_F-(VM-SiO_2)_n-R_F/NBR_{70-5}$ nanocomposites before cross-linking reaction [Fig. 1-12-(B)] as the packing materials.

1.4. Conclusions

Fluoroalkyl end-capped vinyltrimethoxysilane oligomer $[R_F-(VM)_n-R_F]$ was applied to the nanocomposite reactions with NBR under alkaline conditions to afford the corresponding fluorinated oligomeric silica/NBR nanocomposites $[R_F-(VM-SiO_2)_n-R_F/NBR]$. $NBR_{st-zn-s}$ and NBR_{zn-s} containing cross-linkers such as stearic acid (*st*), zinc oxide (*zn*) and S_8 (*s*) were also applied to the nanocomposite reactions with $R_F-(VM)_n-R_F$ oligomer under similar conditions to provide the expected $R_F-(VM-SiO_2)_n-R_F/NBR_{st-zn-s}$ and $R_F-(VM-SiO_2)_n-R_F/NBR_{zn-s}$ nanocomposites, respectively. In these nanocomposites thus obtained, it was demonstrated that the $R_F-(VM-SiO_2)_n-R_F/NBR$ nanocomposites can afford no weight loss behavior corresponding to the contents of NBR even after calcination at 800 °C. Furthermore, these nanocomposites were applied to the surface modification of glass. The modified glass surface treated with the $R_F-(VM-SiO_2)_n-R_F/NBR$ and the $R_F-(VM-SiO_2)_n-R_F/NBR_{st-zn-s}$ nanocomposites were found to afford the highly oleophobic and superhydrophobic characteristics. However, interestingly, it was demonstrated that the $R_F-(VM-SiO_2)_n-R_F/NBR_{zn-s}$ nanocomposites can supply the superoleophilic/superhydrophobic characteristic on the modified glass surface.

The $R_F-(VM-SiO_2)_n-R_F/NBR_{zn-s}$ nanocomposites were also applied to the separation of not only the mixture of oil and water but also the W/O emulsion. The $R_F-(VM-SiO_2)_n-R_F/NBR_{zn-s}$ nanocomposites before cross-linking reaction at 150 °C for 30 min was not effective for the separation of oil/water mixture and the W/O emulsion. However, the $R_F-(VM-SiO_2)_n-R_F/NBR_{zn-s}$ nanocomposites after cross-linking reaction were applicable to the packing material for the column chromatography to separate the mixture of oil/water and W/O emulsion.

References

- 1) S. Sadhu and A. K. Bhowmick, *J. Polym. Sci.: Part B: Polym. Phys.*, **42**, 1573 (2004).
- 2) M. Frounchi, M. Mehrabzadeh, and M. Parvary, *Polym. Int.*, **49**, 163 (2000).
- 3) S.-S. Choi and S.-H. Ha, *J. Ind. Eng. Chem.*, **16**, 238 (2010).
- 4) J.-T. Kim, T.-S. Oh, and D.-H. Lee, *Polym. Int.*, **52**, 1058 (2003).
- 5) J.-T. Kim, T.-S. Oh, and D.-H. Lee, *Polym. Int.*, **52**, 1203 (2003).
- 6) J.-T. Kim, T.-S. Oh, and D.-H. Lee, *Polym. Int.*, **53**, 406 (2004).
- 7) W. Du, H. Zou, M. Tian, L. Zhang, and W. Wang, *Polym. Adv. Technol.*, **23**, 1029 (2012).
- 8) S.-H. Zhu, C.-M. Chan, S. C. Wong, and Y.-W. Mai, *Polym. Eng. Sci.*, **39**, 1998 (1999).
- 9) N. Suzuki, M. Ito, and S. Ono, *J. Appl. Polym. Sci.*, **95**, 74 (2005).
- 10) P. Yu, H. He, C. Jiang, Y. Jia, D. Wang, X. Yao, D. Jia, and Y. Luo, *J. Appl. Polym. Sci.*, **133**, 42922 (2016).
- 11) H. Vargese, S. S. Bhagawan, and S. Thomas, *Eur. Polym. J.*, **31**, 957 (1995).

- 12) G. G. Bandyopadhyay, S. S. Bhagawan, and K. N. Ninan, *Rubber Chem. Technol.*, **70**, 650 (1997).
- 13) J. K. Pandey, K. R. Reddy, A. P. Kumar, and R. P. Singh, *Polym. Degrad. Stab.*, **88**, 234 (2005).
- 14) A. T. Koshy, B. Kuriakose, and S. Thomas, *Polym. Degrad. Stab.*, **36**, 137 (1992).
- 15) D. Lopes, M. J. Ferreira, R. Russo, and J. M. Dias, *J. Cleaner Production*, **92**, 230 (2015).
- 16) P. Jansen and B. G. Soares, *J. Appl. Polym. Sci.*, **79**, 193 (2001).
- 17) X. Ge, Y. Zhang, F. Deng, and U. R. Cho, *Polym. Compos.*, doi:10.1002/pc.23817
- 18) X. Ge, M.-C. Li, X. X. Li, and U. R. Cho, *Appl. Clay Sci.*, **118**, 265 (2015).
- 19) P. C. Thomas, E. T. Jose, G. George, S. Thomas, and K. Joseph, *Polym. Compos.*, **33**, 2236 (2012).
- 20) H. Takahashi and H. Sawada, United States Patent, US 7,144,962 B2 (2006).
- 21) H. Sawada, Y. Matsuki, Y. Goto, S. Kodama, M. Sugiya, and Y. Nishiyama, *Bull. Chem. Soc. Jpn.*, **83**, 75 (2010).
- 22) H. Sawada, *Polym. Chem.*, **3**, 46 (2012).
- 23) H. Sawada and M. Nakayama, *J. Chem. Soc., Chem. Commun.*, 677 (1991).

- 24) M. Akiba and A. S. Hashim, *Prog. Polym. Sci.*, **22**, 475 (1997).
- 25) M. S. A. Rahaman, A. F. Ismail, and A. Mustafa, *Polym. Degrad. Stab.*, **92**, 1421 (2007).
- 26) S. Xiao, B. Wang, C. Zhao, L. Xu, and B. Chen, *J. Appl. Polym. Sci.*, **127**, 2332 (2013).
- 27) G. T. Sivy, B. Gordon, and M. M. Coleman, *Carbon*, **21**, 573 (1983).
- 28) S. Xiao, W. Cao, B. Wang, L. Xu, and B. Chen, *J. Appl. Polym. Sci.*, **127**, 3198 (2013).
- 29) H. Sawada, M. Kabutomori, A. Ratcha, S. Kongparakul, and M. Nishida, *Colloid Polym. Sci.*, **294**, 1173 (2016).
- 30) Y. Oikawa, T. Saito, S. Yamada, M. Sugiya, and H. Sawada, *ACS Appl. Mater. Interfaces*, **7**, 13782 (2015).
- 31) T. Saito, Y. Tsushima, and H. Sawada, *Colloid Polym. Sci.*, **293**, 65 (2015).
- 32) J. Li, H. Wan, Y. Ye, H. Zhou, and J. Chen, *Appl. Surf. Sci.*, **261**, 470 (2012).
- 33) M. Zhang, C. Wang, S. Wang, Y. Shi, and J. Li, *Appl. Surf. Sci.*, **26**, 764 (2012).
- 34) M. Zhang, C. Wang, S. Wang, Y. Shi, and J. Li, *Carbohydrate Polym.*, **97**, 59 (2013).
- 35) T. Arbatan, L. Zhang, X.-Y. Fang, and W. Shen, *Chem. Eng. J.*, **210**, 74 (2012).

- 36) Y. Si and Z. Guo, *Chem. Lett.*, **44**, 874 (2015).
- 37) K. Liu, Y. Tian, and L. Jiang, *Prog. Mater. Sci.*, **58**, 503 (2013).
- 38) T. Darmanin and F. Guittard, *Prog. Polym. Sci.*, **39**, 656 (2014).

CHAPTER 2

Preparation and Thermal Stability of Initiator Fragments

End-Capped Oligomers/Silica Nanocomposites

2.1. Introduction

Fluoroalkyl end-capped oligomers [$R_F-(M)_n-R_F$; R_F = fluoroalkyl groups], which can be synthesized by the oligomerization of the corresponding radical polymerizable monomers (M) initiated by fluoroalkanoyl peroxide [$R_F-(C=O)OO(O=C)-R_F$], can form the nanometer size-controlled self-assembled molecular aggregates with the aggregation of the terminal fluoroalkyl segments in aqueous and organic media.^{1, 2)} These fluorinated molecular aggregates can also interact with silica nanoparticles as a host moiety in the presence of tetraethoxysilane under alkaline conditions (aqueous ammonia) to afford the corresponding fluorinated oligomers/silica nanocomposites [$R_F-(M)_n-R_F/SiO_2$].³⁾ In these nanocomposites, fluorinated oligomers/silica nanocomposites, of whose oligomers possess the amide protons and higher acidic protons such as sulfo groups, can exhibit no weight loss behavior corresponding to the contents of oligomers even after calcination at 800 °C.^{4 ~ 6)} In contrast, the fluorinated oligomers possessing no amide protons and relatively weaker acidic protons such as carboxyl groups than that of sulfo groups can afford the usual flammable characteristic in the silica nanocomposite cores under similar calcination process.^{4 ~ 6)} This nonflammable characteristic is due to the smooth

dehydrofluorination of amide or sulfo protons with fluorines in oligomers catalyzed by ammonia and silica nanoparticles, affording ammonium hexafluorosilicate through the effective interaction between the obtained hydrogen fluoride with silica nanoparticles.⁷⁾

On the other hand, it is well known that polyacrylonitriles (PANs) are widely used as precursors for fabricating high performance carbon fibers.^{8 ~ 15)} The formation of PAN precursor fibers possessing the heat resistance ability by heating 200 ~ 300 °C is due to the change of the chemical structure from the linear molecular chain into ladder structures through a variety of chemical reactions including cyclization of nitrile groups leading to hydronaphthiridine rings, dehydrogenation leading to a certain degree of aromatization, and oxidation reaction leading mainly to acridone and some other structure.^{9, 11, 12)} From this point of view, it is of particular interest to study on the thermal stability of initiator fragments end-capped oligomers, which should be synthesized by using a variety of radical initiators containing not only the nitrile groups but also the 2-methyl-*N*-(2-hydroxyethyl)propionamide and the sulfate ester units. This chapter shows the synthesis and property of the initiator fragments end-capped oligomers by using these radical initiators. In addition, the preparation of the corresponding oligomers/silica

nanocomposites, including their thermal stability was also studied, in comparison with that of the corresponding fluoroalkyl end-capped oligomers/silica nanocomposites.

2.2. Experimental

2.2.1. Measurements

^1H NMR and ^{13}C NMR spectra were recorded using JEOL JNM-ECA 500 (500 MHz) FT NMR SYSTEM (Tokyo, Japan). ^1H magic-angle spinning (MAS) NMR spectra were measured at room temperature using Varian Unity INOVA 300 (Tokyo, Japan). Molecular weight of the initiator fragments end-capped oligomers was measured using a Shodex DS-4 (pump) and Shodex RI-71 (detector) gel permeation chromatography (Tokyo, Japan) calibrated with polystyrene standard using tetrahydrofuran (THF) as the eluent. Fourier transform infrared (FT-IR) spectra were measured with a FT-IR spectrophotometer (FTIR-8400, Shimadzu, Japan). Thermal analyses were recorded by raising the temperature around 800 °C (the heating rate: 10 °C/min) under atmospheric conditions by the use of Bruker axis TG-DTA2000SA differential thermobalance (Kanagawa, Japan). Size [number-average diameter (average hydrodynamic diameter)] of nanocomposites was measured by using Otsuka Electronics DLS-7000 HL (Tokyo, Japan). Field emission scanning electron micrographs (FE-SEM) and energy

dispersive X-ray (EDX) spectra were recorded by means of JEOL JSM-7000 F (Tokyo, Japan).

2.2.2. Materials

Acrylic acid (ACA) and *N*-(1,1-dimethyl-3-oxobutyl)acrylamide (DOBAA) were used as received from Wako Pure Chemical Industries, Ltd. (Osaka, Japan) and KH Neochem Co., Ltd. (Tokyo, Japan), respectively. *N,N*-dimethylacrylamide (DMAA) and acryloylmorpholine (ACMO) were used as received from KJ Chemicals Corp. (Tokyo, Japan). Ammonium persulfate (APS) was purchased from Kanto Chemical Co., Inc. (Tokyo, Japan). Silica-nanoparticle methanol solution [30% (wt.): average particle size 11 nm (Methanol Silica-sol^{TR})] was supplied by Nissan Chemical Industrials Ltd. (Tokyo, Japan). Tetraethoxysilane (TEOS) was purchased from Tokyo Chemical Industry Co., Ltd. (Tokyo, Japan). 2,2'-Azobis(2-methyl-*N*-(2-hydroxyethyl)propionamide) (VA-086), azobisisobutyronitrile (AIBN) and aqueous ammonia were purchased from Wako Pure Chemical Industries, Ltd. (Osaka, Japan).

2.2.3. Synthesis of initiator fragments end-capped oligomers by using APS as a radical initiator

2.2.3.1. Initiator fragments end-capped *N,N*-dimethylacrylamide oligomer

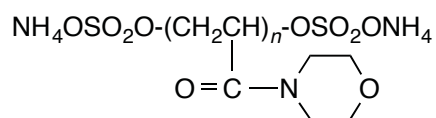
APS (2.00 g) was added to an aqueous solution (150 g) containing *N,N*-dimethylacrylamide (DMAA, 2.00 g). The solution was stirred at 55 °C for 3 h under nitrogen. After evaporating the solvent by the addition of methanol as an azeotropic solvent under reduced pressure, the crude products thus obtained were dialyzed with water to afford the initiator fragments end-capped DMAA oligomer: $\text{NH}_4\text{OSO}_2\text{O}-[\text{CH}_2\text{CHC}(=\text{O})\text{NMe}_2]_n-\text{OSO}_2\text{ONH}_4$ (2.68 g). This oligomer exhibited the following spectra characteristics: FT-IR (v/cm^{-1}) 846 (SO_4), 1097 ~ 1255 ($>\text{N}-\text{C}(=\text{O})$), 1624 ($\text{C}=\text{O}$), 2937 (CH_2), 3300 ~ 3502 (NH_4).

2.2.3.2. Initiator fragments end-capped acrylic acid oligomer

APS (3.19 g) was added to an aqueous solution (150 g) containing ACA. The solution was stirred at 55 °C for 3 h under nitrogen. After evaporating the solvent by the addition of methanol as an azeotropic solvent under reduced pressure, the crude products thus obtained were reprecipitated from the methanol-hexane system to afford the initiator fragments end-capped ACA oligomer: $\text{NH}_4\text{OSO}_2\text{O}-[\text{CH}_2\text{CHC}(=\text{O})\text{OH}]_n-\text{OSO}_2\text{ONH}_4$ (5.81 g). This oligomer exhibited the following spectra characteristics: FT-IR (v/cm^{-1}) 850 (SO_4), 1720 ($\text{C}=\text{O}$), 2937 (CH_2), 3014 ~ 3157 (OH), 3439 and 3520 (NH_4).

Other initiator fragments end-capped oligomers were prepared under similar conditions, and the spectra characteristic of these obtained oligomers is as follows:

$\text{NH}_4\text{OSO}_2\text{O}-[\text{CH}_2\text{CHC}(=\text{O})\text{NHCH}_2\text{CMeCH}_2\text{C}(=\text{O})\text{Me}]_n-\text{OSO}_2\text{ONH}_4$: FT-IR (v/cm^{-1}) 864 (SO_4), 1109 ~ 1288 ($>\text{N}-\text{C}(=\text{O})$), 1654, 1710 ($\text{C}=\text{O}$), 2978 (CH_2), 3076 ~ 3510 (NH_4).



FT-IR (v/cm^{-1}) 844 (SO_4), 1112 ~ 1301 ($>\text{N}-\text{C}(=\text{O})$), 1631 ($\text{C}=\text{O}$), 2924 (CH_2), 3219 ~ 3504 (NH_4).

2.2.4. Synthesis of initiator fragments end-capped oligomers by using VA-086 as a radical initiator

2.2.4.1. Initiator fragments [2-methyl-*N*-(2-hydroxyethyl)propionamide] end-capped

N,N-dimethylacrylamide oligomer

VA-086 (2.90 g) was added to a 2-propanol (200 g) containing DMAA (5.00 g).

The solution was stirred at 80 °C for 9 h under nitrogen. After evaporating the solvent under reduced pressure, the obtained crude products were reprecipitated from the 2-propanol-hexane system to afford the initiator fragments end-capped DMAA oligomer:



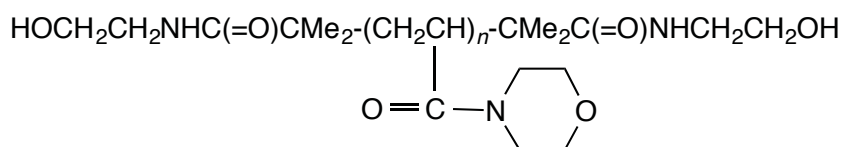
g). This oligomer exhibited the following spectra characteristics: FT-IR (v/cm^{-1})

1062 ~ 1257 ($>\text{N}-\text{C}(=\text{O})$), 1612 ($\text{C}=\text{O}$), 2937 (CH_2), 3325 (OH), 3377 ($-\text{NH}(\text{C}=\text{O})$).

Other initiator fragments end-capped oligomers were prepared under similar conditions, and the spectra characteristic of these obtained oligomers is as follows:

$\text{HOCH}_2\text{CH}_2\text{NHC}(=\text{O})\text{CMe}_2-[\text{CH}_2\text{CHC}(=\text{O})\text{OH}]_n-\text{CMe}_2\text{C}(=\text{O})\text{NHCH}_2\text{CH}_2\text{OH}$: FT-IR (v/cm^{-1}) 1658, 1720 ($\text{C}=\text{O}$), 2937 (CH_2), 3323 (OH), 3383 ($-\text{NH}(\text{C}=\text{O})$).

$\text{HOCH}_2\text{CH}_2\text{NHC}(=\text{O})\text{CMe}_2-[\text{CH}_2\text{CHC}(=\text{O})\text{NHCH}_2\text{CMe}_2\text{CH}_2\text{C}(=\text{O})\text{Me}]_n\text{CMe}_2-\text{C}(=\text{O})\text{NHCH}_2\text{CH}_2\text{OH}$: FT-IR (v/cm^{-1}) 1149 ~ 1267 ($>\text{NC}(=\text{O})$), 1658, 1710 ($\text{C}=\text{O}$), 2937 (CH_2), 3325 (OH), 3377 ($-\text{NH}(\text{C}=\text{O})$).



FT-IR (v/cm^{-1}) 1149 ~ 1267 ($>\text{NC}(=\text{O})$), 1529, 1651 ($\text{C}=\text{O}$), 2937, 2978 (CH_2), 3325 (OH), 3381 ($-\text{NH}(\text{C}=\text{O})$).

2.2.5. Synthesis of initiator fragments end-capped *N,N*-dimethylacrylamide oligomers by using AIBN as a radical initiator

AIBN (2.80 g) was added to a 2-propanol (190 g) containing DMAA (15.0 g). The solution was stirred at 65 °C for 9 h under nitrogen. After evaporating the solvent under reduced pressure, the obtained crude products were reprecipitated from the 2-propanol-hexane system to afford the initiator fragments end-capped DMAA oligomer:

$\text{Me}_2\text{C}(\text{NC})\text{-}[\text{CH}_2\text{CHC}(=\text{O})\text{NMe}_2]_n\text{-C}(\text{CN})\text{Me}_2$: FT-IR (v/cm^{-1}) 1055 ~ 1249 ($>\text{NC}(=\text{O})$), 1529, 1612 (C=O), 2235 (CN), 2926 (CH₂).

2.2.6. Preparation of initiator fragments end-capped *N,N*-dimethylacrylamide oligomers/silica nanocomposites

To a methanol solution (20 ml) of $\text{NH}_4\text{OSO}_2\text{O-}[\text{CH}_2\text{CHC}(=\text{O})\text{NMe}_2]_n\text{-OSO}_2\text{ONH}_4$ (100 mg) were added tetraethoxysilane (TEOS, 0.25 ml), silica-nanoparticle methanol solution [30 % (wt.): 500 mg], and 25 % aqueous ammonia solution (0.25 ml). The mixture was stirred with a magnetic stirring bar at 25 °C for 5 h. After the solvent

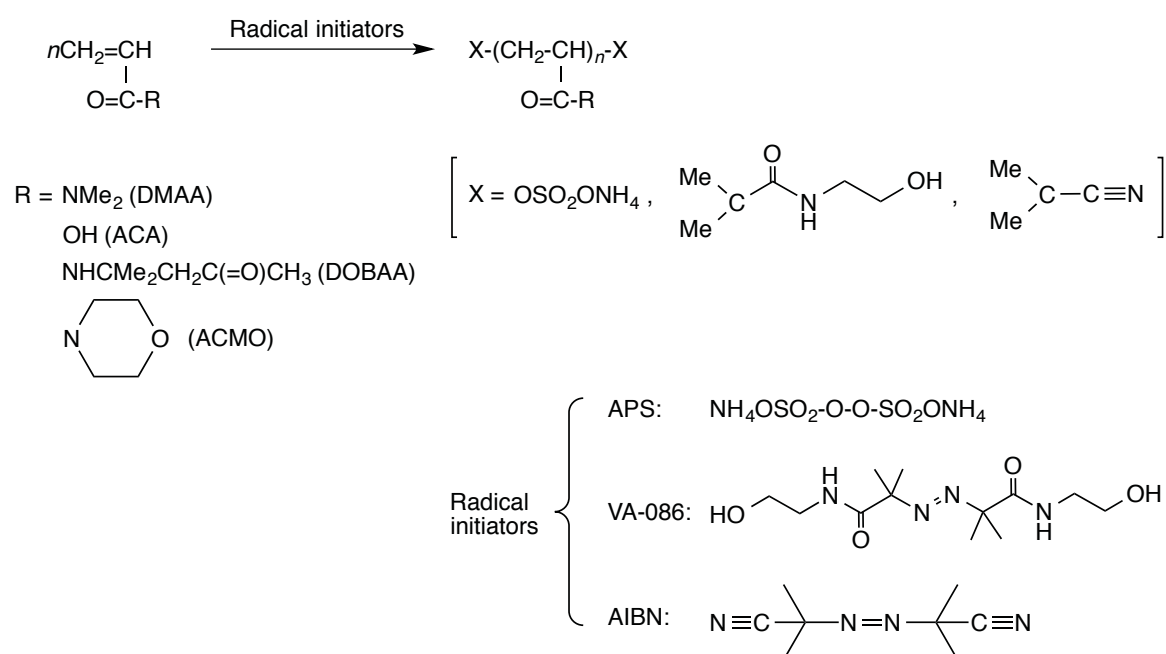
was evaporated off, the methanol (20 ml) was added to the obtained crude products. The methanol solution was stirred with magnetic stirring bar at room temperature for 1 day and then was centrifuged for 30 min. The expected fluorinated nanocomposites were easily separated from the methanol solution and then was washed with methanol in several times. The nanocomposite powders thus obtained were dried in vacuo at 50 °C for 2 days to afford the purified particle powders (540 mg).

Other initiator fragments end-capped oligomers/silica nanocomposites were prepared under similar conditions.

2.3. Results and discussion

2.3.1. Synthesis and solubility of initiator fragments end-capped oligomers

DMAA, ACA, DOBAA, and ACMO were found to afford the initiator fragments end-capped oligomers through the radical oligomerization of the corresponding monomers by the use of APS, VA-086, and AIBN as radical initiators. These results are shown in Scheme 2-1 and Table 2-1.



Scheme 2-1 Synthesis of initiator fragments end-capped oligomers

Table 2-1 Synthesis of initiator fragments end-capped oligomers

Monomer (g) [mmol]	Initiator (g) [mmol]	Product yield ^{a)} (%)	M_n (M_w/M_n) ^{b)}	
APS				
DMAA	2.0 [20]	1.0 [8.8]	67	1040 (1.90)
ACA	5.0 [69]	3.2 [14]	71	1840 (1.03)
DOBAA	5.0 [30]	1.4 [6.1]	75	5750 (1.01)
ACMO	5.0 [35]	1.8 [7.9]	56	5200 (1.04)
VA-086				
DMAA	5.0 [50]	2.9 [10]	70	440 (2.20) [2.2] ^{c)}
ACA	5.0 [69]	4.0 [14]	63	1600 (1.02) [3.2] ^{c)}
DOBAA	5.0 [30]	1.7 [5.9]	61	3570 (1.04) [2.2] ^{c)}
ACMO	5.0 [35]	2.3 [8.0]	87	10180 (1.01) [2.3] ^{c)}
AIBN				
DMAA	15 [151]	2.8 [17.1]	72	870 (1.05) [1.9] ^{c)}

a) Isolated yield based on monomer and radical initiator

b) Determined by gel permeation chromatography

c) Number of initiator fragments end-groups per oligomer molecule calculated from ¹H-NMR spectra and M_n values

As shown in Scheme 2-1 and Table 2-1, two initiator fragments end-capped oligomers ($M_n = 440 \sim 10180$; $M_w/M_n = 1.01 \sim 2.20$) were obtained through the primary radical termination or radical chain transfer to the initiators under the present oligomeric conditions, in which the concentrations of the initiators were almost the same as that of the monomers. The primary radical termination and radical chain transfer to the initiator to give two initiator fragments end-capped polymers are well known as the *iniferter* by Otsu et al.^{16, 17)} It was previously reported that two fluoroalkyl end-capped oligomers

$[R_F-(M)_n-R_F]$; R_F = fluoroalkyl groups; M = radical polymerizable monomers] can be also synthesized by using fluoroalkanoyl peroxide $[R_F-C(=O)OO(O=)C-R_F]$; R_F = fluoroalkyl groups] as a radical initiator under similar oligomeric conditions.^{18, 19)} Under the same feed molar ratio (5/1) of monomers (DMAA, ACA, and DOBAA)/initiator (VA-086) in Table 2-1, DMAA afforded the lowest molecular weight $M_n = 440$, compared with those of other monomers. This finding would be due to its poor radical oligomerizable ability, providing the lower molecular weights for the oligomer with the relatively large dispersibility: $M_w/M_n = 2.20$. 1H NMR spectra for two initiator fragments [the 2-methyl-*N*-(2-hydroxyethyl)propionamide (*HO-Amide*) and the nitrile units] end-capped oligomer show the oligomeric molecule contains two initiator fragments, because the number of initiator fragment end-groups per oligomer molecule is 1.9 ~ 3.2 (see Table 2-1). ^{13}C NMR spectra for the nitrile fragments $[Me_2C(CN)-]$ end-capped DMAA oligomers show the clear signals around 120 ppm related to the presence of -CN groups in the oligomers as shown in Fig. 2-1.

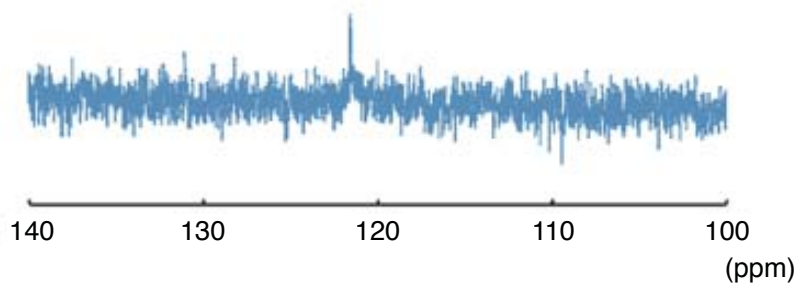


Fig. 2-1 ^{13}C NMR spectra of $\text{Me}_2(\text{NC})\text{C}-(\text{DMAA})_n-\text{C}(\text{CN})\text{Me}_2$ oligomer in CDCl_3

The solubility of the initiator fragments $[\text{NH}_4\text{OSO}_2\text{O}$ (the sulfate ester) and the *HO-Amide*, and the nitrile] end-capped oligomers was also studied. The striking characteristics of these oligomers are to harden not only water but also the traditional organic solvents such as methanol, 2-propanol (IPA), tetrahydrofuran (THF), propylene carbonate (PC) and 1,2-dichloroethane (DE). More interestingly, the sulfate ester fragments end-capped oligomers were found to cause a gelation toward not only these solvents but also non-polar solvent such as hexane. These results are shown in Fig. 2-2.

This unique gelling behavior should be due to the synergistic interaction between the oligomer side chains such as amide or carboxyl segments and the end-capped initiator fragments such as the sulfate esters, the 2-methyl-*N*-(2-hydroxyethyl)propionamide [*HO-Amide*], and the nitrile moieties. To clarify this gelling behavior, the minimum

concentrations (C_{min}) of these oligomers for gelation at 30 °C were measured according to the method reported by Hanabusa et al.^{20, 21)}, and the results are summarized in Table 2-2.

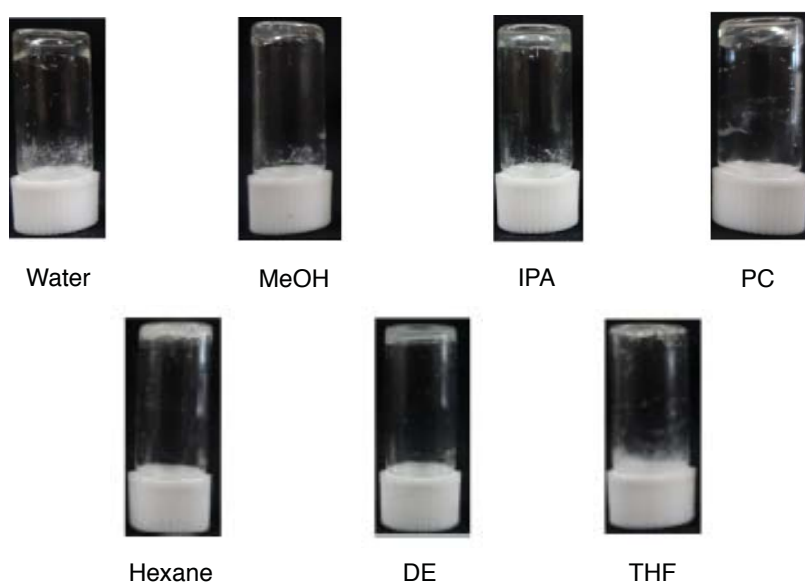


Fig. 2-2 Photograph for the gelation of $H_4NOSO_2O-(DMAA)_n-OSO_2ONH_4$ oligomer in a variety of solvents

Table 2-2 C_{min} values (%) for gelation of the sulfate ester [$X = OSO_2ONH_4$], the *OH-Amide* [$X = CMe_2C(=O)NHCH_2CH_2OH$] and the nitrile [$X = CMe_2CN$] fragments end-capped oligomers [$X-(M)_n-X$]

X in oligomer: solvent	M in oligomer								
	ACA		ACMO		DMAA		DOBAA		
	OSO_2NH_4	<i>HO-Amide</i>	OSO_2NH_4	<i>HO-Amide</i>	OSO_2NH_4	<i>HO-Amide</i>	CMe_2CN	OSO_2NH_4	<i>HO-Amide</i>
Water	29	63	10	59	17	65	76	12	60
MeOH	40	63	29	58	14	74	81	21	61
IPA	31	59	38	65	20	69	78	18	58
PC	34	55	13	50	18	62	69	20	48
Hexane	20	.a)	18	.a)	21	.a)	.a)	31	.a)
DE	49	28	12	42	12	43	70	30	33
THF	16	20	34	20	20	27	75	11	27

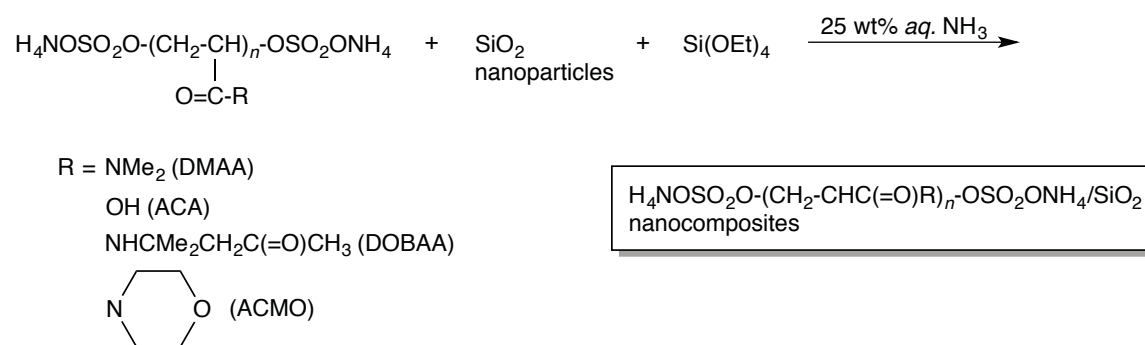
a) No gelation

C_{\min} values indicate that the gelling ability of the sulfate ester fragments end-capped oligomers is in general superior to that of the *HO-Amide* or the nitrile fragments end-capped oligomers. This finding suggests that the sulfate ester fragments end-capped oligomers are likely to promote the gelation with the ionic interaction of the sulfate ester moieties in oligomers, compared with that of the *HO-Amide* or the nitrile fragments end-capped oligomers.

2.3.2. Preparation and thermal stability of the sulfate ester fragments end-capped oligomers/silica nanocomposites

It was previously reported that two fluoroalkyl end-capped acrylic acid oligomer $[\text{R}_F\text{-(ACA)}_n\text{-R}_F]$, *N,N*-dimethylacrylamide oligomer $[\text{R}_F\text{-(DMAA)}_n\text{-R}_F]$ and *N*-(1,1-dimethyl-3-oxobutyl)acrylamide oligomer $[\text{R}_F\text{-(DOBAA)}_n\text{-R}_F]$ can undergo the sol-gel reactions in the presence of tetraethoxysilane (TEOS) and silica nanoparticles under alkaline conditions to afford the $\text{R}_F\text{-(ACA)}_n\text{-R}_F/\text{SiO}_2$ nanocomposites, the $\text{R}_F\text{-(DMAA)}_n\text{-R}_F/\text{SiO}_2$ nanocomposites, and the $\text{R}_F\text{-(DOBAA)}_n\text{-R}_F/\text{SiO}_2$ nanocomposites, respectively.³⁾ In these fluorinated oligomeric silica nanocomposites,

the $R_F-(\text{DOBAA})_n-R_F/\text{SiO}_2$ nanocomposites can supply no weight loss behavior in proportion to the contents of the oligomer in the nanocomposites even after calcination at 800 °C, although the $R_F-(\text{ACA})_n-R_F/\text{SiO}_2$ nanocomposites and the $R_F-(\text{DMAA})_n-R_F/\text{SiO}_2$ nanocomposites provide a usual weight loss corresponding to the contents of the oligomers in the nanocomposites under similar conditions.^{4, 6)} Thus, the initiator fragments end-capped oligomers/ SiO_2 nanocomposites were also prepared under similar sol-gel reactions with TEOS and silica nanoparticles in order to study the thermal stability of these nanocomposites. The results are shown in Scheme 2-2 and Table 2-3.



Scheme 2-2 Preparation of the sulfate ester fragments end-capped oligomers/ SiO_2 nanocomposites

Table 2-3 Preparation of the sulfate ester fragments end-capped oligomers [X-(M)_n-X]/SiO₂ nanocomposites

Run	Oligomer (mg)	SiO ₂ nanoparticles (mg)	TEOS (ml)	25 wt% aq. NH ₃ (ml)	Product yield ^{a)} (%)	Size of nanocomposites ^{b)}	
						Before calcination (nm)	After calcination (nm)
M in oligomer : DMAA							
1	100	500	0.25	0.25	90	218.9 ± 40.0	105.4 ± 15.2
2	150	500	0.25	0.25	68	210.9 ± 32.2	121.3 ± 12.2
3	200	500	0.25	0.25	77	190.7 ± 20.4	98.8 ± 10.4
4	250	500	0.25	0.25	60	200.1 ± 17.4	134.7 ± 20.8
5	300	500	0.25	0.25	75	245.3 ± 41.1	150.3 ± 19.3
6	400	500	0.25	0.25	64	211.4 ± 23.8	119.8 ± 26.4
M in oligomer : ACA							
7	100	500	0.25	0.25	48	207.6 ± 41.4	57.1 ± 12.2
8	150	500	0.25	0.25	61	131.1 ± 24.2	83.1 ± 13.5
9	200	500	0.25	0.25	42	165.3 ± 43.4	96.1 ± 17.4
10	250	500	0.25	0.25	50	197.2 ± 30.1	82.7 ± 15.0
11	300	500	0.25	0.25	41	144.3 ± 14.0	44.2 ± 5.3
12	400	500	0.25	0.25	70	159.2 ± 21.7	96.1 ± 18.3
M in oligomer : DOBAA							
13	100	500	0.25	0.25	63	132.3 ± 23.1	53.5 ± 11.9
14	150	500	0.25	0.25	57	125.1 ± 28.5	71.6 ± 14.4
15	200	500	0.25	0.25	47	123.5 ± 22.5	44.6 ± 11.5
16	250	500	0.25	0.25	61	154.3 ± 21.6	79.1 ± 16.1
17	300	500	0.25	0.25	59	235.2 ± 40.8	103.7 ± 14.6
18	400	500	0.25	0.25	71	161.0 ± 28.5	90.5 ± 14.4
M in oligomer : ACOMO							
19	100	500	0.25	0.25	92	125.9 ± 29.3	37.5 ± 10.8
20	150	500	0.25	0.25	93	208.1 ± 46.4	58.8 ± 13.9
21	200	500	0.25	0.25	90	111.2 ± 23.5	83.3 ± 17.5
22	250	500	0.25	0.25	93	273.0 ± 45.5	101.1 ± 27.2
23	300	500	0.25	0.25	97	154.7 ± 22.8	94.6 ± 12.2
24	400	500	0.25	0.25	94	167.3 ± 28.7	90.4 ± 12.6

a) Isolated yield based on the oligomer, SiO₂ nanoparticles, and TEOS

b) Determined by DLS (dynamic light scattering) measurements in methanol solutions

As shown in Scheme 2-2 and Table 2-3, the expected oligomers/SiO₂ composites were obtained in excellent to moderate isolated yields (41 ~ 97 %). The oligomeric silica composites thus obtained were found to exhibit a good dispersibility and stability toward water and traditional organic solvents such as methanol, ethanol, acetone, tetrahydrofuran, ethyl acetate, 1,2-dichloroethane, and dimethyl sulfoxide.

Thus, the average particle sizes of these composites were measured in methanol by dynamic light scattering (DLS) measurements at 25 °C, and the results are also shown in Table 2-3.

Table 2-3 shows that the present composites are nanometer size-controlled fine particles: 111 ~ 273 nm. Especially, the effective decrease of each oligomeric silica nanocomposites particle size through the calcination was observed as illustrated in Table 2-3. The field emission scanning electron micrograph (FE-SEM) measurements of well-dispersed composite methanol solutions also show the decrease of the nanocomposite particle size after calcination (see Figs. 2-3 ~ 2-6). These findings suggest that the sulfate ester fragments end-capped oligomers should afford the weight loss characteristic in the nanocomposite matrices during the calcination process. To verify this weight loss characteristic, the thermal stability of these oligomeric silica nanocomposites was studied by the use of thermogravimetric analyses (TGA), in which the weight loss of these nanocomposites was measured by raising the temperature around 800 °C at a 10 °C/min heating rate under air atmospheric conditions, and the results are shown in Fig. 2-7.

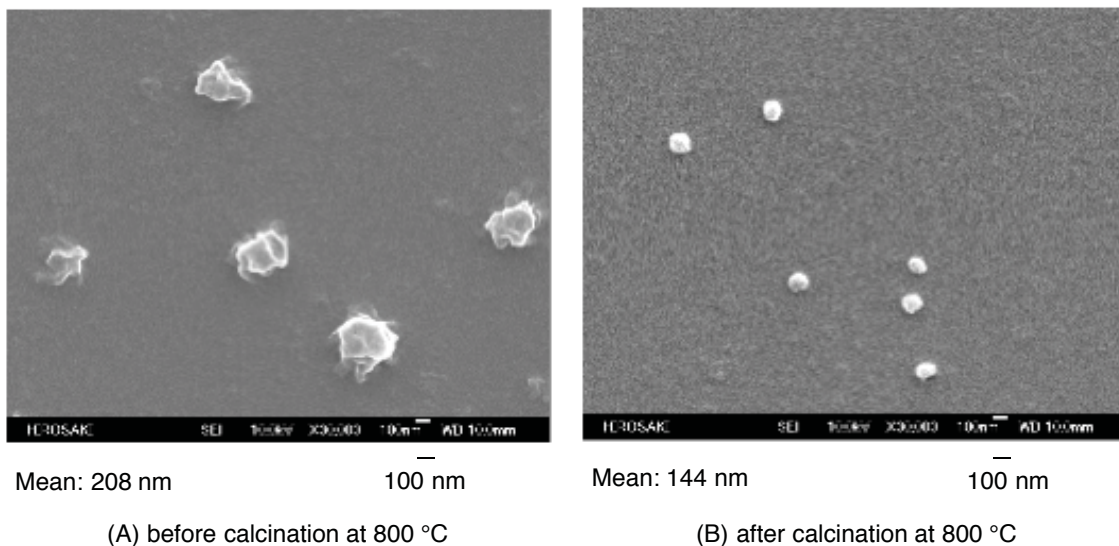


Fig. 2-3 FE-SEM (Field Emission Scanning Electron Microscopy) images of the sulfate ester fragments end-capped DMAA oligomer/SiO₂ nanocomposites (Run 1 in Table 2-3)

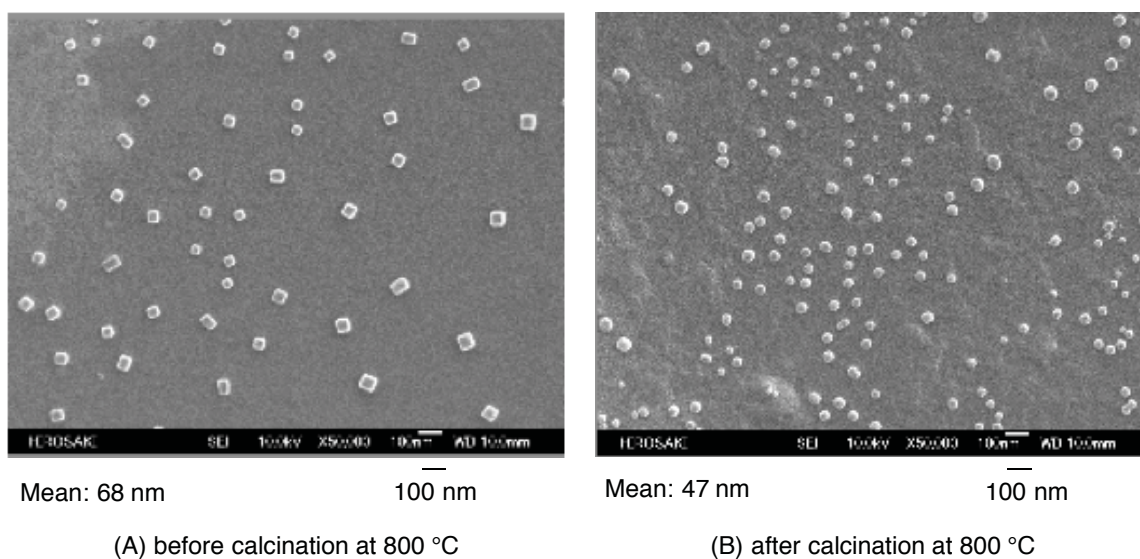


Fig. 2-4 FE-SEM (Field Emission Scanning Electron Microscopy) images of the sulfate ester fragments end-capped ACA oligomer/SiO₂ nanocomposites (Run 7 in Table 2-3)

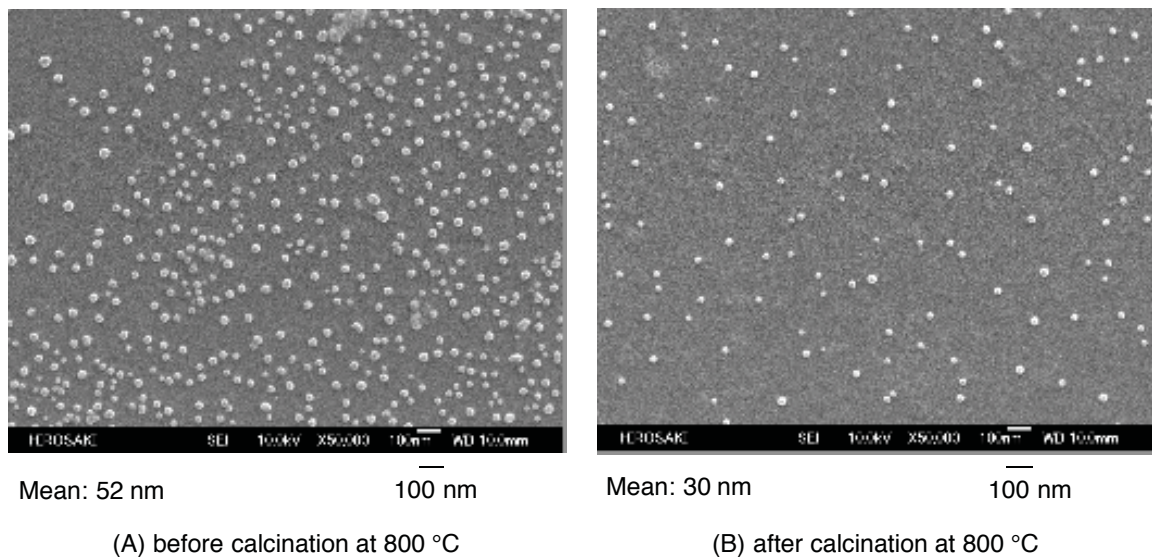


Fig. 2-5 FE-SEM (Field Emission Scanning Electron Microscopy) images of the sulfate ester fragments end-capped DOBAA oligomer/SiO₂ nanocomposites (Run 13 in Table 2-3)

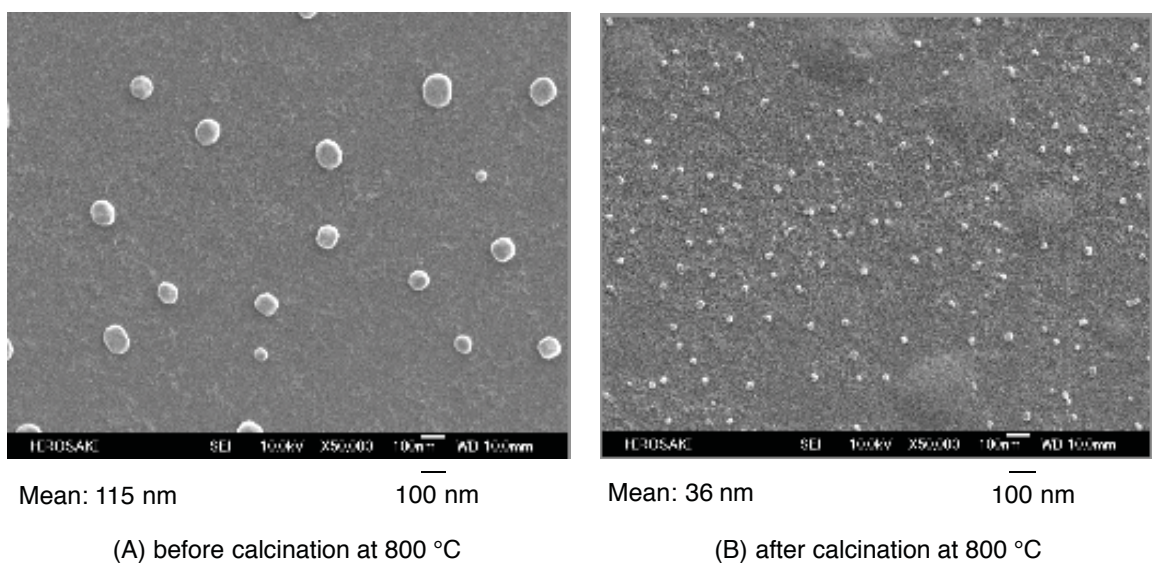


Fig. 2-6 FE-SEM (Field Emission Scanning Electron Microscopy) images of the sulfate ester fragments end-capped ACOMO oligomer/SiO₂ nanocomposites (Run 19 in Table 2-3)

As shown in Fig. 2-7, the sulfate ester fragments end-capped DMAA oligomer/SiO₂ nanocomposites exhibited a clear weight loss corresponding to the contents of oligomer in the composites after calcination at 800 °C. A similar weight loss behavior was

observed in the ACA oligomer/silica nanocomposites (see Fig. 2-8), the DOBAA oligomer/silica nanocomposites (see Fig. 2-9) and the ACOMO oligomer/silica nanocomposites (see Fig. 2-10). FT-IR spectra of these nanocomposites also show the disappearance of the characteristic peaks related to these oligomers in the composites after calcination at 800 °C (data not shown).

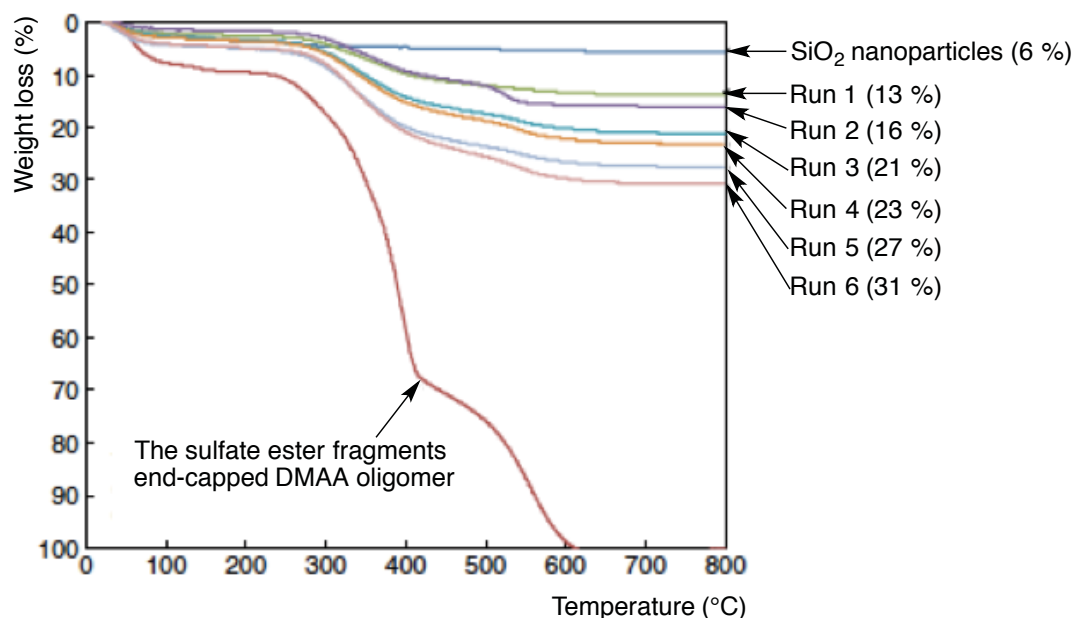


Fig. 2-7 Thermogravimetric analyses of the sulfate ester fragments end-capped DMAA oligomer/SiO₂ nanocomposites (Runs 1 ~ 6 in Table 2-3)

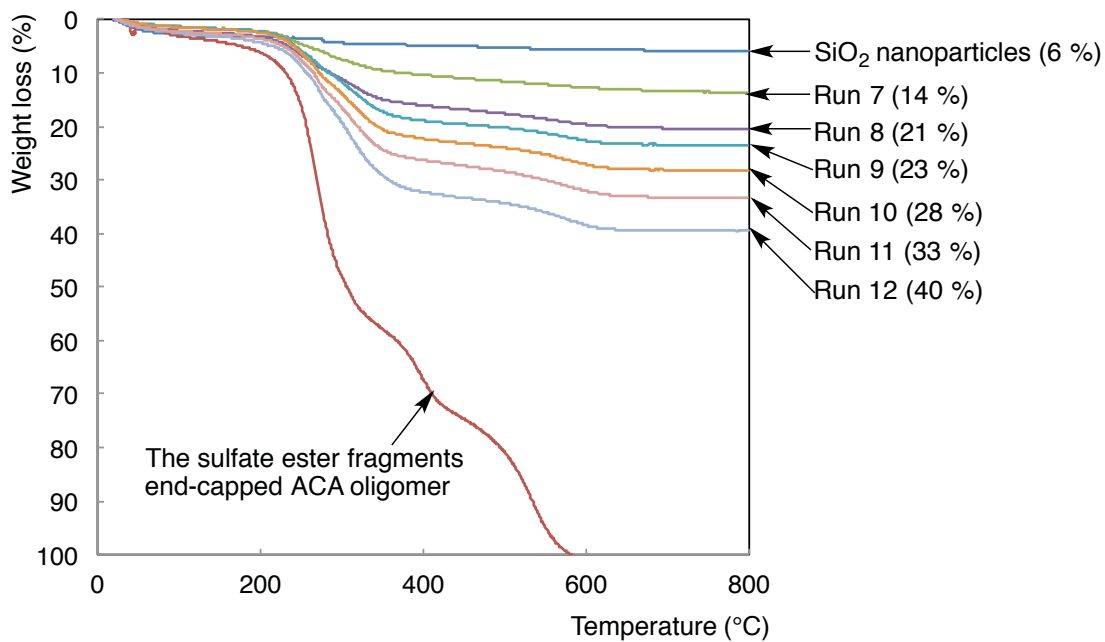


Fig. 2-8 Thermogravimetric analyses of the sulfate ester fragments end-capped ACA oligomer/SiO₂ nanocomposites (Runs 7 ~ 12 in Table 2-3)

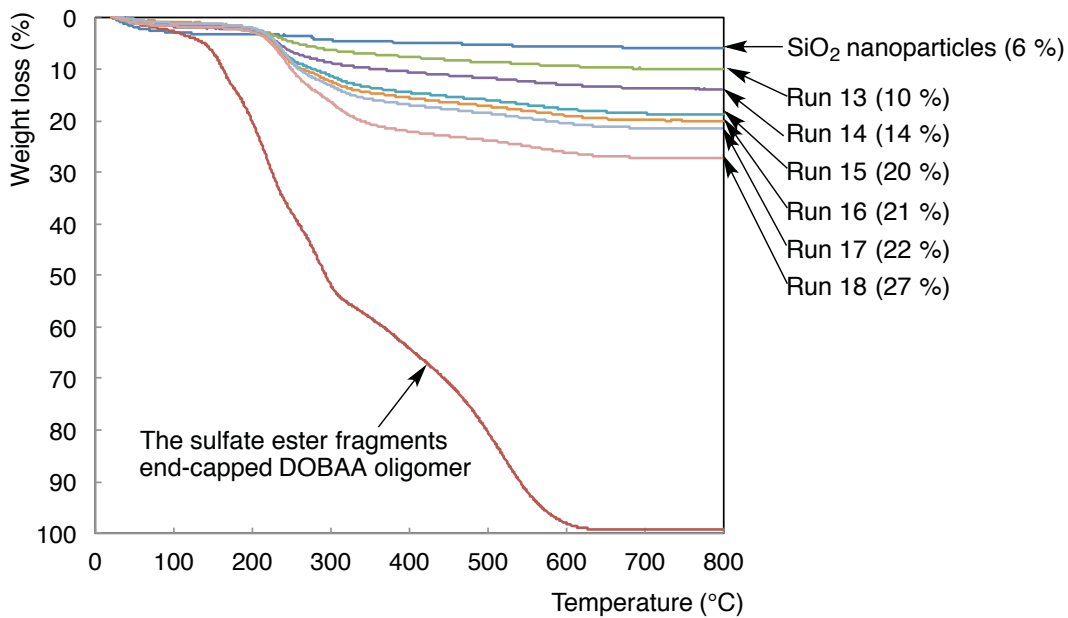


Fig. 2-9 Thermogravimetric analyses of the sulfate ester fragments end-capped DOBAA oligomer/SiO₂ nanocomposites (Runs 13 ~ 18 in Table 2-3)

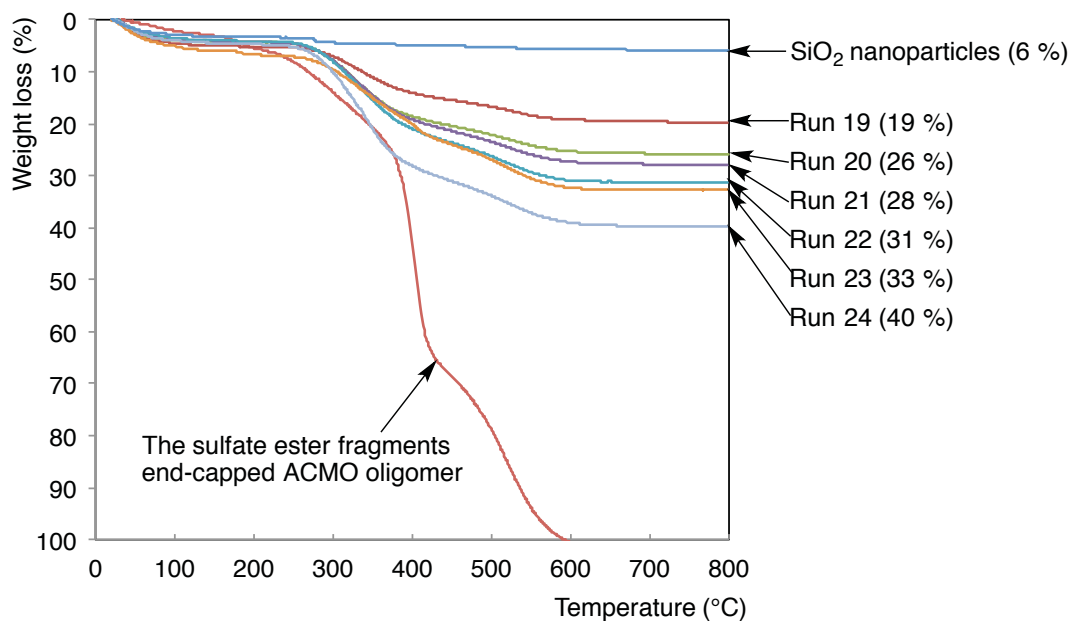
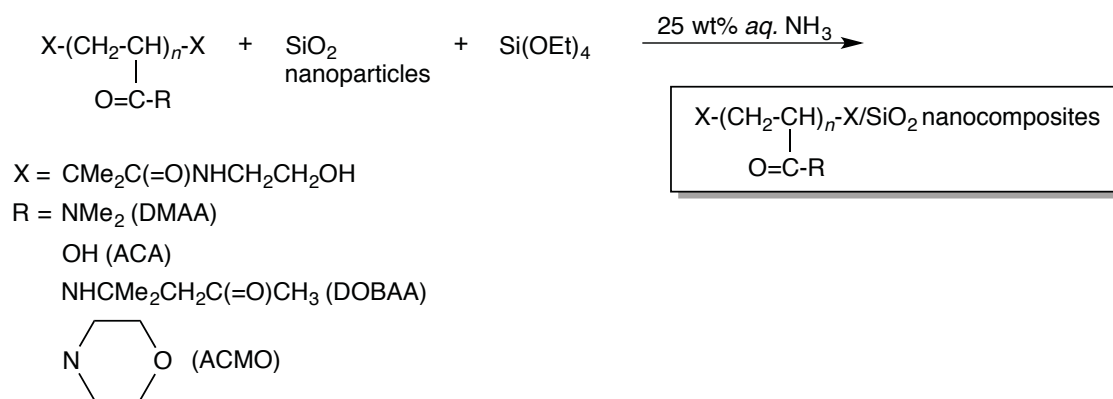


Fig. 2-10 Thermogravimetric analyses of the sulfate ester fragments end-capped ACMO oligomer/SiO₂ nanocomposites (Runs 19 ~ 24 in Table 2-3)

2.3.3. Preparation and thermal stability of the 2-methyl-*N*-(2-hydroxyethyl)propionamide fragments end-capped oligomers/silica nanocomposites

The 2-methyl-*N*-(2-hydroxyethyl)propionamide [*HO-Amide*] fragments end-capped oligomers/silica nanocomposites were prepared by the similar sol-gel reactions with that of the sulfate ester fragments end-capped oligomers/silica nanocomposites in Scheme 2-2.

The results are shown in Scheme 2-3 and Table 2-4.



Scheme 2-3 Preparation of the *OH-Amide* fragments end-capped oligomers [X-(CH₂CHC(=O)R)_n-X]/SiO₂ nanocomposites

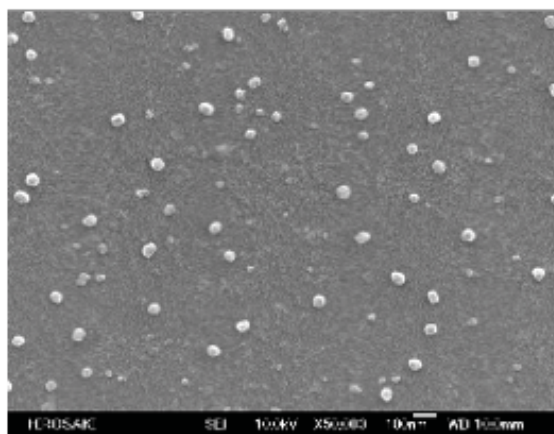
Table 2-4 Preparation of the *HO-Amide* fragments end-capped oligomers [X-(M)_n-X]/SiO₂ nanocomposites

Run	Oligomer (mg)	SiO ₂ nanoparticles (mg)	TEOS (ml)	25 wt% aq. NH ₃ (ml)	Product yield ^{a)} (%)	Size of nanocomposites ^{b)}	
						Before calcination (nm)	After calcination (nm)
M in oligomer : DMAA							
1	100	500	0.25	0.25	76	25.9 ± 5.6	54.1 ± 3.6
2	150	500	0.25	0.25	89	35.3 ± 7.5	38.1 ± 9.2
3	200	500	0.25	0.25	72	36.2 ± 5.6	39.1 ± 5.3
4	250	500	0.25	0.25	67	34.2 ± 9.8	36.5 ± 3.5
5	300	500	0.25	0.25	55	70.4 ± 4.6	88.2 ± 11.2
6	400	500	0.25	0.25	42	55.2 ± 5.3	64.3 ± 6.5
M in oligomer : ACA							
7	100	500	0.25	0.25	80	78.6 ± 10.2	66.0 ± 8.2
8	150	500	0.25	0.25	84	41.9 ± 4.0	39.0 ± 4.8
9	200	500	0.25	0.25	49	94.7 ± 9.0	97.8 ± 11.5
10	250	500	0.25	0.25	53	75.9 ± 9.1	65.5 ± 7.6
11	300	500	0.25	0.25	47	85.1 ± 7.3	74.8 ± 8.8
12	400	500	0.25	0.25	43	63.7 ± 6.4	89.9 ± 11.4
M in oligomer : DOBAA							
13	100	500	0.25	0.25	86	43.1 ± 4.4	78.9 ± 11.2
14	150	500	0.25	0.25	83	47.0 ± 3.1	47.1 ± 3.1
15	200	500	0.25	0.25	76	86.4 ± 9.9	73.2 ± 7.2
16	250	500	0.25	0.25	69	41.3 ± 4.6	53.5 ± 3.4
17	300	500	0.25	0.25	52	33.9 ± 6.1	43.7 ± 5.3
18	400	500	0.25	0.25	31	63.2 ± 6.8	63.6 ± 6.4
M in oligomer : ACMO							
19	100	500	0.25	0.25	70	62.9 ± 5.9	65.7 ± 7.8
20	150	500	0.25	0.25	63	86.8 ± 10.5	88.6 ± 15.1
21	200	500	0.25	0.25	87	44.8 ± 5.7	83.4 ± 8.3
22	250	500	0.25	0.25	62	40.5 ± 2.5	37.5 ± 4.2
23	300	500	0.25	0.25	55	67.0 ± 8.2	67.9 ± 8.4
24	400	500	0.25	0.25	62	63.8 ± 9.1	54.1 ± 6.7

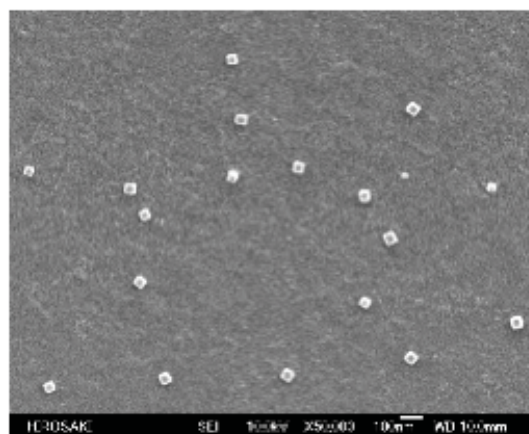
a) Isolated yield based on the oligomer, SiO₂ nanoparticles, and TEOS

b) Determined by DLS (dynamic light scattering) measurements in methanol solutions

As shown in Scheme 2-3 and Table 2-4, the *HO-Amide* fragments end-capped oligomers/silica nanocomposites were obtained in 31 ~ 89 % isolated yields, respectively. These obtained composites were found to afford a good dispersibility and stability toward not only water but also the traditional organic media such as dichloromethane, 2-propanol, 1,2-dichloroethane, methanol, tetrahydrofuran, acetonitrile, *t*-butyl alcohol, acetone, ethanol and ethyl acetate. DLS measurements show that the average particle sizes of these obtained composites are nanometer size-controlled fine particles (26 ~ 87 nm), and the distinct decrease of the particle sizes was not observed through the calcination process. In fact, FE-SEM measurements show that the similar particle sizes of the composites can be observed before and even after calcination at 800 °C (see Figs. 2-11 ~ 2-14).

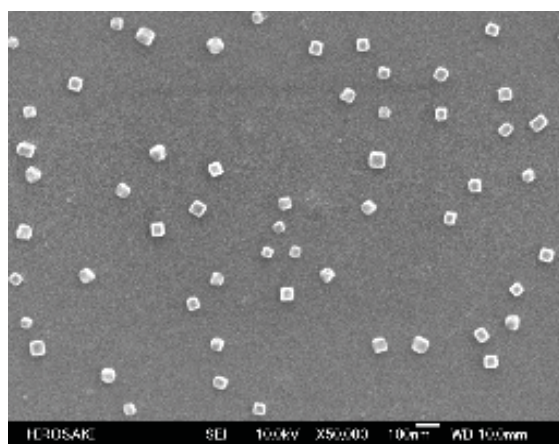


Mean: 60 nm
100 nm
(A) before calcination at 800 °C

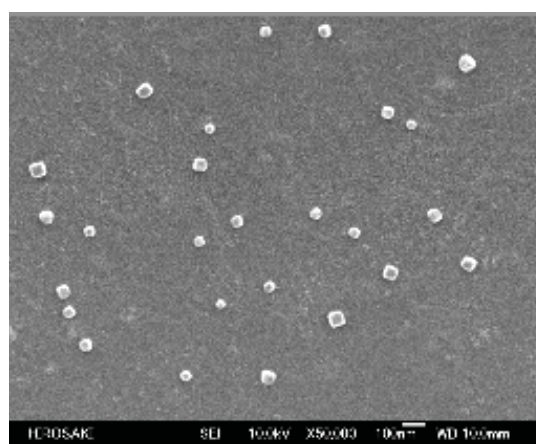


Mean: 54 nm
100 nm
(B) after calcination at 800 °C

Fig. 2-11 FE-SEM (Field Emission Scanning Electron Microscopy) images of the *HO-Amide* fragments end-capped DMAA oligomer/SiO₂ nanocomposites (Run 2 in Table 2-4)

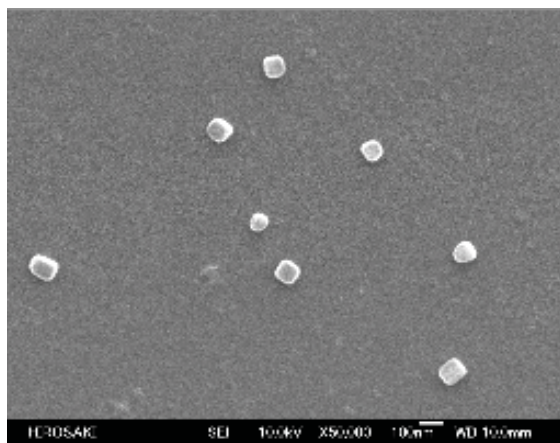


Mean: 60 nm
100 nm
(A) before calcination at 800 °C



Mean: 49 nm
100 nm
(B) after calcination at 800 °C

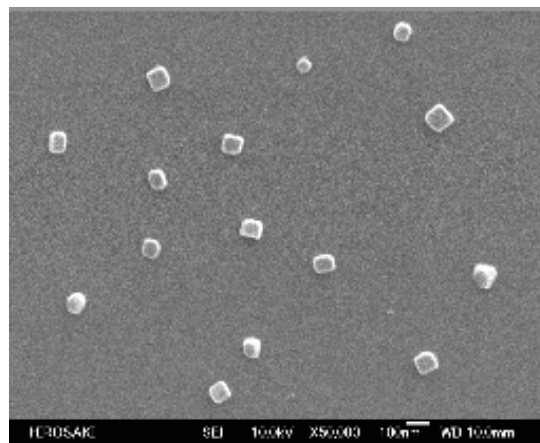
Fig. 2-12 FE-SEM (Field Emission Scanning Electron Microscopy) images of the *HO-Amide* fragments end-capped ACA oligomer/SiO₂ nanocomposites (Run 8 in Table 2-4)



Mean: 80 nm

100 nm

(A) before calcination at 800 °C

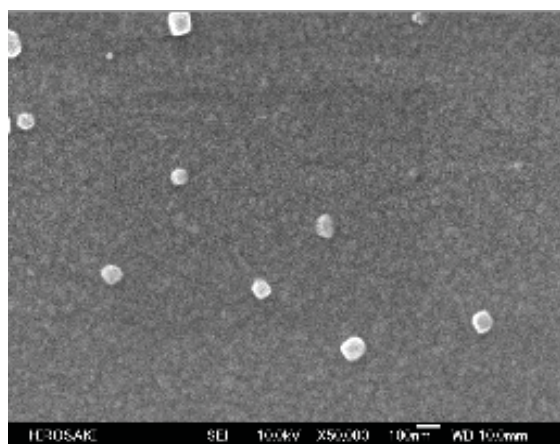


Mean: 81 nm

100 nm

(B) after calcination at 800 °C

Fig. 2-13 FE-SEM (Field Emission Scanning Electron Microscopy) images of the *HO-Amide* fragments end-capped DOBAA oligomer/SiO₂ nanocomposites (Run 13 in Table 2-4)



Mean: 75 nm

100 nm

(A) before calcination at 800 °C



Mean: 88 nm

100 nm

(B) after calcination at 800 °C

Fig. 2-14 FE-SEM (Field Emission Scanning Electron Microscopy) images of the *HO-Amide* fragments end-capped ACMO oligomer/SiO₂ nanocomposites (Run 21 in Table 2-4)

Thermal stability of a variety of the *HO-Amide* fragments end-capped oligomers/silica nanocomposites in Table 2-4 was studied by the use of TGA measurements under similar conditions as those of Fig. 2-7, and the results are shown in Fig. 2-15.

Figure 2-15 shows the TGA curves of the parent silica nanoparticles and the *HO-Amide* fragments end-capped DMAA oligomer in Table 2-4. Interestingly, these DMAA oligomers were unable to exhibit a clear weight loss, which corresponds to the contents of the oligomers in the nanocomposites even after calcination at 800 °C, quite similar to that of the original silica nanoparticles. Similarly, the *HO-Amide* fragments end-capped ACA oligomers, DOBAA oligomers, and ACMO oligomers illustrated in Table 2-4 were found to afford no weight loss corresponding to the contents of the oligomers in the composites even after calcination at 800 °C (see Figs. 2-16 ~ 2-18).

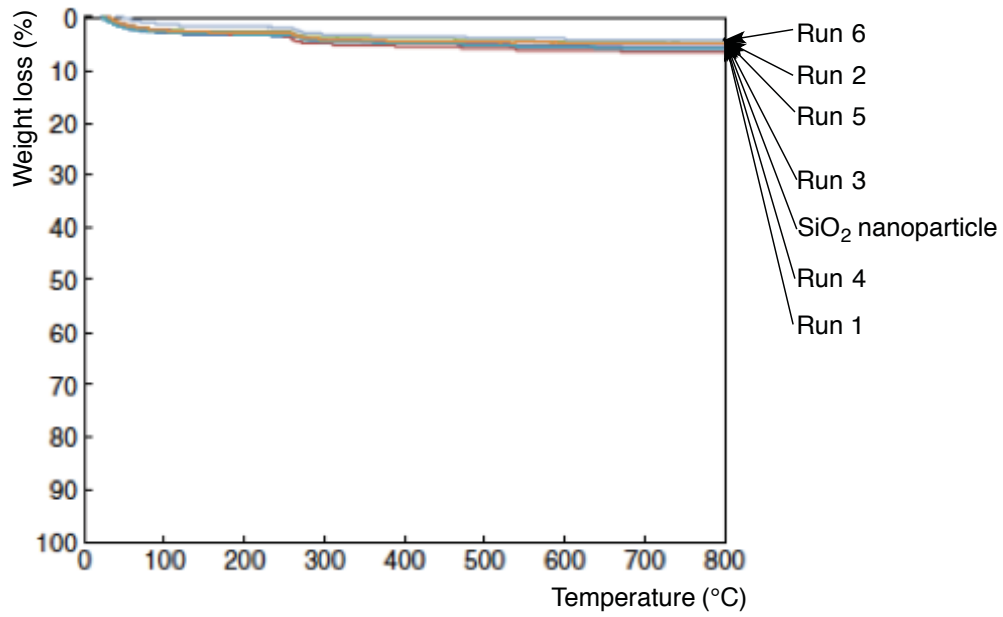


Fig. 2-15 Thermogravimetric analyses of the *HO-Amide* fragments end-capped DMAA oligomer/SiO₂ nanocomposites (Runs 1 ~ 6 in Table 2-4)

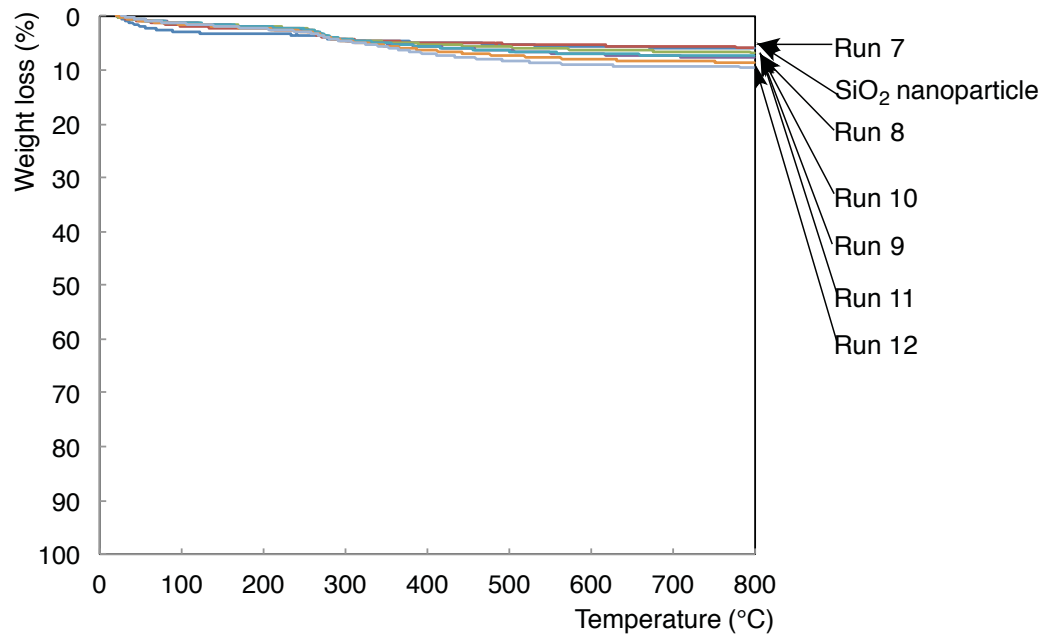


Fig. 2-16 Thermogravimetric analyses of the *HO-Amide* fragments end-capped ACA oligomer/SiO₂ nanocomposites (Runs 7 ~ 12 in Table 2-4)

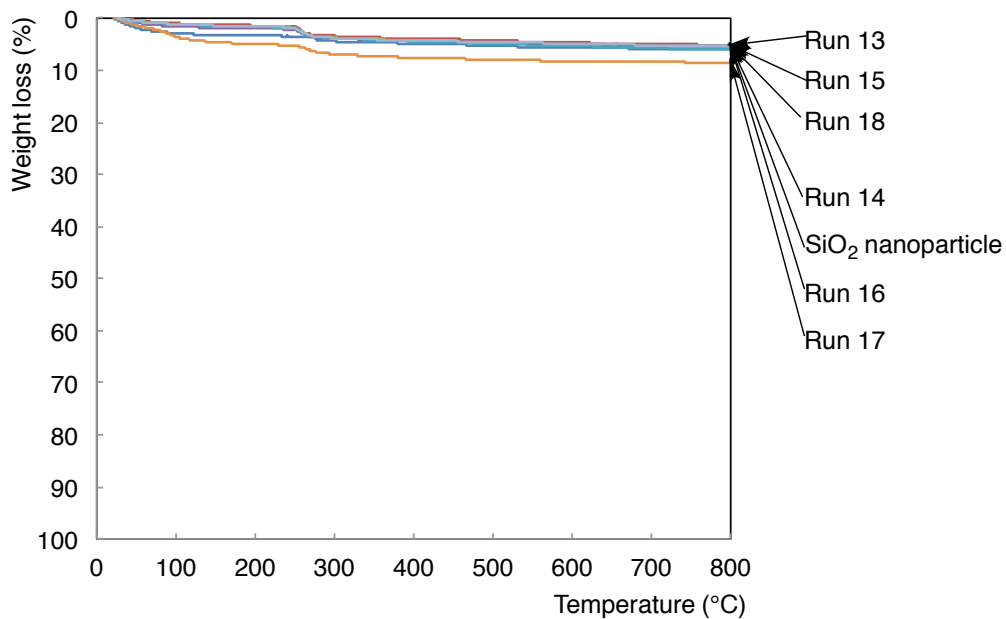


Fig. 2-17 Thermogravimetric analyses of the *HO-Amide* fragments end-capped DOBAA oligomer/SiO₂ nanocomposites (Runs 13 ~ 18 in Table 2-4)

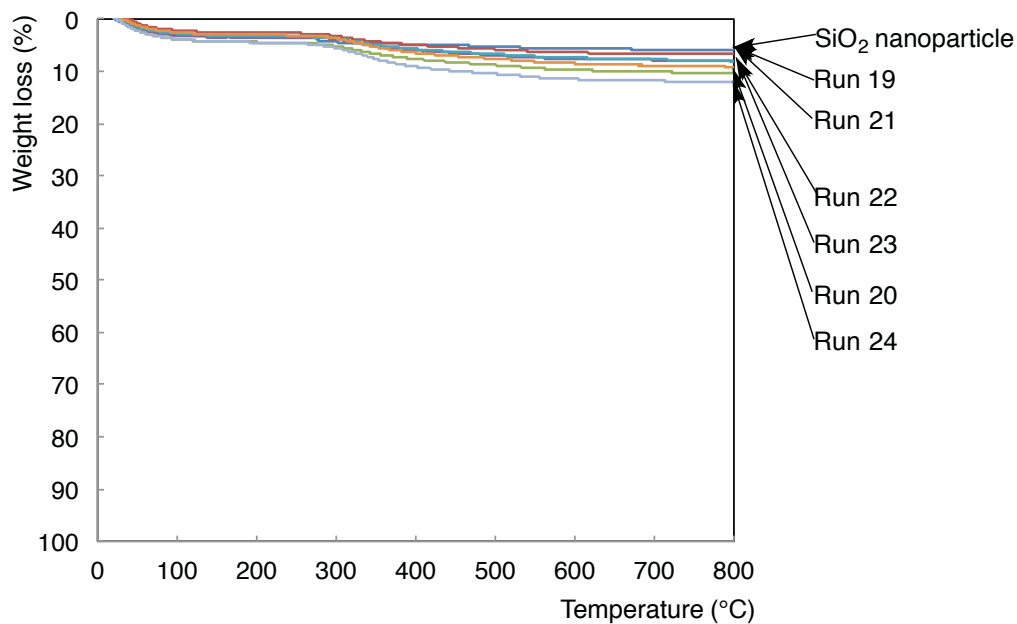


Fig. 2-18 Thermogravimetric analyses of the *HO-Amide* fragments end-capped ACMO oligomer/SiO₂ nanocomposites (Runs 19 ~ 24 in Table 2-4)

In this way, it was demonstrated that the present *HO-Amide* fragments end-capped oligomers can exhibit no weight loss in the silica nanocomposite matrices even after calcination at 800 °C. In order to clarify the presence of these oligomers in the nanocomposites, the contents of the unreacted oligomers isolated from the supernatant solution in the preparation of the oligomeric silica nanocomposites were determined by using the TGA measurements, and the contents of the unreacted and reacted oligomers are as follows:

Run No. in Table 2-4	Used oligomer ^{a)} (mg)	Unreacted oligomer (mg)	Oligomer in the composites [mg] ^{b)}
Run 2	150	116	34 [665] ^{c)} (11 %) ^{d)} (5 %) ^{e)}
Run 8	150	112	38 [485] ^{c)} (14 %) ^{d)} (6 %) ^{e)}
Run 13	100	56	44 [650] ^{c)} (13 %) ^{d)} (6 %) ^{e)}
Run 21	200	136	64 [740] ^{c)} (15 %) ^{d)} (6 %) ^{e)}
Original silica nanoparticles			(6 %) ^{e)}

a) Used oligomer for the preparation of the nanocomposites

b) Content of the oligomer in the nanocomposites derived from the unreacted oligomer

c) Isolated yield of the nanocomposites

d) Theoretical weight loss at 800 °C derived from the contents of the oligomers in the composites

e) Weight loss derived from the TGA curve at 800 °C

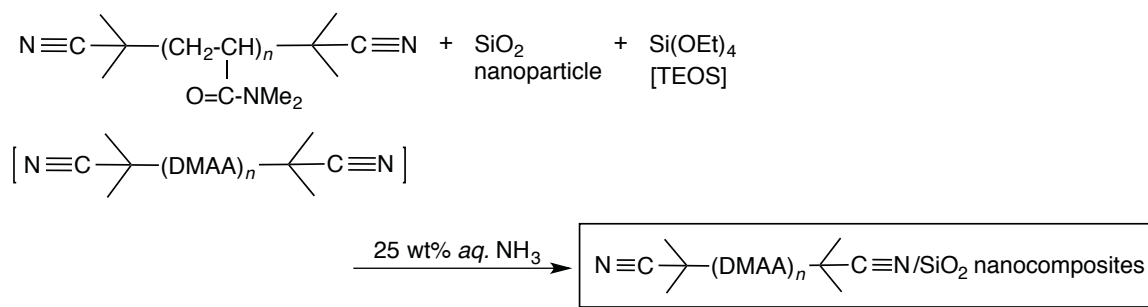
The contents of the oligomers in the nanocomposites were estimated to be from 34 to 64 mg, and the contents of the oligomers based on the isolated nanocomposites were also

estimated to be 5 % (Run 2), 8 % (Run 8), 7 % (Run 13) and 9 % (Run 21), respectively.

Thus, the theoretical weight loss of the nanocomposites at 800 °C based on that (6 %) of the original silica nanoparticles are from 11 to 15 % as mentioned above. However, the *HO-Amide* fragments end-capped oligomers/silica nanocomposites exhibited no weight loss behavior even after calcination at 800 °C, whose TGA curve is quite similar to that of the original silica nanoparticles, indicating that the oligomers can provide no weight loss characteristic in the silica gel matrices even after calcination at 800 °C.

2.3.4. Preparation and thermal stability of the nitrile fragments end-capped *N,N*-dimethylacrylamide oligomers/silica nanocomposites

The nitrile fragments end-capped *N,N*-dimethylacrylamide (DMAA) oligomers/silica nanocomposites were prepared under the similar sol-gel reactions as those of Scheme 2-3, and the results are shown in Scheme 2-4 and Table 2-5.



Scheme 2-4 Preparation of the nitrile fragments end-capped DMAA oligomer/SiO₂ nanocomposites

Table 2-5 Preparation of the nitrile fragments end-capped DMAA oligomer/SiO₂ nanocomposites

Run	Oligomer (mg)	SiO ₂ nanoparticles (mg)	TEOS (ml)	25 wt% aq. NH ₃ (ml)	Product yield ^{a)} (%)	Size of nanocomposites ^{b)}	
						Before calcination (nm)	After calcination (nm)
1	100	500	0.25	0.25	66	60.8 ± 13.1	35.8 ± 8.4
2	150	500	0.25	0.25	77	58.6 ± 12.4	48.8 ± 10.3
3	200	500	0.25	0.25	68	62.6 ± 10.0	52.7 ± 10.0
4	250	500	0.25	0.25	52	74.8 ± 12.7	62.3 ± 11.3
5	300	500	0.25	0.25	11	58.9 ± 15.3	44.5 ± 10.7

a) Isolated yield based on the oligomer, SiO₂ nanoparticles, and TEOS

b) Determined by DLS (dynamic light scattering) measurements in methanol solutions

The nitrile fragments end-capped DMAA oligomer/SiO₂ nanocomposites were obtained in 11 ~ 77 % isolated yields. These obtained DMAA oligomeric silica composites have a good dispersibility and stability toward water and traditional organic media such as dichloromethane, 2-propanol, 1,2-dichloroethane, methanol, tetrahydrofuran, acetonitrile, *t*-butyl alcohol, acetone, ethanol, and ethyl acetate except for hexane and diethyl ether. Thus, the average particle sizes of these composites in methanol

have been measured by using DLS measurements, and the results are also shown in Table 2-5.

As shown in Table 2-5, the average particle sizes of the composites are nanometer size-controlled: 59 ~ 75 nm, and the similar particle sizes: 36 ~ 62 nm were observed even after calcination at 800 °C. FE-SEM pictures of the nitrile fragments end-capped DMAA oligomers (Run 1 in Table 2-5) show the formation of very fine nanoparticles with mean diameters: 60 nm before calcination and 70 nm after calcination, respectively (see Fig. 2-19).

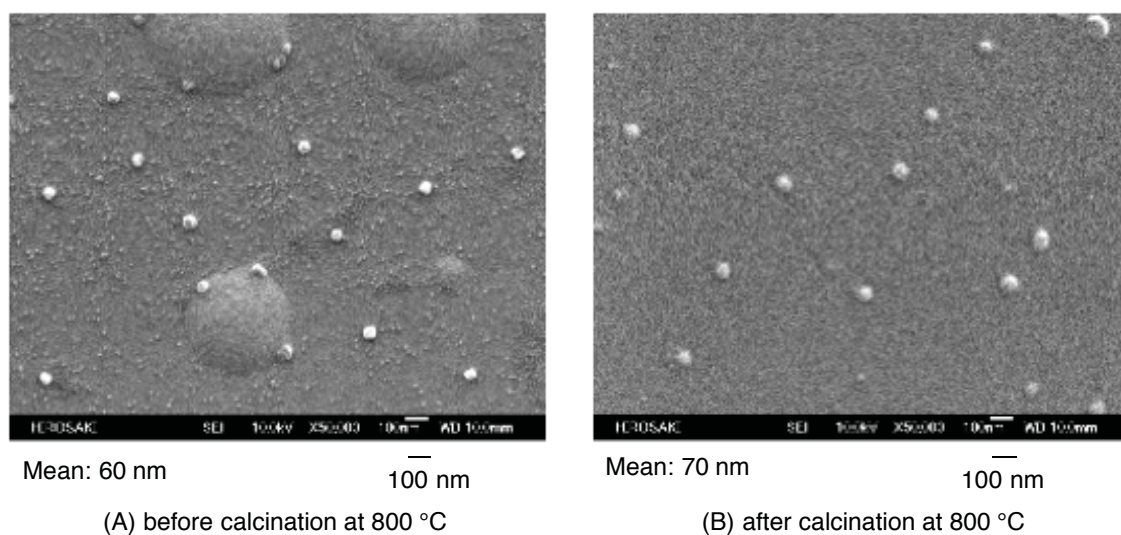


Fig. 2-19 FE-SEM (Field Emission Scanning Electron Microscopy) images of the nitrile fragments end-capped DMAA oligomer/SiO₂ nanocomposites (Run 1 in Table 2-5) in methanol solution

Thermal stability of these obtained nanocomposites was studied by the use of TGA measurements, and the results are shown in Fig. 2-20.

Figure 2-20 shows that each DMAA oligomer/silica nanocomposites can give the quite similar TGA curves to that of the parent silica nanoparticles to indicate no weight loss corresponding to the contents of the oligomer in the nanocomposite matrices even after calcination at 800 °C.

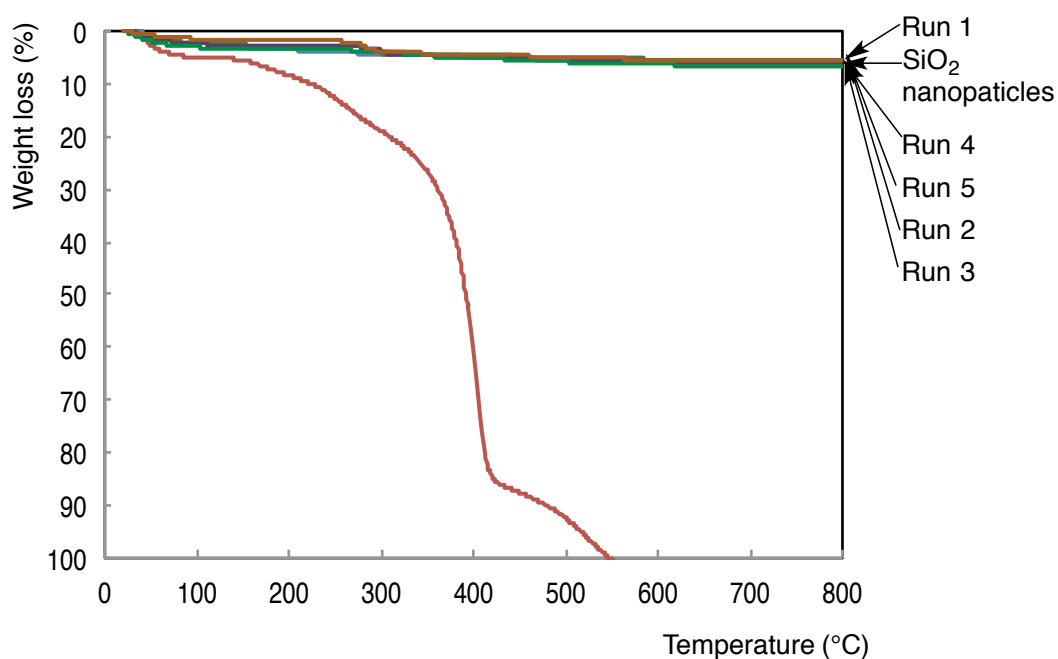


Fig. 2-20 Thermogravimetric analyses of the nitrile fragments end-capped DMAA oligomer/SiO₂ nanocomposites (Runs 1 ~ 5 in Table 2-5)

2.3.5. Discussion on the thermal stability of the initiator fragments end-capped oligomers/silica nanocomposites

To verify such interesting no weight loss behavior, ^1H MAS NMR spectra of the nitrile fragments end-capped DMAA oligomer/silica nanocomposites before and after calcination at $800\text{ }^\circ\text{C}$ were studied, and the results are shown in Fig. 2-21.

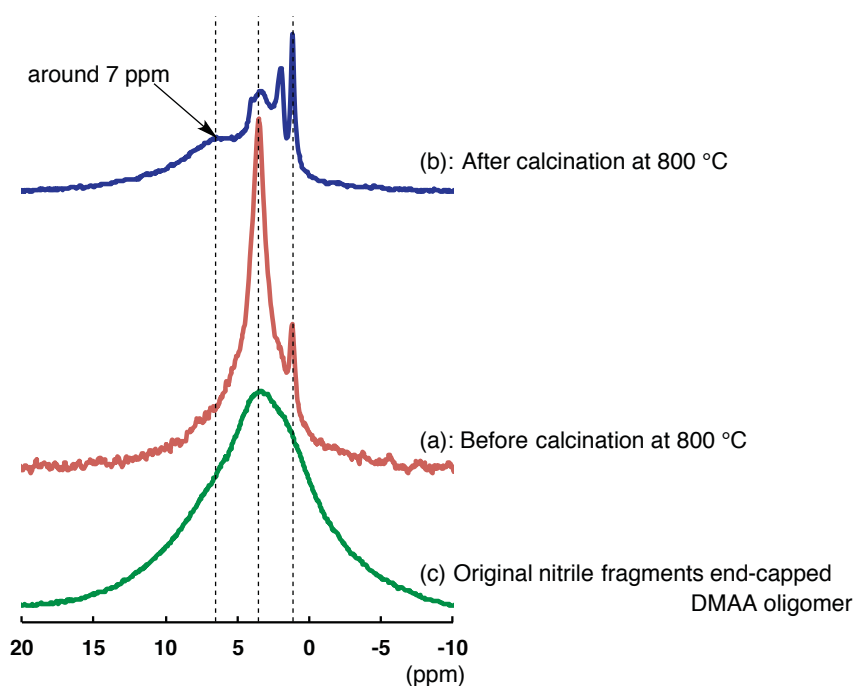
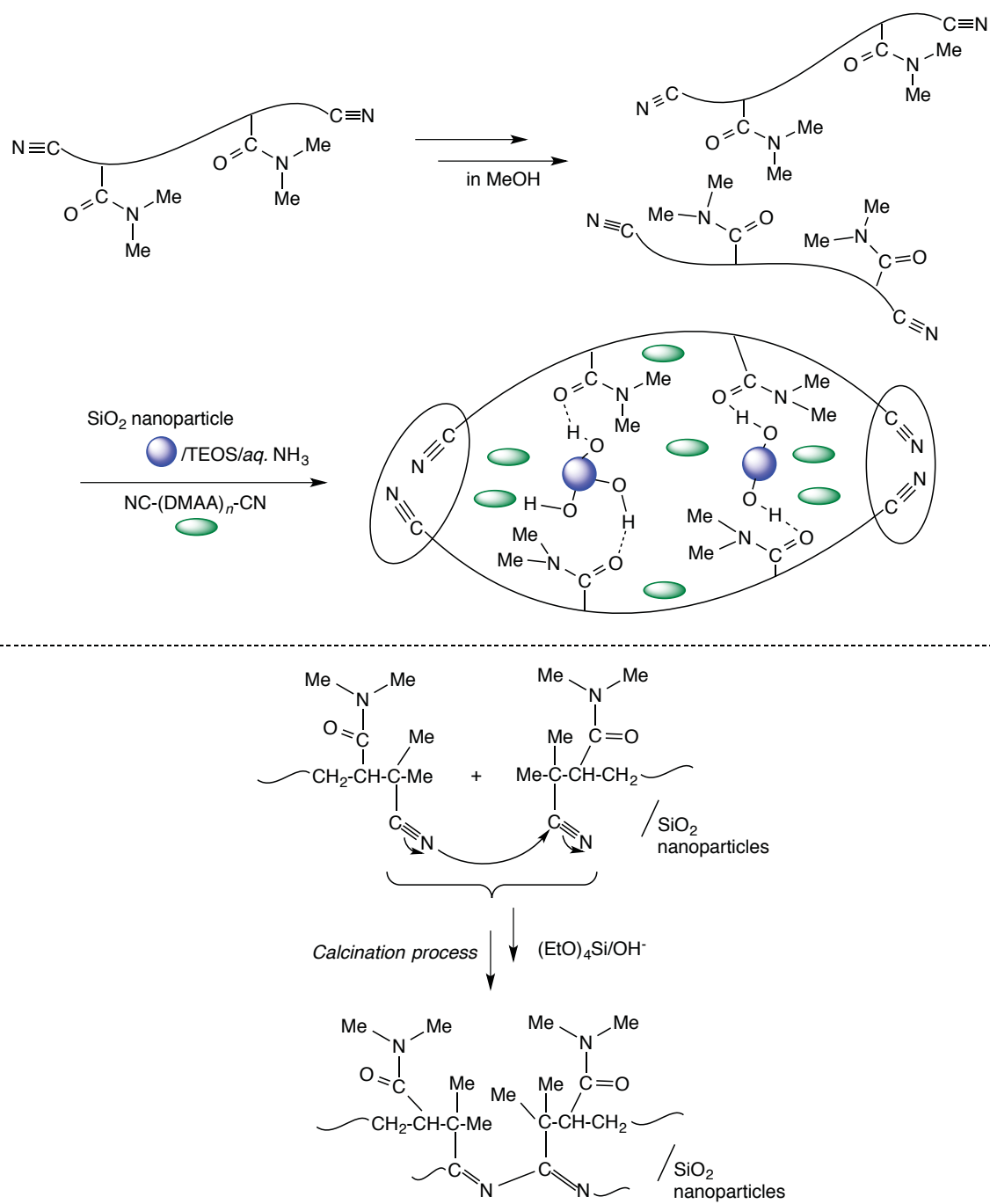


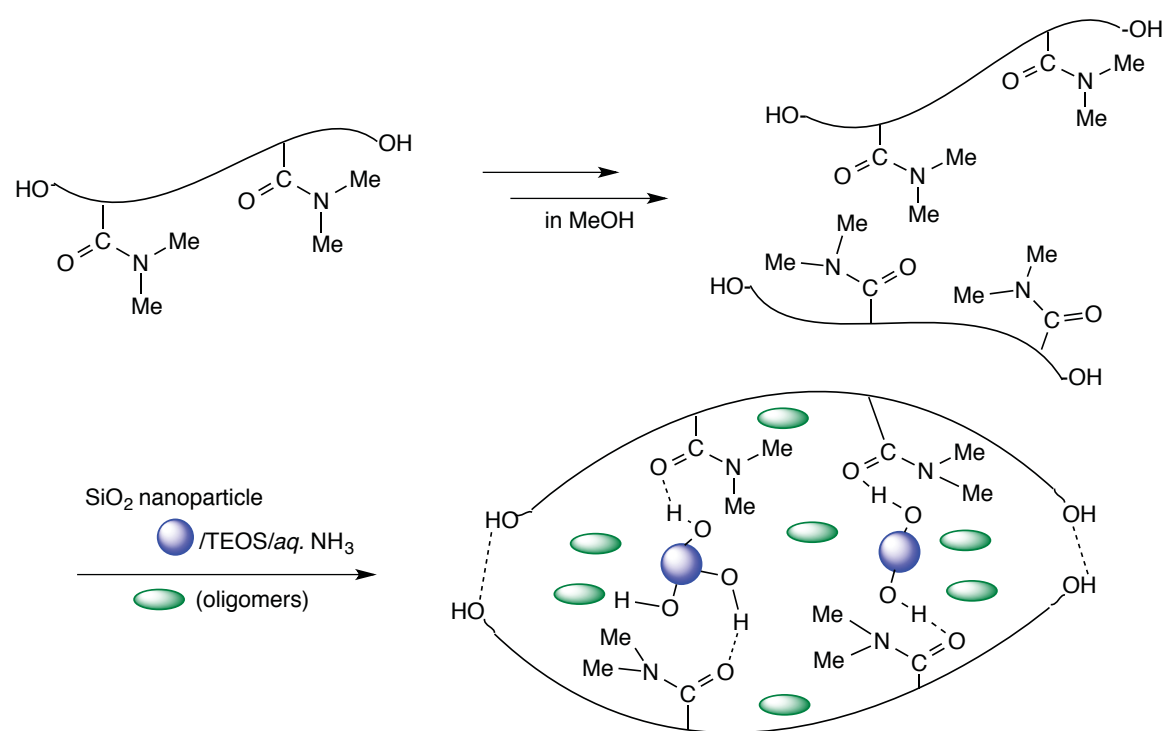
Fig. 2-21 ^1H MAS (magic-angle spinning) NMR spectra of the nitrile fragments end-capped DMAA oligomer/ SiO_2 nanocomposites (Run 1 in Table 2-5) before (a) and after (b) calcination at $800\text{ }^\circ\text{C}$ and original nitrile fragments end-capped DMAA oligomer (c)

As shown in Fig. 2-21, the relatively sharp peaks related to the parent DMAA oligomer [Fig. 2-21-(c)] in the nanocomposites were observed before calcination [Fig. 2-21-(a)] and after calcination [Fig. 2-21-(b)]. Especially, the new signal has been appeared at around 7 ppm after calcination, indicating the formation of imine units after calcination. It is well known that polyacrylonitrile (PAN) $[-(\text{CH}_2\text{CH}(\text{CN})_n-)]$ can enhance its thermal stability due to the cyclization of nitrile groups in PAN leading to the unsaturated $>\text{C}=\text{N}-$ species and the conjugated $>\text{C}=\text{N}-$ species.^{8,9,11)} From these finding, the end-capped nitrile groups in oligomer would interact with each other to form imine units ($>\text{C}=\text{N}\sim$) during the calcination process. Such interaction should afford no weight loss toward the nitrile fragments end-capped DMAA oligomer in the silica nanocomposites matrices as shown in Scheme 2-5 because the DMAA oligomers should be smoothly encapsulated into such oligomeric silica nanocomposite matrices to afford the no weight loss characteristic toward the corresponding oligomers.



Scheme 2-5 Schematic illustration for the preparation of the nitrile fragments end-capped DMAA oligomer/SiO₂ nanocomposites: formation of the >C=N- units in the nanocomposites

As mentioned above, the *HO-Amide* fragments end-capped DMAA oligomer/, ACA oligomer/, DOBAA oligomer/ and ACOMO oligomer/silica nanocomposites can provide no weight loss characteristic corresponding to the contents of these oligomers in the silica gel matrices even after calcination. This no weight loss behavior would be due to the effective intermolecular hydrogen-bonding interactions between the end-capped *HO-Amide* fragments to form the *HO-Amide* fragments end-capped oligomeric silica nanocomposites as shown in Scheme 2-6. Especially, the oligomers should be predominantly encapsulated into such oligomeric silica nanocomposite cores to provide no weight loss behavior even after calcination.



Scheme 2-6 Schematic illustration for the preparation of the *HO-Amide* fragments end-capped oligomers/SiO₂ nanocomposites

In addition, the energy dispersive X-ray analyses (EDX) of the *HO-Amide* fragments end-capped oligomers/silica nanocomposites (Runs 2, 8, 13, and 21 in Table 2-4) have been measured to verify the presence of the corresponding oligomer in the silica nanocomposite cores before and after calcination at 800 °C, and the results are as follows:

Run	Atomic contents (atm, %)							
	Before calcination				After calcination			
	C	N	O	Si	C	N	O	Si
2	14.0	21.1	55.6	9.3	15.5	20.6	52.5	11.4
6	10.2	-	64.0	25.8	10.5	-	70.7	18.8
13	10.2	21.0	53.9	14.9	12.4	21.3	53.7	12.6
21	15.5	20.9	54.3	9.3	16.9	20.4	41.6	21.1

Interestingly, the *HO-Amide* fragments end-capped oligomers/silica nanocomposites after calcination at 800 °C exhibited the similar atomic (carbon and nitrogen) content values to those before calcination, indicating that the present nanocomposites should provide no weight loss behavior corresponding to the contents of the oligomers in the composite cores even after calcination at 800 °C.

On the other hand, the sulfate ester fragments end-capped DMAA oligomer/, ACA oligomer/, DOBAA oligomer/ and ACMO oligomer/silica nanocomposites afford a

clear weight loss corresponding to the contents of these oligomers in the composite matrices after calcination as shown in Fig. 2-7. Hitherto, it is well known that the sulfate esters $[(RO)_2SO_2]$ decompose to afford the corresponding alcohol (ROH) with the formation of sulfuric acid.²²⁾ Thus, it is suggested that the sulfate ester fragments end-capped oligomers $[NH_4OSO_2O-(M)_n-OSO_2ONH_4]$ /silica nanocomposites should supply the directly hydroxyl groups end-capped oligomers $[HO-(M)_n-OH]$ during the calcination process. In fact, FT-IR spectra of the original $NH_4OSO_2O-(M)_n-OSO_2ONH_4$ oligomer show the disappearance of the peak at around 846 and 3524 cm^{-1} related to the sulfate esters and ammonium units, respectively, after calcination at 300 °C. In contrast, the peak related to the hydroxyl groups has been newly appeared at around 3311 cm^{-1} under similar conditions (see Fig. 2-22). Such directly hydroxyl groups end-capped oligomers are unable to lead the formation of oligomeric silica nanocomposites through the intermolecular hydrogen-bonding interaction of such end-capped hydroxyl groups due to their non-flexible end-capped groups.

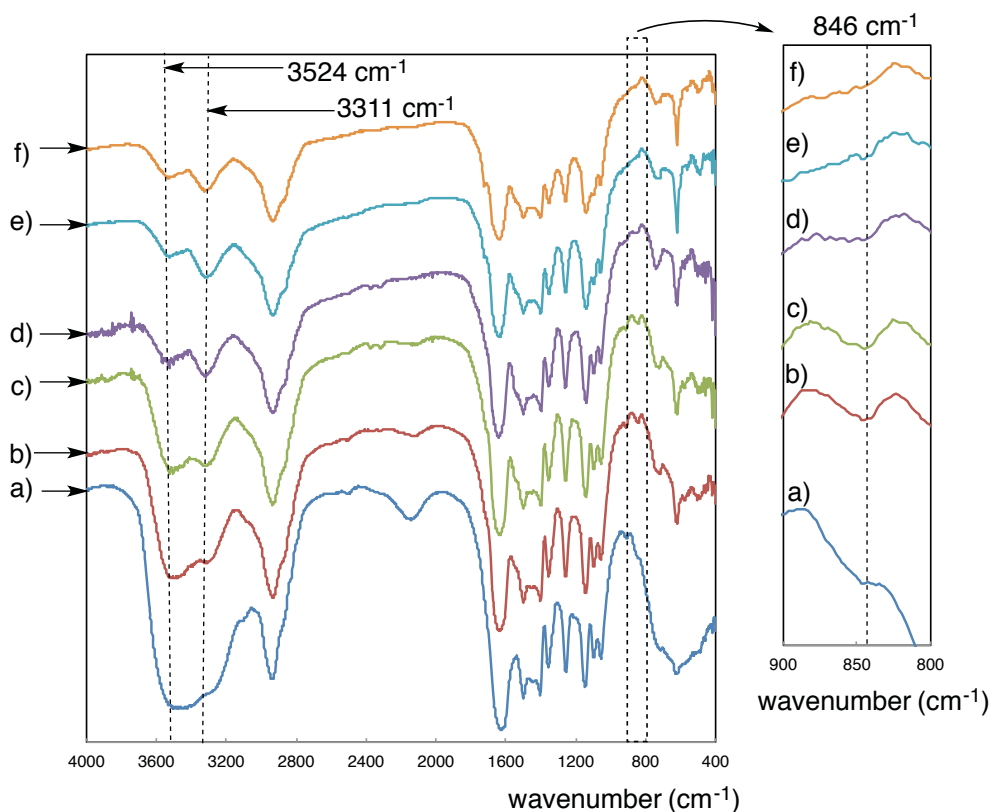


Fig. 2-22 FT-IR spectra of $\text{NH}_4\text{OSO}_2\text{O}-(\text{DMAA})_n-\text{OSO}_2\text{ONH}_4$ oligomer before calcination: (a), and after calcination at 100 °C: (b), 150 °C: (c), 200 °C: (d), 250 °C: (e) and 300 °C: (f)

In this way, the sulfate ester fragments end-capped DMAA, ACA, DOBAA, and ACMO oligomers/silica nanocomposites were found to supply a usual weight loss toward the oligomers in the composites during the calcination process. However, it was verified that the *HO-Amide* fragments end-capped DMAA, ACA, DOBAA, and ACMO oligomers/silica nanocomposites can afford no weight loss corresponding to the contents of these oligomers in the composites even after calcination at 800 °C. The nitrile fragments end-capped DMAA oligomer/silica nanocomposites can also provide the

similar no weight loss even after calcination. Such no weight loss behavior toward the oligomers in the silica nanocomposite cores has been already observed in the fluoroalkyl end-capped DOBAA oligomer/silica nanocomposites.^{4, 6)} However, fluoroalkyl end-capped DMAA, ACA, and ACMO oligomers/silica nanocomposites can provide the usual weight loss in proportion to the contents of these oligomers in the composites.^{5, 6)} This no weight loss behavior is due to the dehydrofluorination between the amide protons in oligomer and fluorines in the end-capped fluoroalkyl groups catalyzed by ammonia in the presence of silica nanoparticles as co-catalyst to afford the ammonium hexafluorosilicate: $(\text{NH}_4)_2\text{SiF}_6$.⁷⁾

In contrast, the present initiator fragments end-capped DMAA, ACA, ACMO, and DOBAA oligomers, end-capped fragments such as the *HO-Amide* and the nitrile enable their oligomers to provide no weight loss characteristic in the silica nanocomposite cores even after calcination. Thus, these initiator fragments can be clearly differentiated with the end-capped fluoroalkyl groups.

2.4. Conclusions

A variety of initiator fragments end-capped DMAA, ACA, DOBAA, and ACOMO oligomers were prepared by the oligomerizations of the corresponding monomers initiated by APS, VA-086, and AIBN as the radical initiators. It was demonstrated that under these oligomeric conditions, in which the concentration of the initiators are almost the same as that of the monomers, the initiator fragments end-capped oligomers can be obtained in excellent to moderate isolated yields. These obtained oligomers can cause a gelation, where the ionic or hydrogen-bonding interactions related to the end-capped fragments and the oligomer side chains such as amide or carboxyl segments are involved in establishing a physical gel network not only in water but also in traditional organic media including non-polar solvent such as hexane. The initiator fragments end-capped oligomers were applied to the preparation of the corresponding oligomers/silica nanocomposites through the sol-gel reactions of these oligomers with tetraethoxysilane in the presence of the silica nanoparticles under alkaline conditions. In these obtained oligomers/silica nanocomposites, the sulfate ester fragments end-capped oligomers in the composites afforded a clear weight loss after calcination at 800 °C.

However, interestingly, it was demonstrated that the *HO-Amide* fragments end-capped oligomers can supply no weight loss behavior in the silica nanocomposite cores even after calcination, In addition the nitrile fragments end-capped DMAA oligomer/silica nanocomposites were also found to afford no weight loss characteristic corresponding to the contents of the oligomer in the composites under similar conditions. Therefore, the present oligomeric silica nanocomposites have high potential for new functional oligomeric material possessing an excellent thermal stability.

References

- 1) H. Sawada “*Fluoropolymer Nanocomposites*” Smith DW Jr. Iacono ST, Iyer SS (eds) *Handbook of Fluoropolymer Science and Technology*, 4th edn., Wiley, Hoboken, pp. 59 ~ 82 (2014).
- 2) H. Sawada, *Polym. Chem.*, **3**, 46 (2012).
- 3) H. Sawada, T. Narumi, A. Kajiwara, K. Ueno, and K. Hamazaki, *Colloid Polym. Sci.*, **284**, 551 (2006).
- 4) H. Sawada, T. Narumi, S. Kodama, M. Kamijo, R. Ebara, M. Sugiya, and Y. Iwasaki, *Colloid Polym. Sci.*, **285**, 977 (2007).
- 5) H. Sawada, M. Kikuchi, and M. Nishida, *J. Polym. Sci. Part A: Polym. Chem.*, **49**, 1070 (2011).
- 6) H. Sawada, T. Tashima, H. Kakchi, Y. Nishiyama, M. Kikuchi, M. Miura, Y. Sato, and N. Isu, *Polym. J.*, **42**, 167 (2010).
- 7) H. Sawada, T. Tashima, Y. Nishiyama, M. Kikuchi, G. Kostov, Y. Goto, and B. Ameduri, *Macromolecules*, **44**, 1114 (2011).

- 8) M. S. A. Rahaman, A. F. Ismail, and A. Mustafa, *Polym. Degrad. Stab.*, **92**, 1421 (2007).
- 9) S. Xiao, B. Wang, C. Zhao, L. Xu, and B. Chen, *J. Appl. Polym. Sci.*, **127**, 2332 (2013).
- 10) G. T. Sivy, B. Gordon, and M. M. Coleman, *Carbon*, **21**, 573 (1983).
- 11) S. Xiao, W. Cao, B. Wang, L. Xu, and B. Chen, *J. Appl. Polym. Sci.*, **127**, 3198 (2013).
- 12) Y. Xue and J. Liang, *J. Appl. Polym. Sci.*, **127**, 237 (2013).
- 13) B. Wang, S. Xiao, W. Cao, X. Shi, and L. Xu, *J. Appl. Polym. Sci.*, **124**, 3412 (2012).
- 14) T. Sun, Y. Hou, and H. Wang, *J. Appl. Polym. Sci.*, **118**, 462 (2010).
- 15) S. Xiao, H. Lv, Y. Tong, L. Xu, and B. Chen, *J. Appl. Polym. Sci.*, **122**, 480 (2011).
- 16) T. Otsu and M. Yoshida, *Makromol. Chem. Rapid Commun.*, **3**, 127 (1982).
- 17) T. Otsu, M. Yoshida, and Y. Tazaki, *Makromol. Chem. Rapid Commun.*, **3**, 133 (1982).
- 18) H. Sawada, Y. F. Gong, Y. Minoshima, T. Matsumoto, M. Nakayama, M. Kosugi, and T. Migita, *J. Chem. Soc. Chem. Commun.*, **537**, 537 (1992).
- 19) H. Sawada, Y. Minoshima, and H. Nakajima, *J. Fluor. Chem.*, **65**, 169 (1993).

- 20) K. Hanabusa, R. Tanaka, M. Suzuki, M. Kimura, and H. Shirai, *Adv. Mater.*, **9**, 1095 (1997).
- 21) K. Hanabusa, K. Okui, K. Karaki, M. Kimura, and H. Shirai, *J. Colloid Interface Sci.*, **195**, 86 (1997).
- 22) P. Lundquist, J. Martensson, B. Sorbo, and S. Ohman, *Clin. Chem.*, **26(8)**, 1178 (1980).

CHAPTER 3

**Wettability Control Between Superoleophobic and Superoleophilic
Characteristics on the Modified Superhydrophobic Surfaces Treated
with Fluoroalkyl End-Capped Vinyltrimethoxysilane Oligomeric
Silica/Poly(styrene-*co*-butadiene) Nanocomposites:
Application to the Separation of Oil and Water**

3.1. Introduction

The oil resistance of a rubber is the key characteristic from the practical viewpoint in the automotive, industrial and seal applications.¹⁾ However, traditional rubbers such as ethylene-propylene-non-conjugated dienes rubber [EP(D)M], isoprene rubber, butyl rubber, natural rubber, butadiene rubber and styrene-butadiene rubber (SBR) have a high oil swelling characteristic, because their structures are quite similar to that of the oil itself.^{1 ~ 6)} The compositization of such rubbers with highly oleophobic materials possessing longer fluoroalkyl groups is of particular interest, from the developmental viewpoint of the rubber possessing highly oleophobic characteristic. The creation of the modified surface possessing superamphiphobic, superoleophilic/superhydrophobic and superoleophobic/superhydrophilic characteristics has been recently developed by using fluoroalkyl end-capped vinyltrimethoxysilane oligomer $[\text{R}_F-(\text{CH}_2\text{CHSi}(\text{OMe})_3)_n-\text{R}_F$; $\text{R}_F = \text{CF}(\text{CF}_3)\text{OC}_3\text{F}_7$, $n = 2, 3$; $\text{R}_F-(\text{VM})_n-\text{R}_F]$ as a key intermediate.^{7 ~ 13)} For example, fluoroalkyl end-capped vinyltrimethoxysilane oligomer/calcium silicide nanocomposites $[\text{R}_F-(\text{VM}-\text{SiO}_2)_n-\text{R}_F/\text{CaSi}_2]$, which were prepared by the sol-gel reaction of the corresponding oligomer in the presence of calcium silicide particles under alkaline

conditions, can exhibit a superoleophobic characteristic imparted by fluoroalkyl segments in the composites on the modified glass surface.¹⁴⁾ This chapter shows that the $R_F-(VM)_n-R_F$ oligomer can undergo the sol-gel reactions in the presence of SBR under alkaline or acidic conditions to provide the corresponding fluorinated oligomeric silica/SBR nanocomposites. It has been found that the $R_F-(VM-SiO_2)_n-R_F/SBR$ nanocomposites, which were obtained under alkaline conditions, can give the superoleophobic/superhydrophobic (superamphiphobic) characteristic on the modified glass surface. In contrast, the $R_F-(VM-SiO_2)_n-R_F/SBR$ nanocomposites, which were prepared under acidic conditions, can give the superoleophilic/superhydrophobic characteristic on the modified surface, and these fluorinated nanocomposite particle powders were applied to the packing materials for the column chromatography to separate the mixture of oil and water. Especially, the transparent colorless oil was isolated from the mixture of oil and water even after the reuse of these nanocomposite powders as the packing material under similar conditions. These results will be described in this chapter.

3.2. Experimental

3.2.1. Measurements

^1H NMR spectra were recorded using a JEOL JNM-ECA 500 (500 MHz) FT NMR SYSTEM (Tokyo, Japan). Molecular weight and copolymer compositions of SBR $[-(\text{CH}_2\text{CHPh})_x-(\text{CH}_2-\text{CH}=\text{CH}-\text{CH}_2)_y-]$: $x : y = 45 : 55$; $M_n = 14390$, $M_w/M_n = 1.79$] and NBR $[-(\text{CH}_2\text{CHCN})_x-(\text{CH}_2-\text{CH}=\text{CH}-\text{CH}_2)_y-]$: $x : y = 34 : 66$; $M_n = 10780$, $M_w/M_n = 1.12$] were measured using a Shodex DS-4 (pump) and Shodex RI-71 (detector) gel permeation chromatography (Tokyo, Japan) calibrated with polystyrene standard using tetrahydrofuran (THF) as the eluent and ^1H NMR spectra, respectively. Size [number - average diameter (average hydrodynamic diameter)] of nanocomposite was measured by using Otsuka Electronics DLS-7000F (Tokyo, Japan). Contact angles were measured using a Kyowa Interface Science Drop Master 300 (Saitama, Japan). Dynamic force microscope (DFM) was recorded by using SII Nano Technology Inc. E-sweep (Chiba, Japan). Optical and fluorescence microscopies were measured by using OLYMPUS Corporation BX51 (Tokyo, Japan).

3.2.2. Materials

SBR [poly(styrene-*co*-butadiene)] and NBR [poly(acrylonitrile-*co*-butadiene): Nipol DN3380^{TR}] were used as received from Sigma-Aldrich Japan (Tokyo, Japan) and Zeon Corporation (Tokyo, Japan), respectively. Vinyltrimethoxysilane was used as received from Dow Corning Toray Co., Ltd. (Tokyo, Japan). Fluoroalkyl end-capped vinyltrimethoxysilane oligomer [$R_F-(CH_2-CHSi(OMe)_3)_n-R_F$: the mixture of dimer and trimer; $R_F = CF(CF_3)OC_3F_7$] was synthesized by reaction of fluoroalkyl peroxide with the corresponding monomer according to the previously reported method.¹⁵⁾ Glass plate (borosilicate glass) [micro cover glass: 18 mm × 18 mm] was purchased from Matunami glass Ind. Ltd. (Osaka, Japan) and was used after washing well with 1,2-dichloroethane.

3.2.3. Preparation of $R_F-(VM-SiO_2)_n-R_F$ /SBR nanocomposites

To an 1,2-dichloroethane solution (5.0 ml) containing fluoroalkyl end-capped vinyltrimethoxysilane oligomer [100 mg; $R_F-(CH_2CHSi(OMe)_3)_n-R_F$: $R_F-(VM)_n-R_F$; $R_F = CF(CF_3)OC_3F_7$; $n = 2, 3$] were added SBR (10 mg) and 1N HCl solution (1.0 ml).

The mixture was stirred with a magnetic stirring bar at room temperature for 5 h. 1,2-Dichloroethane was added to the obtained crude products after the solvent was evaporated off. The 1,2-dichloroethane suspension was stirred with magnetic stirring bar at room temperature for 1 day. After centrifugal separation of this solution, the obtained products were washed well with 1,2-dichloroethane several times, and dried in vacuo to afford the expected white powdery product (75 mg). 25 wt% aqueous ammonia (1.0 ml) solution was used instead of 1N HCl solution for the preparation of the $R_F-(VM-SiO_2)_n-R_F/SBR$ nanocomposites under similar conditions (see Scheme 3-1).

3.2.4. Preparation of modified glass treated with the $R_F-(VM-SiO_2)_n-R_F/SBR$ nanocomposites by casting method

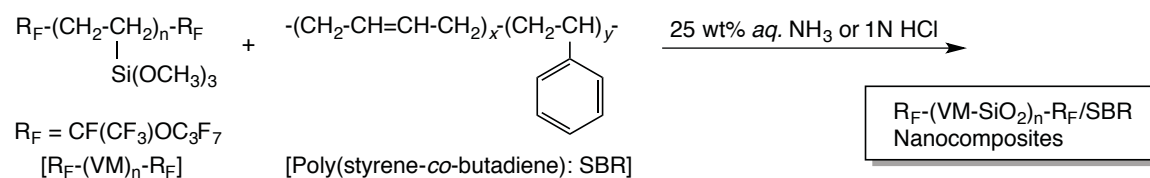
To an 1,2-dichloroethane solution (5.0 ml) containing $R_F-(VM)_n-R_F$ oligomer (100 mg) were added SBR (10 mg) and 1N HCl solution (1.0 ml). The mixture was stirred with a magnetic stirring bar at 25 °C for 5 h. The modified glass was prepared by casting the 1,2-dichloroethane solution of $R_F-(VM-SiO_2)_n-R_F/SBR$ nanocomposites thus obtained on glass plate (18 × 18 mm² pieces). The solvent was evaporated at room

temperature and dried at room temperature for 1 day under vacuum to afford the modified glass. The $R_F-(VM-SiO_2)_n-R_F/SBR$ nanocomposites, which were prepared under alkaline conditions, were also used for the surface modification of glass under similar conditions.

3.3. Results and discussion

3.3.1. Preparation of the $R_F-(VM-SiO_2)_n-R_F/SBR$ nanocomposites

The sol-gel reactions of fluoroalkyl end-capped vinyltrimethoxysilane oligomer [$R_F-(CH_2-CHSi(OMe)_3)_n-R_F$; $R_F = CF(CF_3)OC_3F_7$; $R_F-(VM)_n-R_F$] were found to proceed smoothly in the presence of SBR under acidic conditions to provide the corresponding fluorinated oligomeric silica/SBR composites [$R_F-(VM-SiO_2)_n-R_F/SBR$] in excellent to moderate isolated yields: 54 ~ 68 %. Similarly, the sol-gel reactions under alkaline conditions afforded the expected composites in 34 ~ 56 % isolated yields. The results are shown in Scheme 3-1 and Table 3-1.



Scheme 3-1 Preparation of $R_F-(VM-SiO_2)_n-R_F/SBR$ nanocomposites

Table 3-1 Preparation of the $R_F-(VM-SiO_2)_n-R_F/SBR$ nanocomposites

Run	$R_F-(VM)_n-R_F$ (mg)	SBR (mg)	25 wt% aq. NH_3 (ml)	1N HCl (ml)	Product yield (%) ^{a)}	Size of the composites ^{b)} (nm) \pm STD
1	100	10	1	-	56	40.4 \pm 2.5
2	100	20	1	-	47	54.4 \pm 4.8
3	100	50	1	-	34	33.2 \pm 5.4
4	100	100	1	-	56	647 \pm 67
5	100	10	-	1	68	29.1 \pm 3.5
6	100	20	-	1	59	35.9 \pm 3.1
7	100	50	-	1	57	589 \pm 78
8	100	100	-	1	54	349 \pm 49

a) Yields are based on $R_F-(VM)_n-R_F$ and SBR

b) Determined by dynamic light scattering measurements in 1,2-dichloroethane

These obtained composites in Table 3-1 can give a good dispersibility and stability toward the traditional organic solvents such as methanol, ethanol, 1,2-dichloroethane, tetrahydrofuran and 2-propanol except for water. Thus, the size of these composites was measured by using dynamic light scattering (DLS) measurements at 25 °C, and the results are also shown in Table 3-1.

Table 3-1 shows that these SBR composites are nanometer size-controlled particles, of whose mean diameters are from 29 to 647 nm. Thus, in order to clarify the formation of the nanocomposites, the field emission scanning electron micrographs (FE-SEM) of methanol solution of the $R_F-(VM-SiO_2)_n-R_F/SBR$ nanocomposites (Runs 1 and 5 in Table 3-1) have been measured and the results are illustrated in Fig. 3-1.

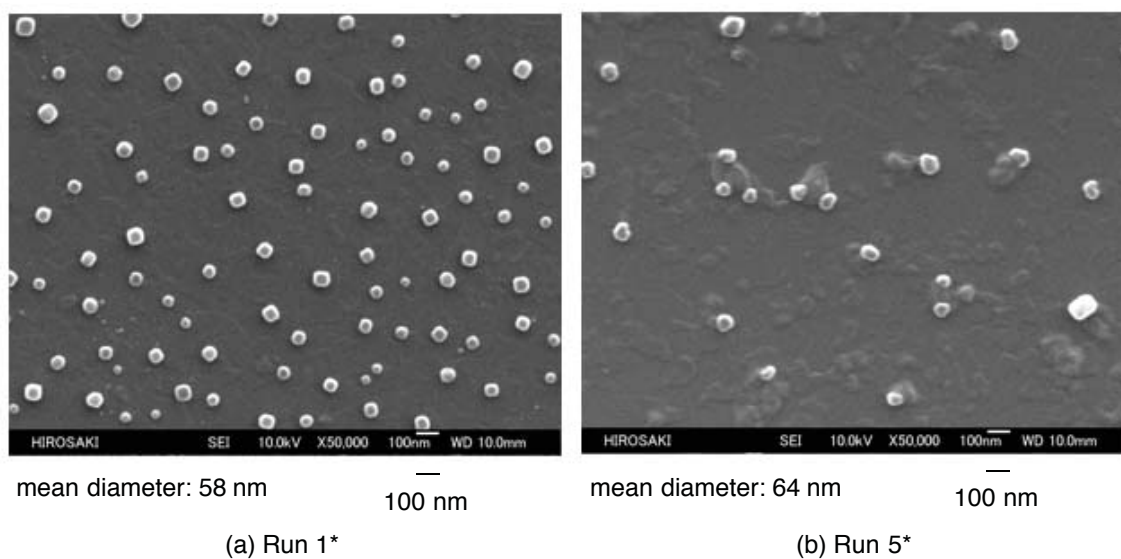


Fig. 3-1 Field emission scanning electron microscopy (FE-SEM) images of well-dispersed in methanol solution of the $R_F-(VM-SiO_2)_n-R_F/SBR$ nanocomposites under alkaline (Run 1*) and acidic (Run 5*) conditions

* Each Run No. corresponds to that of Table 3-1

As shown in Fig. 3-1, the obtained SBR composites, which were prepared under alkaline and acidic conditions are very fine spherical particles with mean diameter: 58 nm and 64 nm, respectively, and the similar particle sizes were observed by the DLS measurements illustrated in Table 3-1. The $R_F-(VM)_n-R_F$ oligomer can undergo the sol-gel reaction in methanol under alkaline conditions to afford the corresponding $R_F-(VM-SiO_2)_n-R_F$ oligomeric nanoparticles through the base-catalyzed hydrolysis of the trimethoxysilyl segment $[(MeO)_3Si\sim]$ in the oligomer.¹⁶⁾ Similarly, the sol-gel reaction of $R_F-(VM)_n-R_F$ oligomer in the absence of SBR in 1,2-dichloroethane under alkaline or acidic conditions illustrated in Scheme 3-1 were found to provide the $R_F-(VM-SiO_2)_n-R_F$

oligomeric nanoparticles with mean diameter: 101 ± 17 nm and 103 ± 17 nm, respectively. Thus, the different sizes of the obtained nanocomposites, compared with that of the parent $R_F-(VM-SiO_2)_n-R_F$ oligomeric nanoparticles show that the present sol-gel reaction in Scheme 3-1 should proceed smoothly to afford the expected nanocomposites which consist of the core-corona type nanoparticles, of whose core units correspond to the SBR and the $R_F-(VM-SiO_2)_n-R_F$ oligomeric siloxane networks will be defined as the core units.

3.3.2. Surface modification of glass by using the $R_F-(VM-SiO_2)_n-R_F/SBR$ nanocomposites

The $R_F-(VM-SiO_2)_n-R_F$ oligomeric nanoparticles have been reported to be applicable to the surface modification of glass to afford the superhydrophobic surface (water contact angle value: 180°) with good oleophobicity.¹⁶⁾ Thus, the modified glasses treated with the $R_F-(VM-SiO_2)_n-R_F/SBR$ nanocomposites have been prepared in Table 3-1, and the contact angles of dodecane and water on these modified glass surfaces were measured. The results are shown in Table 3-2.

Table 3-2 Contact angles of water and dodecane on the modified glass treated with the $R_F-(VM-SiO_2)_n-R_F/SBR$ nanocomposites

Run ^{a)}	Contact angle (Degree)							
	Dodecane	Water						30
		Time (min)						
		0	5	10	15	20	25	
1	114	180	.b)	.b)	.b)	.b)	.b)	.b)
2	113	180	.b)	.b)	.b)	.b)	.b)	.b)
3	107	180	.b)	.b)	.b)	.b)	.b)	.b)
4	88	180	.b)	.b)	.b)	.b)	.b)	.b)
5	0	180	.b)	.b)	.b)	.b)	.b)	.b)
6	0	180	.b)	.b)	.b)	.b)	.b)	.b)
7	0	180	.b)	.b)	.b)	.b)	.b)	.b)
8	0	180	.b)	.b)	.b)	.b)	.b)	.b)

a) Each Run No. corresponds to that of Table 3-1

b) No change

As shown in Runs 1 ~ 4 in Table 3-2, the dodecane contact angle values on the modified glass surface treated with the $R_F-(VM-SiO_2)_n-R_F/SBR$ nanocomposites, which were prepared under alkaline conditions, are sensitive to the feed ratios of SBR employed, increasing with greater feed ratios of SBR from 10 to 100 mg to provide from superoleophobic to highly oleophobic characteristics. Because, the dodecane contact angle values were found to decrease from 114 ~ 113 to 107 ~ 88 degrees. The modified glass surface also afforded a superhydrophobic property (water contact angle value: 180 degrees) in each case. In fact, as shown in Fig. 3-2-(B), oil (dodecane) droplet had a

strong repellent characteristic toward the modified surface treated with the $R_F\text{-(VM-SiO}_2)_n\text{-R}_F\text{/SBR}$ nanocomposites to give the superoleophobic characteristic (dodecane contact angle value: 114 degrees) on the surface. In addition, the contact angle values of not only dodecane but also other oils such as toluene, *p*-xylene, 1-heptanol and 1-butanol were measured on the modified surface (Run 1 in Table 3-2). The results are as followings:

Contact angle (Degree)			
Toluene	<i>p</i> -Xylene	1-Heptanol	<i>n</i> -Butanol
90	99	86	52

Interestingly, the similar higher contact angle values (52 ~ 99 degrees) were observed for the other oil droplets such as toluene, *p*-xylene, 1-heptanol, and 1-butanol. These findings suggest that the present modified surface can afford highly oleophobic characteristic toward a variety of oils including dodecane.

The modified glass surface also afforded a superhydrophobic property (water contact angle value: 180 degrees) in each case. Especially, the water droplets cannot deposit on this modified surface due to the superhydrophobic characteristic (water contact angle

value: 180 degrees) even after pull-up process of the needle from the modified surface as illustrated in Figs. 3-2-(A)-(b) and 3-2-(A)-(c).

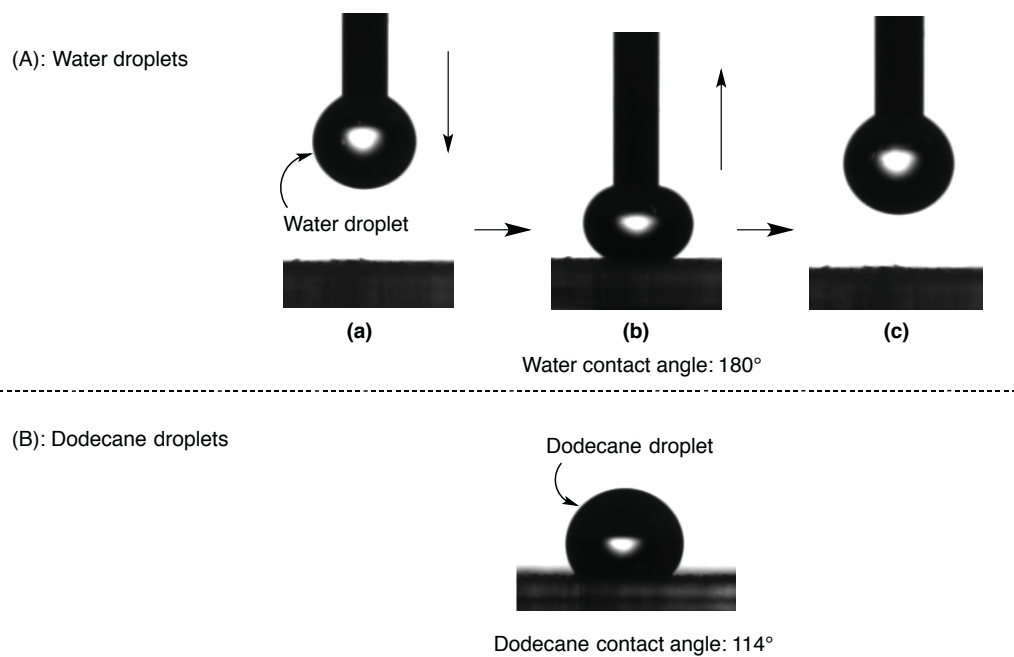


Fig. 3-2 CCD (Charge Couple Device) camera images of the water droplet (A) and the dodecane droplet (B) on the modified glass surface treated with the $R_F-(VM-SiO_2)_n-R_F/SBR$ nanocomposites (Run 1 in Table 3-1)

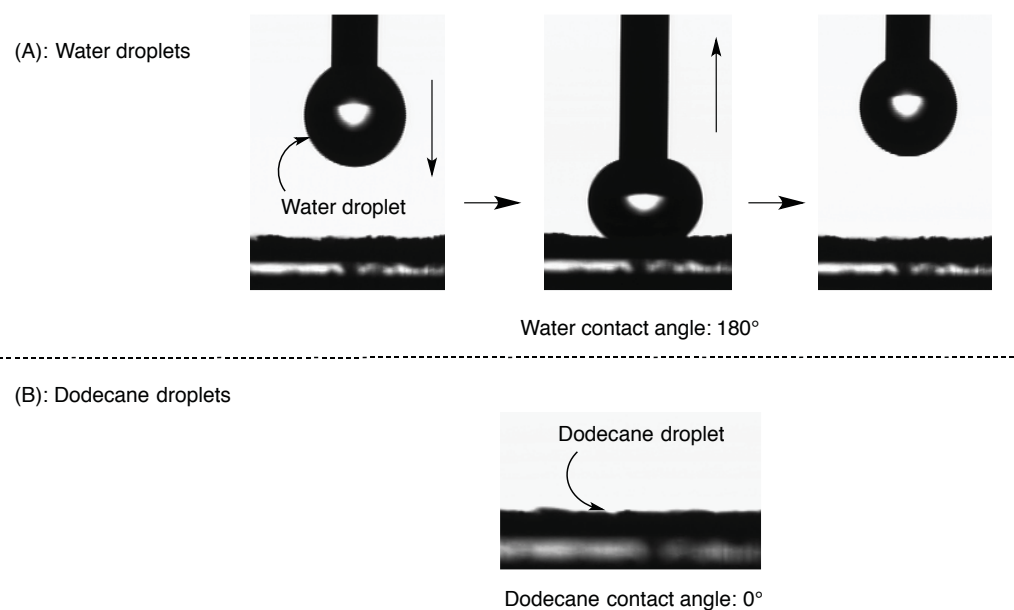


Fig. 3-3 CCD (Charge Couple Device) camera images of the water droplet (A) and the dodecane droplet (B) on the modified glass surface treated with the $R_F-(VM-SiO_2)_n-R_F/SBR$ nanocomposites (Run 5 in Table 3-1)

However, of particular interest, the $R_F-(VM-SiO_2)_n-R_F/SBR$ nanocomposites, which were prepared under acidic conditions, were found to supply not the superoleophobic but the superoleophilic characteristic (dodecane contact angle value: 0 degree; see Fig. 3-3-(B)) with the superhydrophobic property (water contact angle value: 180 degrees; see Fig. 3-3-(A)) on each modified surface as shown in Runs 5~8 in Table 3-2. The modified surface (Run 5 in Table 3-2) was also found to provide a similar superoleophilic characteristic toward not only dodecane but also other oils such as toluene, *p*-xylene, 1-heptanol and 1-butanol as followings:

Contact angle (Degree)			
Toluene	<i>p</i> -Xylene	1-Heptanol	<i>n</i> -Butanol
0	0	0	0

In this way, it was verify that the wettability between superoleophobic and superoleophilic characteristics on the modified surface can be easily controlled by changing the preparative conditions (alkaline or acidic conditions) of the expected nanocomposites.

In general, a lower surface energy and enhancement of the surface roughness are very effective for creation a superoleophobic surface.^{17 ~ 19)} The fabrication of the

superoleophobic surface is difficult due to the lower surface tension of oils than that of water.¹²⁾ In contrast, the superhydrophobic surface is in general realized by enhancing the surface roughness. Thus, the superhydrophobic surface can be easily prepared by using longer alkyl chains-containing silica nanocomposites to create the roughness surface.^{20 ~ 22)} To confirm the present unique different wettability between these modified surfaces, the surface morphology of the modified glass surface treated with the $R_F-(VM-SiO_2)_n-R_F/SBR$ nanocomposites have been studied by FE-SEM (Field emission scanning electron micrographs) and DFM (Dynamic force microscopy) measurements. These results are shown in Figs. 3-4 and 3-5.

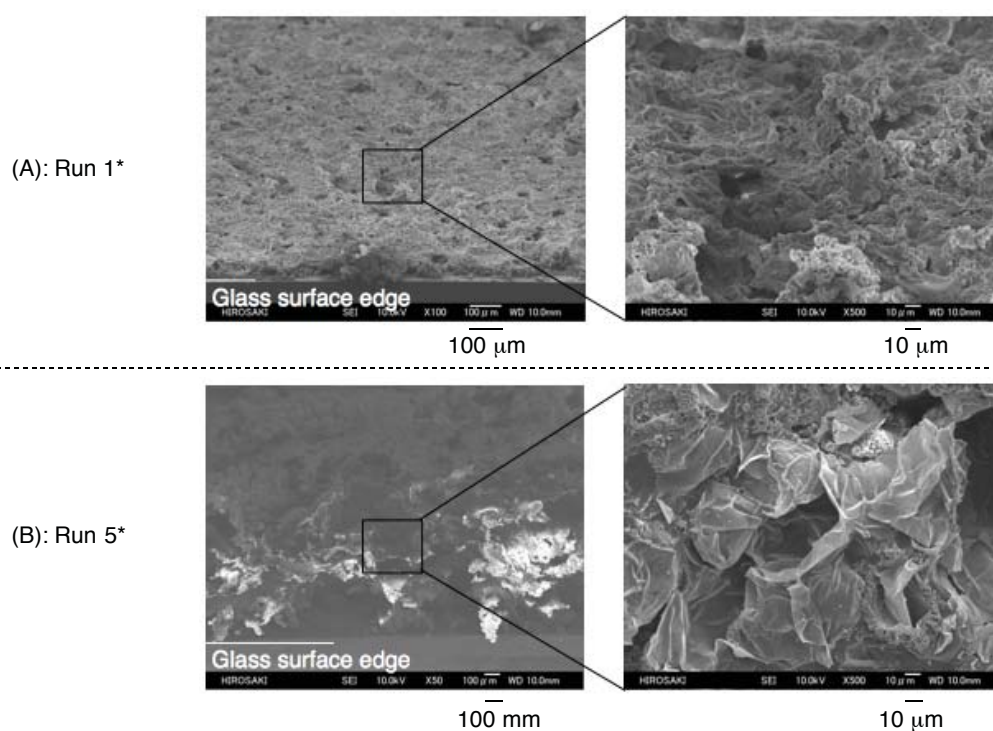


Fig. 3-4 FE-SEM images of the modified glass surface treated with the $R_F-(VM-SiO_2)_n-R_F/SBR$ nanocomposites, which were prepared under alkaline condition (A: Run 1*) and acidic conditions (B: Run 5*)
 * Each Run No. corresponds to that of Table 3-1

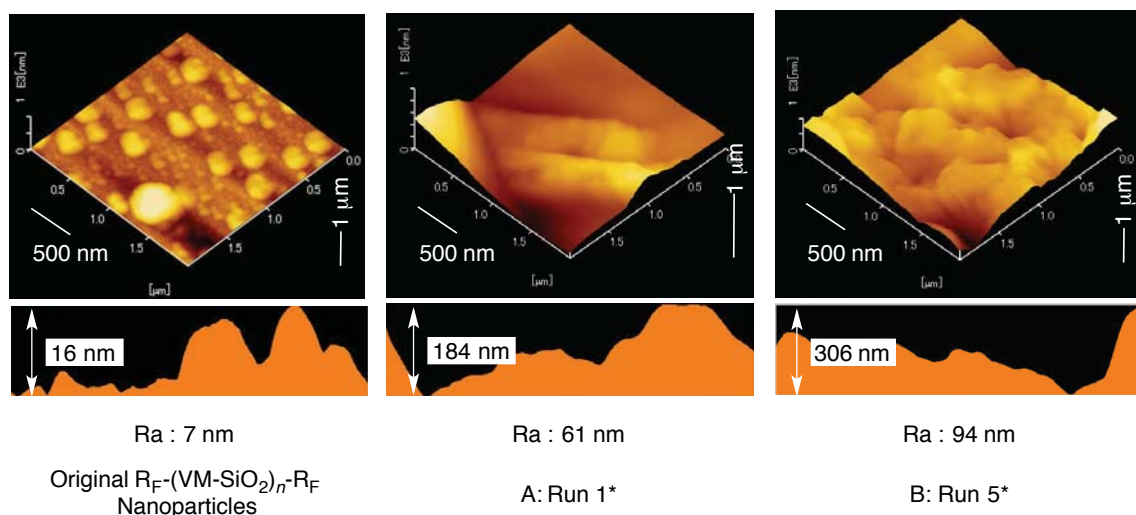


Fig. 3-5 DFM topographic images of the modified glasses surface treated with parent $R_F-(VM-SiO_2)_n-R_F$ nanoparticles and the $R_F-(VM-SiO_2)_n-R_F/SBR$ nanocomposites, which were prepared under alkaline (A: Run 1*) and acidic (B: Run 5*) conditions
 * Each Run No. corresponds to that of Table 3-1

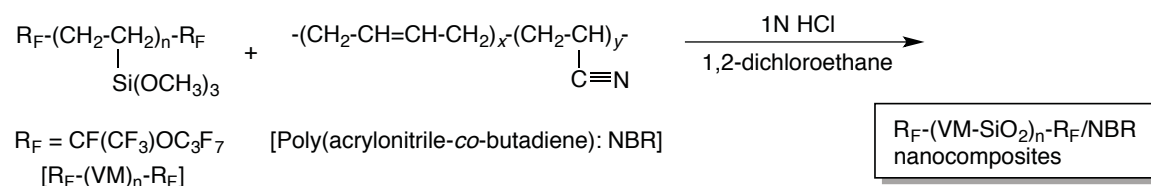
As shown in Figs. 3-4-(A) and (B), the architecture of the effective roughness was observed on the modified surfaces treated with the $R_F-(VM-SiO_2)_n-R_F/SBR$ nanocomposites (Runs 1 and 5 in Table 3-1). Especially, the higher roughness surface was observed on the modified surface (B) possessing a superoleophilic/superhydrophobic characteristic. In fact, DFM measurements show that the topographical image of each modified surface can provide a roughness characteristic, and a higher roughness average value (Ra: 94 nm) was observed in the $R_F-(VM-SiO_2)_n-R_F/SBR$ nanocomposites possessing superoleophilic/superhydrophobic characteristic [see Fig. 3-5-(B)], compared with the nanocomposites possessing a

superoleophobic/superhydrophobic characteristic [Ra: 61 nm: see Fig. 3-5-(A)] or the parent $R_F-(VM-SiO_2)_n-R_F$ oligomeric nanoparticles (Ra: 7 nm: see Fig. 3-5).

In the FE-SEM pictures illustrated in Fig. 3-4-(B), the formation of the clear void moieties was observed on the modified surface treated with the $R_F-(VM-SiO_2)_n-R_F/SBR$ nanocomposites possessing a superoleophilic/superhydrophobic characteristic, quite different from that [Fig. 3-4-(A)] of the nanocomposites possessing a superoleophobic/superhydrophobic property. This finding suggests that such void moieties should interact smoothly with oil droplets to afford the superoleophilic characteristic through the oil-adsorption process on the modified surface, due to the lower surface tension (25 mN/m levels) of oils than that (72 mN/m) of water. In contrast, such roughness surface (Ra value: 61 nm) possessing few void moieties can afford a superoleophobic/superhydrophobic surface due to the presence of fluoroalkyl segments in the nanocomposites on the roughness surface [see Fig. 3-4-(A)].

It is suggested that clear void formation on the modified surface illustrated in Fig. 3-4-(B) would be also due to the presence of relatively bulky benzene units in the fluorinated SBR nanocomposites. Recently, the $R_F-(VM-SiO_2)_n-R_F/NBR$ [poly(acrylonitrile-*co*-butadiene)] nanocomposites have been prepared by the sol-gel

reaction of the corresponding oligomer in the presence of NBR under alkaline conditions.²³⁾ The modified glass surface treated with the $R_F-(VM-SiO_2)_n-R_F/NBR$ nanocomposites can give the similar highly oleophobic (dodecane contact angle values: 74 ~ 95 degrees)/superhydrophobic (water contact angle values: 180 degrees) characteristic to those of the present $R_F-(VM-SiO_2)_n-R_F/SBR$ nanocomposites, which were prepared under alkaline conditions as shown in Table 3-2.²³⁾ NBR can possess no bulky substituents, quite different from SBR. Thus, it is suggested that the $R_F-(VM-SiO_2)_n-R_F/NBR$ nanocomposites, which were prepared under not alkaline but acidic conditions, would be unable to supply the similar superoleophilic/superhydrophobic characteristic due to the absence of bulky substituents. In fact, the $R_F-(VM-SiO_2)_n-R_F/NBR$ nanocomposites were prepared under acidic conditions, and the results are shown in Scheme 3-2 and Table 3-3.



Scheme 3-2 Preparation of $R_F-(VM-SiO_2)_n-R_F/NBR$ nanocomposites

Table 3-3 Preparation of the $R_F-(VM-SiO_2)_n-R_F/NBR$ nanocomposites under acidic conditions (used 1N HCl: 1.0 ml)

Run	$R_F-(VM)_n-R_F$ (mg)	NBR (mg)	Product yield (%) ^{a)}	Size of the composites ^{b)} (nm) \pm STD
9	100	10	49	44.7 \pm 2.5
10	100	20	39	65.6 \pm 4.8
11	100	50	46	48.3 \pm 5.7

a) Yields are based on $R_F-(VM)_n-R_F$ and NBR

b) Determined by dynamic light scattering measurements in 1,2-dichloroethane

As shown in Scheme 3-2 and Table 3-3, the expected $R_F-(VM-SiO_2)_n-R_F/NBR$ nanocomposites were obtained in 39 ~ 49 % isolated yields. The obtained composites were found to exhibit the similar dispersibility and stability to that of the $R_F-(VM-SiO_2)_n-R_F/SBR$ nanocomposites. Thus, the size of these nanocomposites in 1,2-dichloroethane has been measured by using DLS measurements at 25 °C, and the results are also shown in Table 3-3.

The sizes of these composites determined by DLS measurements are nanometer size-controlled particles from 45 to 66 nm, and FE-SEM picture (see Fig. 3-6) shows that the shape of the composite particles (Run 9 in Table 3-3) is very fine spherical particles, similar to that of the $R_F-(VM-SiO_2)_n-R_F/SBR$ nanocomposites illustrated in Run 5 in

Fig. 3-1. Especially, Figure 3-6 shows that the average particle size of composites is 55 nm, of whose value is quite similar to that (45 nm) determined by DLS measurements.

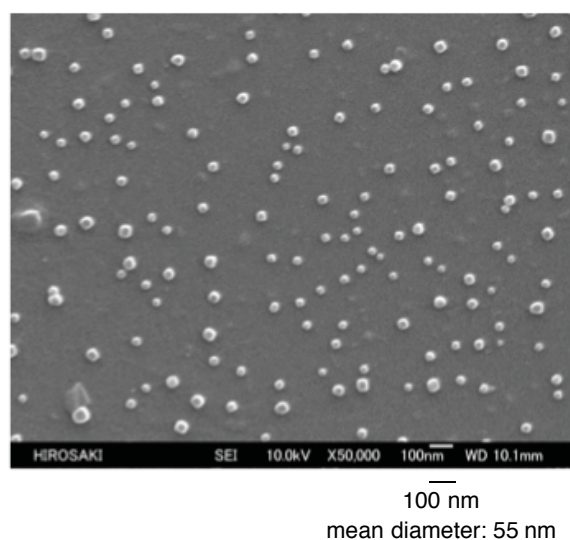


Fig. 3-6 FE-SEM image of the $R_F-(VM-SiO_2)_n-R_F/NBR$ nanocomposites (Run 9 in Table 3-3) in methanol solutions

Additionally, the dodecane and water contact angle values on the modified glass surface treated with the $R_F-(VM-SiO_2)_n-R_F/NBR$ nanocomposites were measured, and the results are as followings:

Run No*	Contact angle (degree)	
	Dodecane	Water
9	100	180
10	94	180
11	93	180

* Each Run No. corresponds to that of Table 3-3

Each modified glass surface was found to exhibit a highly oleophobic/superhydrophobic characteristic, indicating a quite different wettability from that of the $R_F-(VM-SiO_2)_n-R_F/SBR$ nanocomposites, which were prepared under acidic conditions illustrated in Table 3-2. In order to verify such different wettability, the FE-SEM and DFM measurements on the modified glass surface treated with the $R_F-(VM-SiO_2)_n-R_F/NBR$ nanocomposites (Run 9 in Table 3-3) have been studied, and the results are depicted in Fig. 3-7.

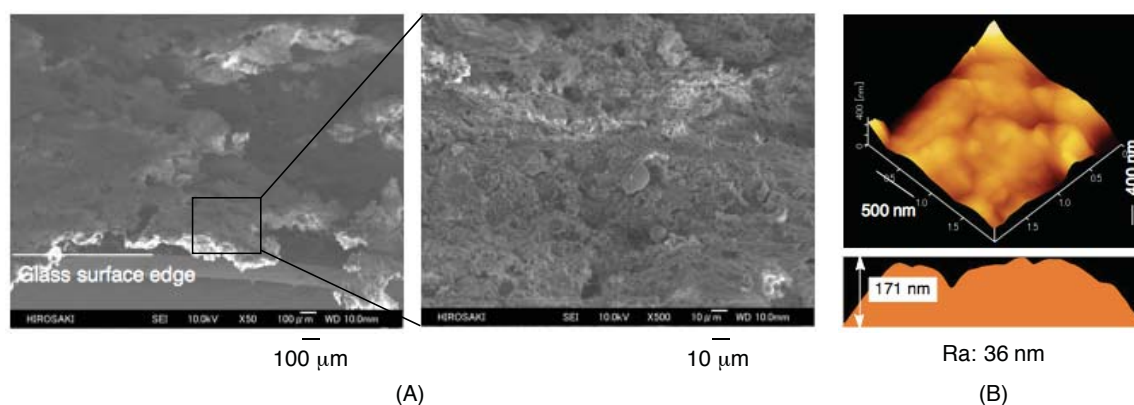


Fig. 3-7 FE-SEM images (A) and DFM topographic images (B) of the modified glass surfaces treated with the $R_F-(VM-SiO_2)_n-R_F/NBR$ nanocomposites (Run 9 in Table 3-3)

As shown in Fig. 3-7-(A), the clear void formation cannot be observed, compared with that of the corresponding $R_F-(VM-SiO_2)_n-R_F/SBR$ nanocomposites illustrated in Fig. 3-4-(B), although this modified surface has a relatively high roughness average value

[Ra: 36 nm: see Fig. 3-7-(B)]. Such surface morphology should afford the highly oleophobic/superhydrophobic characteristic, as well as that of the $R_F\text{-(VM-SiO}_2)_n\text{-R}_F\text{/SBR}$ nanocomposites, which were prepared under alkaline conditions.

3.3.3. Separation of the mixture of oil and water and water-in-oil (W/O) emulsion by using the $R_F\text{-(VM-SiO}_2)_n\text{-R}_F\text{/SBR}$ nanocomposites as a packing material

The superoleophilic surface can supply a good affinity toward oils. The present $R_F\text{-(VM-SiO}_2)_n\text{-R}_F\text{/SBR}$ nanocomposites, which were prepared under acidic conditions, can exhibit a superoleophilic/superhydrophobic characteristic. It is strongly suggested that such nanocomposite particle powders can simultaneously repels water and strongly absorb oils. Thus, these nanocomposite powders should be applicable as the packing materials for the column chromatography for the separation of the mixture of oil and water. In fact, the separation of the mixture of the blue-colored water (water was colored with $\text{CuSO}_4\cdot 5\text{H}_2\text{O}$) and 1,2-dichloroethane has been studied by the use of the $R_F\text{-(VM-SiO}_2)_n\text{-R}_F\text{/SBR}$ nanocomposites (Run 5 in Table 3-1) as the packing material for the column chromatography. The silica gel (Wakogel^{TR} C-500HG) was also used as the

packing material under similar conditions, for comparison. These results are shown in

Fig. 3-8.

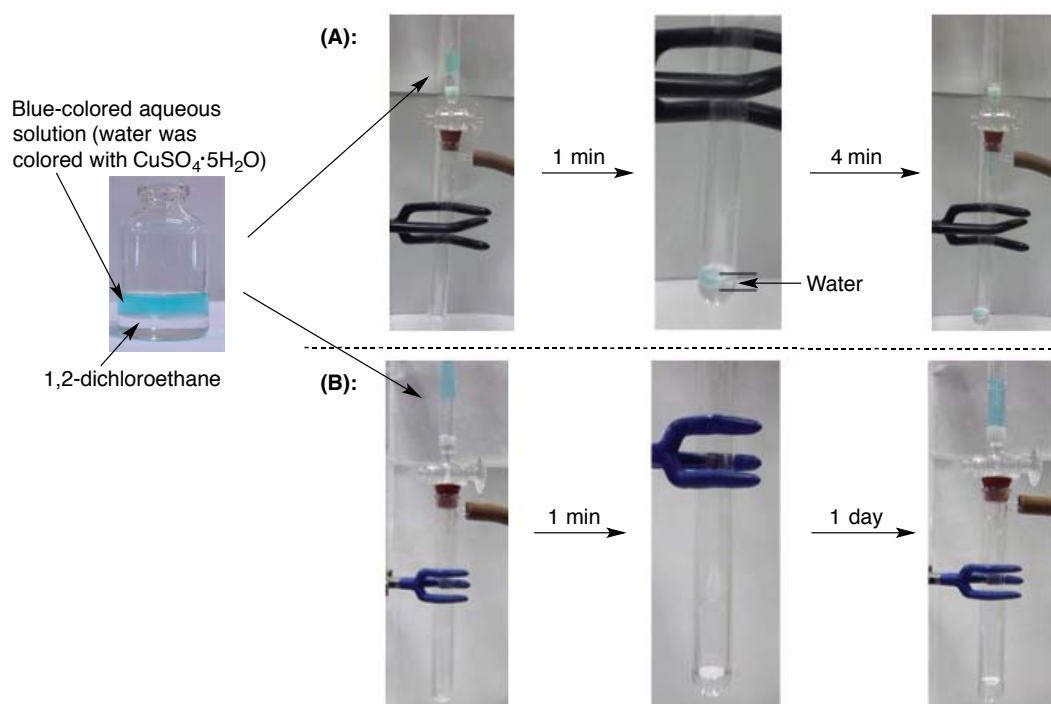


Fig. 3-8 Separation of mixture of blue-colored water and 1,2-dichloroethane by using the silica gel (Wakogel^{TR} C-500HG) (A) and the $R_F-(VM-SiO_2)_n-R_F/SBR$ composite powders (Run 5 in Table 3-1), (B) under reduced pressure conditions

As shown in Fig. 3-8-(A), the silica gel (Wakogel^{TR} C-500HG) was not effective for the separation of the mixture of oil and water under reduced pressure; however, the transparent colorless oil can be isolated under similar reduced pressure conditions by using the $R_F-(VM-SiO_2)_n-R_F/SBR$ nanocomposite powders as packing material.

Interestingly, the blue-colored water was not isolated at all even after 1 day as shown in Fig. 3-8-(B), due to the superhydrophobic characteristic of the nanocomposite powders.

The $R_F-(VM-SiO_2)_n-R_F/SBR$ nanocomposites have been applied to the separation of not only the mixture of oil and water but also the W/O emulsion, of whose emulsion consists of 1,2-dichloroethane (5.0 ml), water (0.05 ml) and surfactant (Span 80: 30.0 mg), and the results are depicted in Fig. 3-9.

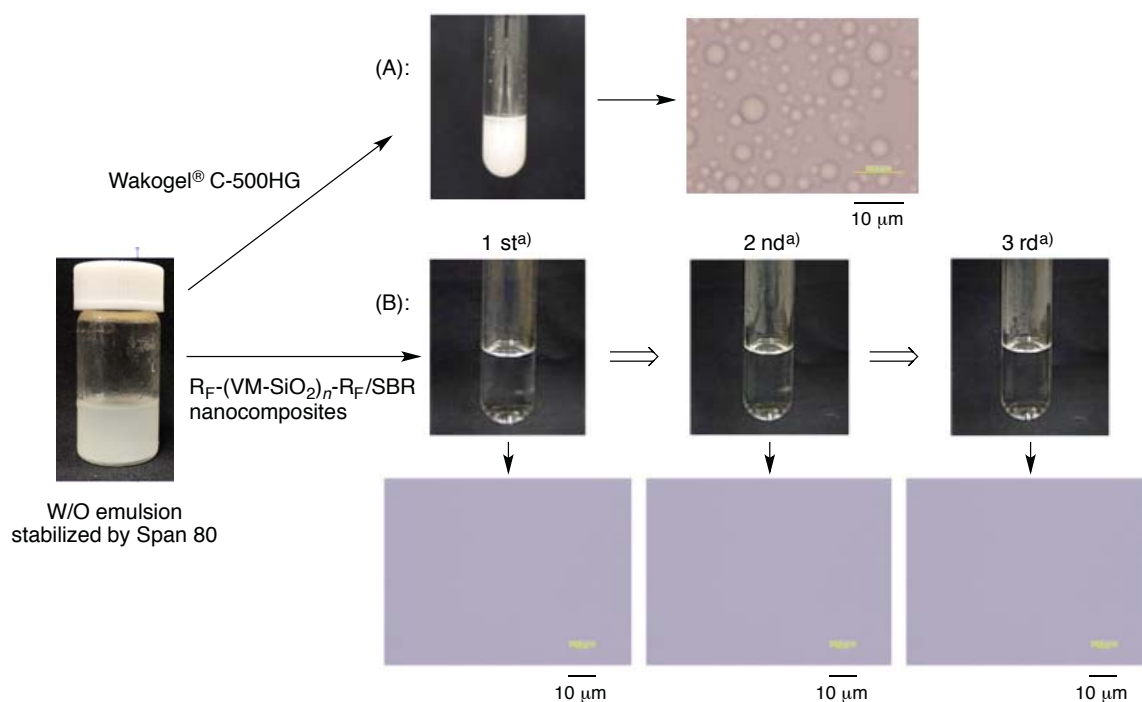


Fig. 3-9 Optical microscopy images of the eluent after the separation of the W/O (oil: 1,2-dichloroethane) emulsion stabilized by span 80 by using the column chromatography with Wakogel^{TR} C500-HG (A) and the $R_F-(VM-SiO_2)_n-R_F/SBR$ nanocomposites (Run 5 in Table 3-1) (B)
a) Number of cycles

As shown in Fig. 3-9-(A), the original silica gel (Wakogel^{TR} C500-HG) cannot be applied to the packing material for the separation of the W/O emulsion under reduced pressure. In contrast, only transparent colorless oil was isolated by using the R_F-(VM-SiO₂)_n-R_F/SBR nanocomposite particle powders (Run 5 in Table 3-1) as the packing material for the column chromatography for the separation of the W/O emulsion [see Fig. 3-9-(B)]. Optical micrograph also showed that the water droplet cannot be detected at all in the isolated colorless oil as shown in Fig. 3-9-(B), although the water droplet can be easily detected in the W/O emulsion which flowed out from the column chromatography by the use of silica gel as the packing material [see Fig. 3-9-(A)]. More interestingly, it was clarified that the present nanocomposite powders have a good reusability as the packing material for the separation of the W/O emulsion, and any water droplets in the isolated colorless oil cannot be detected at all even after the separation of the W/O emulsion three times as the following recovered ratios: first time 90 %; second time 85 %; third time 86 % [see Fig. 3-9-(B)], indicating that the SBR in the nanocomposites can possess a good oil resistance ability toward 1,2-dichloroethane.

Application of SBR into a wide variety of fields has been hitherto very limited, due to the poor oil resistance of SBR.^{24 ~ 28)} However, the present R_F-(VM-SiO₂)_n-R_F/SBR

nanocomposites, which were prepared under alkaline conditions, can exhibit a superoleophobic/superhydrophobic characteristic. The present $R_F-(VM-SiO_2)_n-R_F/SBR$ nanocomposites, which were prepared under acidic conditions, can supply a superoleophilic/superhydrophobic characteristic; however, this composite is applicable to the packing material for the column chromatography to isolate the transparent colorless oil from the mixture of oil/water possessing a good reusability. Therefore, the present fluorinated SBR nanocomposites have high potential for new development of SBR into a wide variety of fields.

3.4. Conclusions

The $R_F-(VM-SiO_2)_n-R_F/SBR$ nanocomposites were prepared by the sol-gel reactions of the corresponding oligomer $[R_F-(VM)_n-R_F]$ in the presence of SBR under alkaline and acidic conditions, respectively. The $R_F-(VM-SiO_2)_n-R_F/SBR$ nanocomposites, which were prepared under alkaline conditions, can provide the superoleophobic/superhydrophobic characteristic on the modified glass surface. In contrast, the nanocomposites, which were prepared under acidic conditions, can supply superoleophilic/superhydrophobic characteristic on the modified surface. Therefore, it was demonstrated that the wettability between superoleophobic and superoleophilic characteristics on the modified superhydrophobic glass surface can be easily controlled by changing the preparative conditions (alkaline or acidic conditions) of the expected nanocomposites. In addition, the $R_F-(VM-SiO_2)_n-R_F/SBR$ nanocomposites possessing the superoleophilic/superhydrophobic characteristic were applied to the packing material for the column chromatography for the separation of the mixture of oil and water. Especially, a good reusability of the nanocomposite powders for the packing material was observed for the separation of the W/O emulsions, and the transparent colorless oil was isolated

even after the use of this packing material three times. In general, SBR is well-known to have a poor oil resistance ability; however, the present nanocomposites can exhibit a good oil resistance ability for the use of packing material. Furthermore, it was verified that the present nanocomposites have a superoleophobic property with the superhydrophobicity. Thus, the present fluorinated SBR nanocomposites may be developed into a wide variety of fields as promising fluorinated SBR nanocomposite materials possessing a good oil resistance ability.

References

- 1) M. van Duin and H. Dikland, *Polym. Degrad. Stab.*, **92**, 2287 (2007).
- 2) W. Wu and D. Chen, *J. Appl. Polym. Sci.*, **120**, 3695 (2011).
- 3) H. Ismail and S. Suzaimah, *Polym. Testing*, **19**, 879 (2000).
- 4) J. Korb, *J. Appl. Polym. Sci.*, **6**, 240 (1962).
- 5) H. Ismail and H. M. Hairunezam, *Eur. Polym. J.*, **37**, 39 (2001).
- 6) C. Shan, Z. Gu, L. Wang, P. Li, G. Song, Z. Gao, and X. Yang, *J. Appl. Polym. Sci.*, **119**, 1185 (2011).
- 7) Y. Oikawa, T. Saito, S. Yamada, M. Sugiya, and H. Sawada, *ACS Appl. Mater. Interfaces*, **7**, 13782 (2015).
- 8) J. Suzuki, Y. Takegahara, Y. Oikawa, M. Chiba, S. Yamada, M. Sugiya, and H. Sawada, *J. Sol-Gel Sci. Technol.*, **81**, 611 (2017).
- 9) K. Yamashita, S. Sasahara, and H. Sawada, *J. Coat. Technol. Res.*, DOI:10.1007/s11998-016-9910-5.
- 10) H. Sawada, Y. Suto, T. Saito, Y. Oikawa, K. Yamashita, S. Yamada, M. Sugiya, and J. Suzuki, *Polymers*, **9**, 92 (2017).

- 11) Y. Goto, H. Takashima, K. Takishita, and H. Sawada, *J. Colloid Interface Sci.*, **362**, 375 (2011).
- 12) H. Sawada, "Fluorinated Polymers, Volume 2: Applications, Edited by B. Ameduri and H. Sawada, Chap 12, pp353 ~ 365, RSC, UK (2016).
- 13) H. Sawada, *Polym. Chem.*, **3**, 46 (2012).
- 14) T. Saito, Y. Tsushima, and H. Sawada, *Colloid Polym. Sci.*, **293**, 65 (2015).
- 15) H. Sawada and M. Nakayama, *J. Chem. Soc., Chem. Commun.*, 677 (1991).
- 16) H. Sawada, T. Suzuki, H. Takashima, and K. Takishita, *Colloid Polym. Sci.*, **286**, 1569 (2008).
- 17) X. Deng, L. Mammen, H.-J. Butt, and D. Vollmer, *Science*, **335**, 67 (2012).
- 18) X. Yao, Y. Song, and L. Jiang, *Adv. Mater.*, **23**, 719 (2011).
- 19) A. K. Kota, Y. Li, J. M. Mabry, and A. Tuteja, *Adv. Mater.*, **24**, 5838 (2012).
- 20) Y. Si and Z. Guo, *Chem. Lett.*, **44**, 874 (2015).
- 21) J. Li, H. Wan, Y. Ye, H. Zhou, and J. Chen, *Appl. Surface Sci.*, **261**, 470 (2012).
- 22) K. Liu, Y. Tian, and L. Jiang, *Prog. Mater. Sci.*, **58**, 503 (2013).
- 23) A. Ratcha, T. Saito, R. Takahashi, S. Kongparakul, and H. Sawada, *Colloid Polym. Sci.*, **294**, 1529 (2016).

- 24) R. Manshaie, S. Nouri Khorasani, S. Jahanbanai Veshare, and M. Rezaei Adadchi, *Rad. Phys, Chem.*, **80**, 100 (2011).
- 25) M. M. Hassan, R. O. Aly, S. E. Abdel Aal, A. M. El-Masry, and E. S. Fathy, *J. Ind. Eng. Chem.*, **19**, 1735 (2013).
- 26) J. Li, A. I. Isayev, X. Ren, and M. D. Soucek, *Polymer*, **60**, 144 (2015).
- 27) Y.-I. Tai, J.-S. Qian, J.-B. Miao, R. Xia, Y.-C. Zhang, and Z.-G. Yang, *Materials Design*, **34**, 522 (2012).
- 28) F. Touaiti, P. Alam, M. Toivakka, and M. P. Ansell, *Mechanics Materials*, **49**, 1 (2012).

Conclusions

The results obtained from this study are summarized as follows:

1. Fluoroalkyl end-capped vinyltrimethoxysilane oligomer/poly(acrylonitrile-*co*-butadiene) $[R_F-(VM-SiO_2)_n-R_F/NBR]$ nanocomposites were prepared by the sol-gel reactions of the corresponding fluorinated oligomer $[R_F-(VM)_n-R_F]$ with NBR under alkaline conditions. Not only the NBR but also the NBR containing stearic acid, zinc oxide and sulfur $[NBR_{st-zn-s}]$, and NBR containing zinc oxide and sulfur $[NBR_{zn-s}]$ were also prepared under similar conditions. Thermogravimetric analyses measurements show that the $R_F-(VM-SiO_2)_n-R_F/NBR$ nanocomposites were found to give no weight loss corresponding to the content of NBR even after calcination at 800 °C. The modified glass surfaces treated with the $R_F-(VM-SiO_2)_n-R_F/NBR$ and $/NBR_{st-zn-s}$ nanocomposites can provide a highly oleophobic - superhydrophobic characteristic; however, the $R_F-(VM-SiO_2)_n-R_F/NBR_{zn-s}$ nanocomposites can afford superoleophilic - superhydrophobic characteristic. In addition, the $R_F-(VM-SiO_2)_n-R_F/NBR_{zn-s}$ nanocomposites possessing superoleophilic/superhydrophobic characteristic, which were prepared by the cross-linking reaction at 150 °C for 30 min, were applicable to packing material for column chromatography to separate not only the mixture of oil and water but also water-in-oil emulsion.

2. A variety of initiator fragments end-capped oligomers were prepared by radical oligomerization of the corresponding monomers such as acrylic acid (ACA), acryloylmorpholine (ACMO), *N*-(1,1-dimethyl-3-oxobutyl)acrylamide (DOBAA) and *N,N*-dimethylacrylamide (DMAA) by using a variety of radical initiators such as ammonium persulfate (APS), 2,2'-azobis(2-methyl-*N*-(2-hydroxyethyl)propionamide) (VA-086) and azobisisobutyronitrile (AIBN). These obtained initiator fragments [the sulfate ester, the *HO-Amide* and the nitrile] end-capped oligomers were found to exhibit good dispersibility and stability in traditional organic solvents including water. Interestingly, these obtained initiator fragments end-capped oligomers can cause a gelation toward not only water but also traditional organic solvents including non-polar solvent such as hexane. In addition, the initiator fragments end-capped oligomers can react with tetraethoxysilane in the presence of the silica nanoparticles through the sol-gel reaction under alkaline conditions to provide the corresponding initiator fragments end-capped oligomers/silica nanocomposites. The obtained *HO-Amide* fragments end-capped DMAA, ACA, DOBAA, and ACMO oligomers/silica nanocomposites can give no weight loss behavior even after calcination at 800 °C, although the sulfate ester fragment DMAA, ACA, DOBAA, and ACMO oligomers/silica nanocomposites can afford a clear weight loss under similar conditions. In addition, the nitrile fragments end-capped DMAA oligomer/silica nanocomposites were also found to afford no weight loss characteristic through the formation of imine units during the calcination process.

3. Fluoroalkyl end-capped vinyltrimethoxysilane oligomer/poly(styrene-*co*-butadiene) [R_F-(VM-SiO₂)_n-R_F/SBR] nanocomposites were prepared by the sol-gel reaction of the corresponding fluorinated oligomer [R_F-(VM)_n-R_F] with SBR under alkaline and acidic conditions. These nanocomposites thus obtained can exhibit a good dispersibility and stability in traditional organic solvents. 1,2-Dichloroethane sol solution of the R_F-(VM-SiO₂)_n-R_F/SBR nanocomposites, which were prepared under alkaline conditions, were effective for the surface modification of glass through the casting technique to exhibit superamphiphobic (superoleophobic/superhydrophobic) characteristic on the modified glass surface. In contrast, 1,2-dichloroethane sol solutions enabled the R_F-(VM-SiO₂)_n-R_F/SBR nanocomposites, which were prepared under acidic conditions, to exhibit the superoleophilic and superhydrophobic characteristics on the modified glass surface through casting the glass into these sol solutions. Therefore, the wettability between superoleophobic and superoleophilic characteristics on the modified superhydrophobic glass surfaces can be easily controlled by changing the preparative conditions (alkaline or acidic conditions). Furthermore, these obtained nanocomposites possessing the superoleophilic and superhydrophobic characteristics were applied to the packing material for the column chromatography to separate not only the mixture of oil and water but also the water-in-oil emulsion.

Publications

- 1) A. Ratcha, T. Saito, R. Takahashi, S. Kongparakul, and H. Sawada, "Preparation and Thermal Stability of Fluoroalkyl End-capped Vinyltrimethoxysilane Oligomeric Silica/Poly(acrylonitrile-*co*-butadiene) Nanocomposites - Application to the Separation of Oil and Water", *Colloid Polym. Sci.*, **294**, 1529 - 1539 (2016).
- 2) H. Sawada, M. Kabutomori, A. Ratcha, S. Kongparakul, and M. Nishida, "Preparation and Thermal Stability of Initiator Fragments End-capped Oligomers/Silica Nanocomposites", *Colloid Polym. Sci.*, **294**, 1173 - 1186 (2016).
- 3) A. Ratcha, R. Takahashi, S. Kongparakul, and H. Sawada, "Wettability Control Between Superoleophobic and Superoleophilic Characteristics on the Modified Superhydrophobic Surfaces Treated with Fluoroalkyl End-capped Vinyltrimethoxysilane Oligomeric Silica/Poly(styrene-*co*-butadiene) Nanocomposites: Application to the Separation of Oil and Water", *J. Coat. Technol. Res.*, DOI: 10.1007/s1198-017-0003-x.

(not described in this thesis)

- 4) A. Ratcha, B. Yoosuk, and S. Kongparakul, "Grafted Methyl Methacrylate and Butyl Methacrylate onto Natural Rubber Foam for Oil Sorbent", *Adv. Mater. Res.*, **844**, 385 - 390 (2014).
- 5) A. Ratcha, C. Samart, B. Yoosuk, and S. Kongparakul, "Reusable Modified Natural Rubber Foam for Petroleum-based Liquid Removal", *Macromolecular Symp.*, **354**, 177 - 183 (2015).
- 6) A. Ratcha, C. Samart, B. Yoosuk, H. Sawada, P. Reubroycharoen, and S. Kongparakul, "Polyisoprene Modified Poly(alkyl acrylate) Foam as Oil Sorbent Material", *J. Appl. Polym. Sci.*, **132**, 42688 - 42696 (2015).

Acknowledgements

This thesis was well succeeded due to the kind support and cooperation from many persons as follows:

First of all, the author would like to express her sincerest gratitude and appreciation to Professor Hideo Sawada for his valuable suggestion, encouragement, supportive and giving his knowledge throughout of this thesis.

Secondly, she deeply thanks to Professor Isoshi Nukatsuka, Associate Professor Masaki Hagihara, Associate Professor Fumihiko Kitagawa and Associate Professor Masanobu Sagisaka for their kind advice and discussions. She would also like thanks to all students in Sawada Laboratory, especially Dr. Tomoya Saito, Ms. Yuri Oikawa and Mr. Masakazu Kabutomori for their cooperation, great advice and great help during the three years.

Finally, all most of all, she would like to express special thanks to her family who the most important people in her life for their love, support and encouragement and throughout her entire study.